Sedimentary Geology 504 (2026) 107173

Contents lists available at ScienceDirect

Sedimentary Geology

journal homepage: www.elsevier.com/locate/sedgeo

Sedimentary and biotic responses to climate-driven terrigenous input in the lower Priabonian of the South Pyrenean foreland basin (Centelles, Ebro Basin)☆

Laura Acosta [a,*], Carles Ferràndez-Cañadell [a], Julio Aguirre [b], Alessandro Mancini [c], Telm Bover-Arnal [d]

[a] Departament de Dinàmica de la Terra i de l'Oceà, Universitat de Barcelona, Barcelona, Spain
[b] Departamento de Estratigrafía y Paleontología, Facultad de Ciencias, Universidad de Granada, Granada, Spain
[c] Department of Chemical and Geological Sciences, University of Cagliari, "Cittadella Universitaria, Blocco A" S.S. 554 bivio per Sestu, Monserrato, Italy, 09042
[d] Departament de Mineralogia, Petrologia i Geologia Aplicada, Universitat de Barcelona, Barcelona, Spain

ARTICLE INFO

Editor: Dr. Michal Gradzinski

Keywords:
Platform carbonates
Larger foraminifera
Coralline algae
Palaeoecology
Late Eocene

ABSTRACT

The lower Priabonian (SBZ 18b-c) La Tossa Formation in Centelles (south-eastern margin of the Ebro Basin) records an upward transition from the siliciclastic-dominated Centelles Sandstone to the carbonate-dominated Collsuspina Limestone, with an intervening mixed siliciclastic-carbonate interval. This long-term decline in terrigenous supply is interpreted to mark the onset of increasing aridity and seasonal climatic variability in the region during the early Priabonian. This aridification, also indicated by palaeobotanical and pedogenic records from the Iberian Peninsula, likely resulted from large-scale atmospheric reorganisation driven by Southern Hemisphere cooling and enhanced equatorial warming, which expanded subtropical dry belts. Through an integrated analysis of macro- and microfacies, combined with biostratigraphy and palaeoecology of larger foraminifera and coralline algae, this study reconstructs the facies architecture of a low-gradient homoclinal ramp. The results show a progressive ecological shift from larger foraminifera-dominated assemblages and cluster coral reefs to coralline algal-rich communities and frame-reef buildups, reflecting the influence of climate-mediated terrigenous fluxes on carbonate factory dynamics in a Priabonian shallow-marine platform.

1. Introduction

The late Eocene recorded the transition between the greenhouse conditions prevailing in the middle Eocene and the icehouse state that became established at the onset of the Oligocene (Zachos et al., 2001; Katz et al., 2008; Hutchinson et al., 2021). In this context, Westerhold et al. (2020) interpreted the Eocene–Oligocene Transition (EOT) as a shift from a warmhouse to a coolhouse climate, reserving the term icehouse for the later development of extensive ice sheets in the Northern Hemisphere around the Pliocene–Pleistocene boundary. Regardless of this conceptual framework, the Priabonian was characterised by an overall progressive cooling trend that mainly resulted from the uplift of the Alpine orogenic belt and the gradual restriction of the Tethys, which reshaped oceanic and atmospheric circulation patterns (Allen and Armstrong, 2008; Hamon et al., 2013; Torfstein and Steinberg, 2020; Straume et al., 2025). In addition, a possible long-term decline in atmospheric CO_2 concentrations (Pearson et al., 2009; Anagnostou et al., 2016; Hutchinson et al., 2021) and orbital forcing (Ladant et al., 2014; Wei et al., 2020) likely contributed to intensifying this cooling trend, which triggered the early growth of ice sheets in Antarctica (Zachos et al., 2001, 2008). The increase in Antarctic ice mass during the Priabonian initiated a global regression that led to the drainage of epicontinental seas and widespread environmental change (Jaramillo-Vogel et al., 2016; Hutchinson et al., 2021; De Lira Mota et al., 2023), causing a decline in marine and terrestrial biodiversity among taxa adapted to earlier greenhouse conditions (Corliss, 1981; Thomas, 2007; Pearson et al., 2008; Sun et al., 2014; Akhmetiev et al., 2017; Houben et al., 2019; Buffan et al., 2025).

However, the documented widespread Priabonian cooling trend was not linear (see e.g., Cramer et al., 2009), but was instead characterised

☆ This article is part of a Special issue entitled: 'Carbonate' published in Sedimentary Geology.

* Corresponding author.
E-mail address: laura.acosta@ub.edu (L. Acosta).

https://doi.org/10.1016/j.sedgeo.2026.107173
Received 1 June 2026; Received in revised form 31 July 2026; Accepted 4 August 2026
Available online 6 August 2026
0037-0738/© 2026 The Authors. Published by Elsevier B.V. This is an open access article under the CC BY license (http://creativecommons.org/licenses/by/4.0/).

by alternating intervals of warmer and cooler conditions (Katz et al., 2008; Persico and Villa, 2004; Pascher et al., 2015; Śliwińska et al., 2019; Hutchinson et al., 2021; Botté et al., 2026), with the cooler phases leading to the development of partial and/or ephemeral ice sheets over Antarctica (Zachos et al., 2001, 2008; Carter et al., 2017; Van Breedam et al., 2022). Moreover, this long-term cooling trend would not have occurred uniformly across the globe, as several regional records reveal climatic heterogeneity during the late Eocene. Notably, Tremblin et al. (2016) documented a phase of warming in the equatorial and North Atlantic beginning ~4 Myr before the EOT, highlighting a divergence in temperature trends between the cooling Southern Ocean and lower latitudes, and proposed that this accumulation of low-latitude heat may have contributed to the onset of permanent Antarctic glaciation.

The first well-defined and widely recognised episode of transient glaciation following the Middle Eocene Climatic Optimum (MECO) in the late Eocene is known as the Priabonian Oxygen Isotope Maximum (PrOM). This was followed by further transitional glacial intervals (e.g., Pascher et al., 2015; Śliwińska et al., 2019) that ultimately led to the major glaciation at the Eocene–Oligocene transition (~34 Ma), recorded as the Oxygen Isotope 1 event (Oi-1) (Miller et al., 1991). The PrOM was first identified by Scher et al. (2014) based on analyses of $\delta^{18}O$ in benthic foraminifera recovered from deep-sea sedimentary cores off the eastern Antarctic margin. Documented within the lower Priabonian record, it corresponds to a pronounced positive $\delta^{18}O$ excursion accompanied by an abrupt change in the provenance of Antarctic terrigenous sediments, indicating a combination of cooling and nascent ice sheet development in East Antarctica. This cooling episode has been dated to ~37 Ma, within magnetochron C17n.1n, and spanned c.140.000 years (Scher et al., 2014).

Despite its significance, the relatively recent recognition of the PrOM, together with the coeval episode of equatorial warming documented by Tremblin et al. (2016), leaves their potential expression and impact in shallow-marine, low- to mid-latitude settings poorly constrained, and correlations with coeval shallow-platform records remain limited and unresolved.

In this regard, extensive carbonate and mixed siliciclastic-carbonate systems flourished in low- to mid-latitude regions along the broad Tethys seaway and in marginal basins connected to the Atlantic, such as the studied area, which was part of the South Pyrenean foreland basin during the Priabonian (e.g., Travé et al., 1996; Nebelsick et al., 2005; Morsilli et al., 2012; Pomar et al., 2017; Tomassetti and Benedetti, 2020; Coletti et al., 2021; Mancini et al., 2025). Such shallow marine environments were dominated by larger foraminifera, commonly associated with coralline algae and hermatypic corals (e.g., Bassi, 1998; Morsilli et al., 2012; Dimou et al., 2024; Erkızan et al., 2025). These carbonate factories had already been shaped by a climatic shift across the middle–late Eocene transition, which triggered a major biotic crisis in larger foraminiferal assemblages and led to a progressive reduction in their diversity (Hottinger, 1998, 2001; Renema, 2002; Less and Özcan, 2012; Whidden and Jones, 2012; Lunt and Luan, 2022; Benedetti et al., 2024). The Bartonian–Priabonian turnover was characterised by the extinction of once-abundant groups, such as the *Alveolina-Glomalveolina* group, which was reduced to one single species, as well as of several groups of nummulitids and orthophragmines (Hottinger, 1983; Serra-Kiel et al., 1998; Less and Özcan, 2012; Özcan et al., 2018). This decline in larger foraminifera diversity coincided with the expansion of coralline algae communities and coral reef systems, which, together with larger foraminifera, constituted the dominant carbonate producers on low- to mid-latitude shallow-marine platforms (Bassi, 2005; Nebelsick et al., 2000; Nebelsick et al., 2005; Pomar et al., 2017; Król et al., 2018; Mancini et al., 2025).

The present study investigates the lower Priabonian La Tossa Formation (Ferrer, 1971a), a shallow-water mixed siliciclastic-carbonate succession in the eastern Ebro Basin (north-eastern Iberia). During the Lutetian-earliest Priabonian, this area corresponded to the eastern sector of the South Pyrenean foreland basin, a marine elongated gulf connected to the Atlantic. According to recent correlations between shallow benthic zones and polarity chrons, the studied interval falls within the episode of equatorial and North Atlantic warming documented by Tremblin et al. (2016), contemporaneous with the Antarctic PrOM glacial event. By integrating macro- and microfacies analysis with coralline algae and larger foraminifera taxonomy, and constraining the age of the succession through foraminiferal biostratigraphy, this study reconstructs the facies architecture and palaeoecological evolution of this mixed siliciclastic-carbonate system, and evaluates how climate-driven changes in terrigenous influx conditioned carbonate factories, favouring certain biological groups over others and resulting in a diverse array of mixed siliciclastic-carbonate facies.

2. Geological setting

The study area is located in the south-eastern sector of the Ebro Basin (Fig. 1), where Priabonian strata deposited along the south-eastern margin of the South Pyrenean foreland basin are currently exposed. The Pyrenean foreland basin developed in response to flexural subsidence and tectonic loading associated with the uplift of the Pyrenean orogen during convergence between the Iberian and Eurasian plates (Muñoz, 1992; Beaumont et al., 2000).

The South Pyrenean foreland basin infill comprises a succession of marine and continental deposits spanning from the Upper Cretaceous to the upper Eocene. During the Palaeocene and Eocene, the basin was a marine corridor connected to the Atlantic at the Bay of Biscay (e.g., Plaziat, 1981; Anadón et al., 1989a, 1989b; Garcés et al., 2020). By the late Eocene, the progressive tectonic uplift of the western Pyrenees restricted this connection, leading to the basin's isolation and the widespread deposition of evaporites marking the terminal phase of marine sedimentation in the region (Puigdefàbregas et al., 1992; Travé et al., 1996; Taberner et al., 1999).

Following the cessation of marine connections, the basin evolved into the endorheic Ebro Basin, which exhibits a relatively triangular shape, delimited by three distinct mountain ranges: the Pyrenees to the north, the Iberian Chain to the southwest, and the Catalan Coastal Chain to the southeast (Vergés et al., 2002). The basin's geometry was primarily controlled by the progressive, southward emplacement of north-margin Pyrenean thrust sheets, following a piggyback sequence (Riba et al., 1975, 1983; Puigdefàbregas et al., 1986; Vergés and Muñoz, 1990; Barnolas, 1992).

Under endorheic conditions, extensive alluvial and lacustrine systems developed from the late Priabonian to the Late Miocene (Alonso-Zarza et al., 2002; Costa et al., 2010). The final stage of sedimentation, recorded from the Middle to Late Miocene, coincided with the establishment of a regional drainage into the Mediterranean, which triggered lithospheric uplift of the south-eastern margin and widespread erosion across the basin (Muñoz, 1992; Vergés et al., 1998).

The south-eastern sector of the Ebro Basin can be subdivided into three areas of marine sedimentation during the Eocene, when it corresponded to the South Pyrenean foreland basin: the Igualada to the southwest and Vic to the northwest, commonly referred to in the literature as the “Igualada sub-basin” and “Vic sub-basin”, respectively (e.g., Romero et al., 1999; Salas, 1979) and, between them, the Manresa area, which includes the Montserrat and Sant Llorenç del Munt fan-delta complexes (Del Santo et al., 2000; López-Blanco et al., 2000; López-Blanco, 2002, 2006; Gómez-Paccard et al., 2011) (Fig. 1B). The studied succession is located along the south-eastern margin of the Vic sub-basin, in the Centelles high (Fig. 2) (Reguant, 1967; Taberner et al., 1999; Waltham et al., 2000). The sedimentary fill of the sub-basin ranges from Palaeocene to Oligocene in age (Lutetian-Oligocene in the Centelles area) and forms a monoclinal structure that dips gently (~5–10°) toward the northwest (Reguant, 1967). Its Eocene record documents the final phase of open-marine sedimentation within the south-eastern sector of the Pyrenean foreland basin, immediately prior

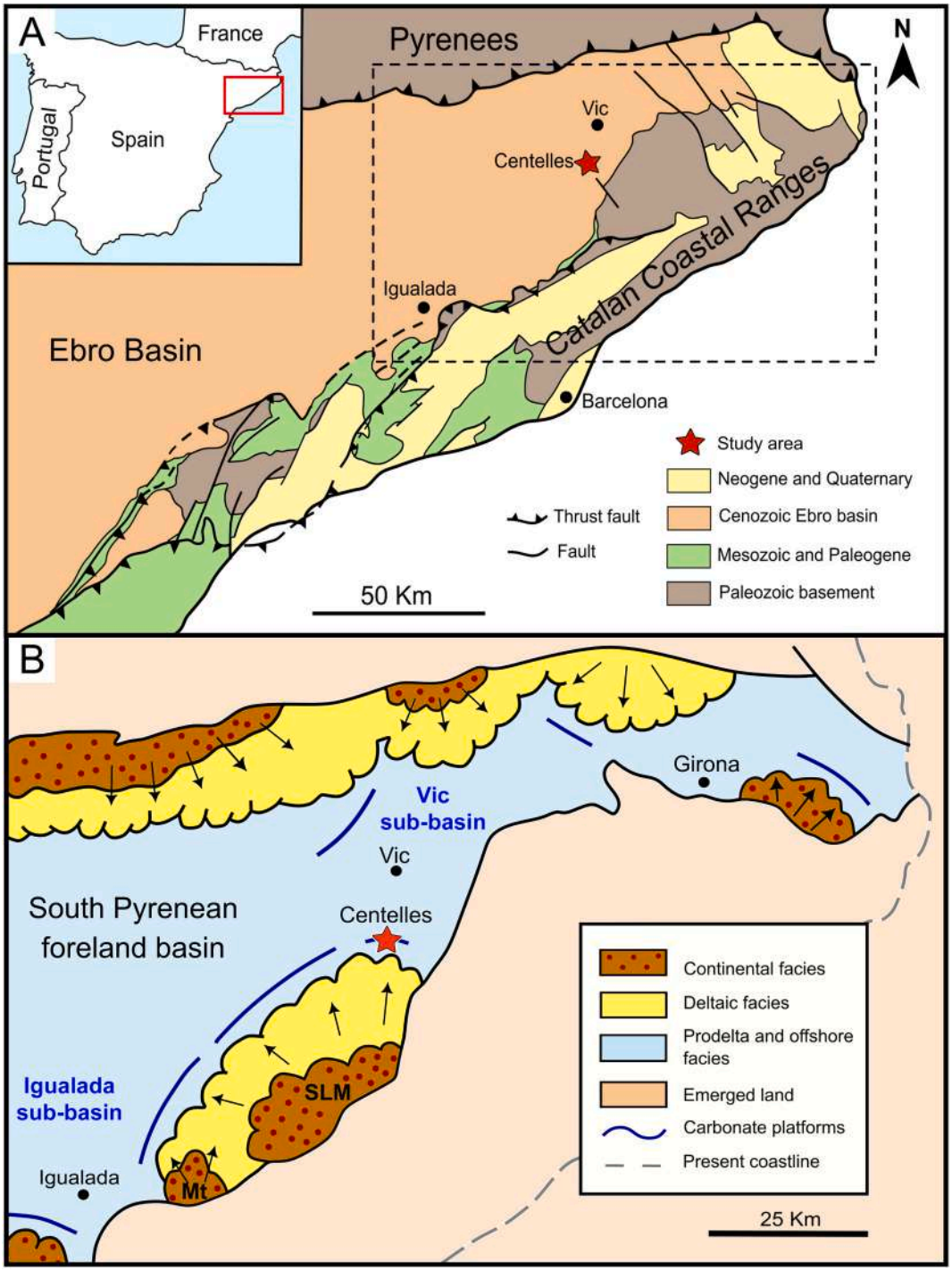


Fig. 1. (A) Simplified geological map of the north-eastern part of the Iberian Peninsula. The box indicates the location of panel B, and the study area is marked by a red star (after Barnolas et al., 1981). (B) Palaeogeography of the eastern sector of the South Pyrenean foreland basin during the late Bartonian–early Priabonian, showing the location of the studied succession near Centelles, as well as the Igualada and Vic sub-basins and the present-day Montserrat (Mt) and Sant Llorenç de Munt (SLM) massifs. Modified from Barnolas et al. (2019).

to the transition to continental alluvial, lacustrine and evaporitic deposition (Taberner, 1984; Taberner et al., 1999). According to palaeogeographic reconstructions, the Vic sub-basin was located at approximately 33° N during the Priabonian (~37 Ma; van Hinsbergen et al., 2015, 2026), corresponding to a lower mid-latitude setting within the subtropical belt.

2.1. Stratigraphy

In the south-eastern margin of the Ebro Basin, the middle–upper Eocene record comprises a thick marine to continental succession that can be subdivided into the following lithostratigraphic units: a lower continental unit (Pontils Group), followed by a marine unit (Santa Maria Group), the transitional deposits of the Terminal Complex, the evaporitic Cardona Formation, and the continental Artés Formation (Fig. 3).

The Pontils Group is a set of continental and transitional deposits,

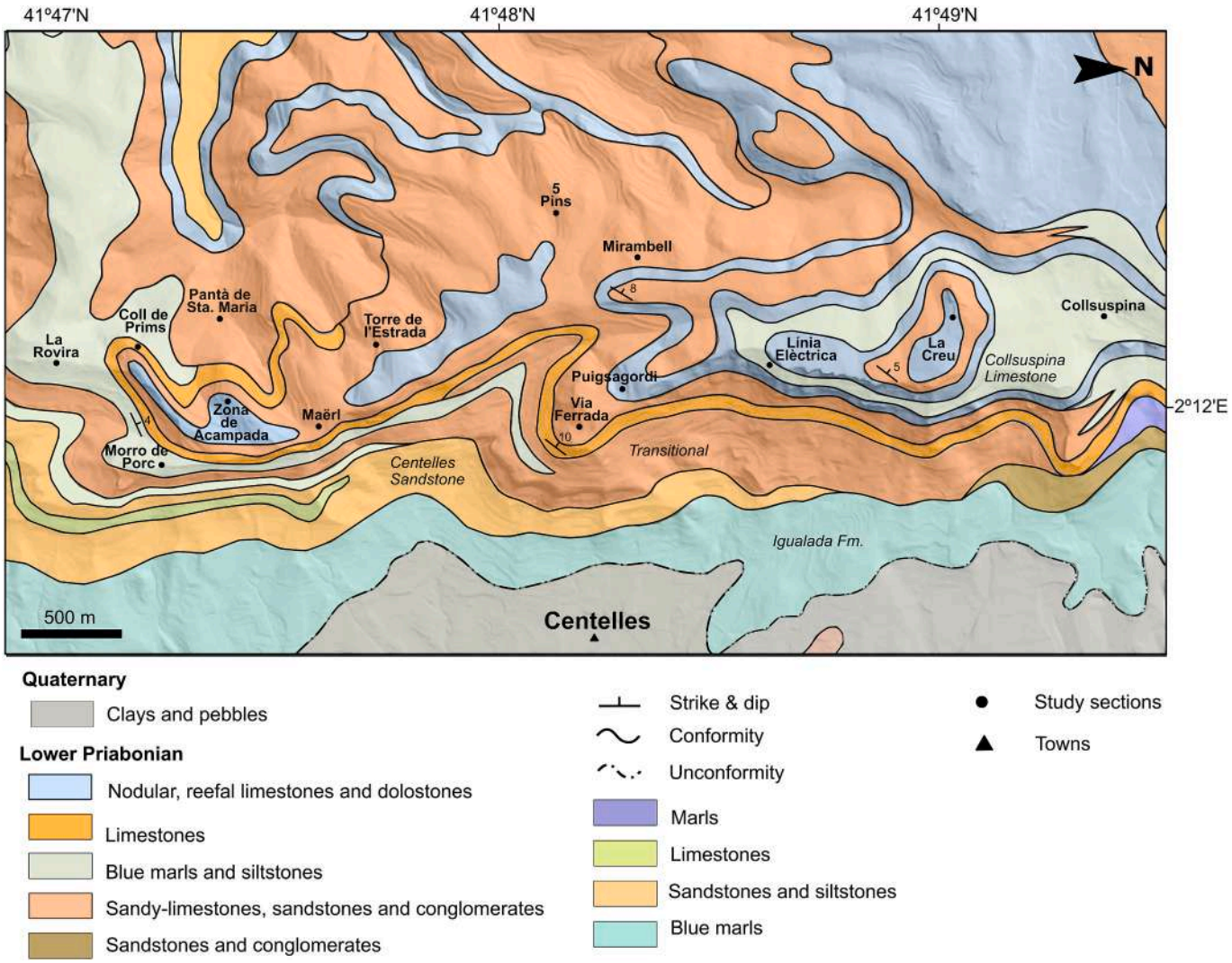


Fig. 2. Geological map of the western part of Centelles showing the study area and the location of the stratigraphic sections. Modified from the Institut Cartogràfic i Geològic de Catalunya (ICGC) (2024), scale 1:50.000.

predominantly composed of red mudstones, interbedded with carbonate and evaporitic materials (Anadón, 1978). Its age is attributed to the Lutetian and Bartonian stages, based on biozonation established by charophytes and mammal remains (Anadón and Feist, 1981; Anadón et al., 1983). The overlying Santa Maria Group (Ferrer et al., 1968; Ferrer, 1971a, 1971b) comprises the following formations: i) the Collbàs Formation, represented by a complex association of sandstones, occasionally conglomeratic, limestones, sandy-limestones and marls, indicative of a nearshore depositional environment; ii) the Vic-Igualada Formation, including its three members, Manlleu, La Guixa, and Vespella, characterised by a thick succession of marls and siltstones with sporadic, thin intercalations of marly limestones. This formation is interpreted as prodelta deposits associated with the basin-margin deltaic complexes of Centelles and Sant Martí Xic, spanning the Bartonian–-Priabonian boundary. According to Burbank et al. (1992) and Vergés and Burbank (1995), the base of this unit (the Manlleu Member) is constrained to the late Lutetian, while its uppermost section (the Vespella Member) marks the Bartonian–Priabonian boundary. Finally, iii) the La Tossa Formation and its lateral equivalent in the northern Vic sub-basin, the Sant Martí Xic Formation, comprise platform carbonates dominated by coral bioconstructions, larger foraminifera, and coralline algae interbedded with conglomerates and sandstones (Fig. 3). These formations are attributed to the early Priabonian (Ferrer, 1967, 1971a; Romero et al., 1999; Taberner et al., 1999; Costa et al., 2013).

The Santa Maria Group succession exhibits a transgressive character along the eastern Ebro Basin, with its lower boundary placed at the base of the Collbàs Formation (Teixell and Serra-Kiel, 1988). This sequence culminates in a final marine regression comprising the middle part of the Igualada and the La Tossa formations, followed by the shallow-water deposits of the "Terminal Complex" (Travé, 1992; Travé et al., 1996), characterised by porcelaneous foraminifera, corals, coralline algae, oolitic bars, and microbial mats, interbedded with unfossiliferous marls and sandstones. The succession is capped by the extensive evaporite deposits of the saline Cardona Formation (Puigdefàbregas et al., 1986). Finally, the Artés Formation, consisting of alluvial materials ranging from the middle Priabonian to late Miocene, represents the continental deposits in the central part of the Ebro Basin (Ferrer et al., 1968; Colom et al., 1970; Sanjuan et al., 2012).

The studied succession belongs to the La Tossa Formation, which comprises a mixed siliciclastic-carbonate platform that developed along the south-eastern margin of the Igualada-Vic sub-basins (Serra-Kiel et al., 2003a, 2003b; Romero et al., 1999; Travé et al., 1999) (Fig. 1). In the study area, this formation has been subdivided herein into three distinct units based on lithology and fossil content. From base to top, these units are: the Centelles Sandstone, a transitional mixed siliciclastic-carbonate interval (hereafter referred to as Transitional), and the Collsuspina Limestone (Figs. 4 and 5).

The age of the La Tossa Formation has been the subject of

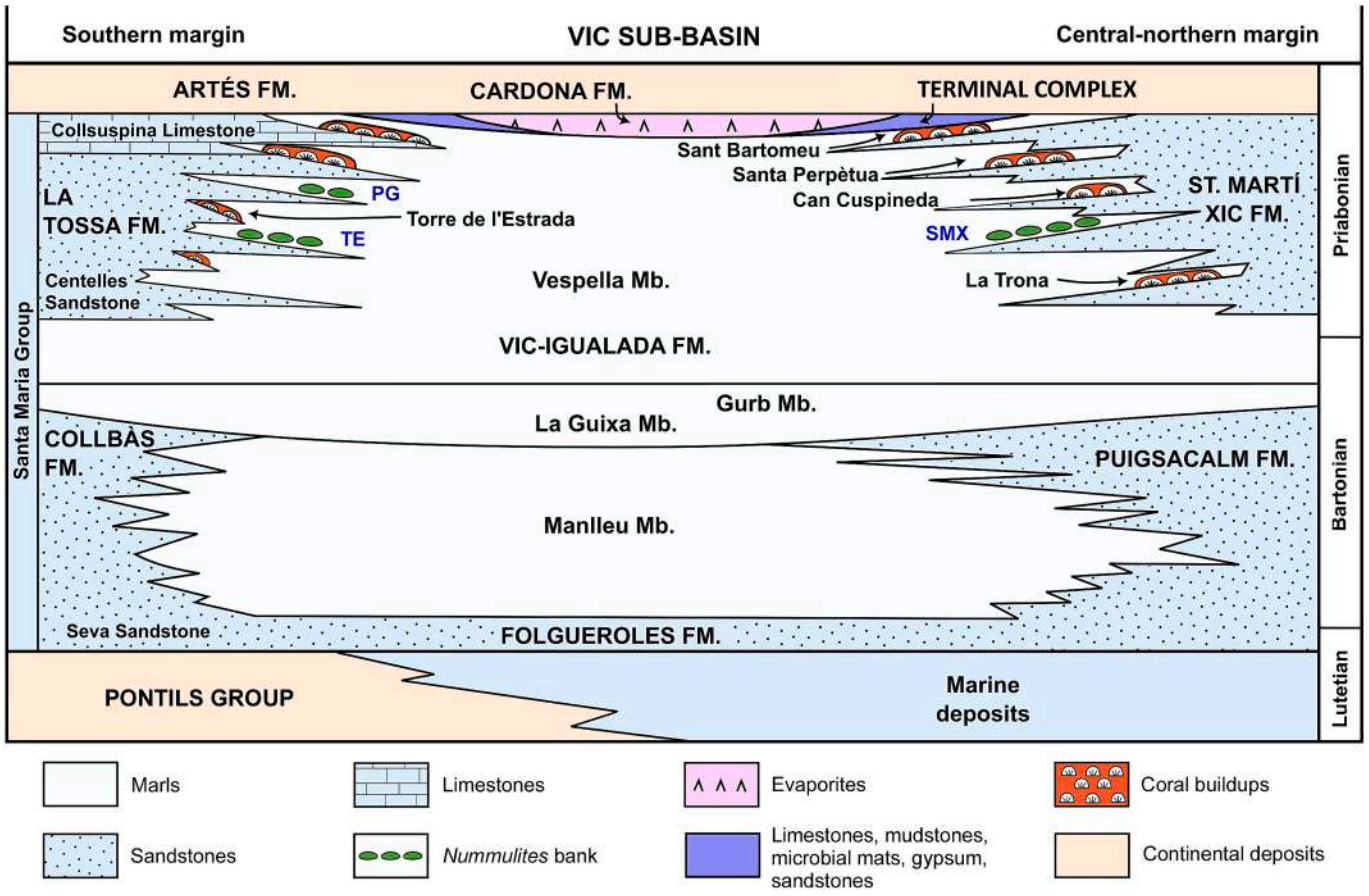


Fig. 3. Middle to upper Eocene lithostratigraphic chart of the south-eastern Pyrenean foreland basin. The study area is part of the La Tossa Formation (modified after Busquets et al., 1997 and Acosta et al., in press). TE: Torre de l'Estrada, PG: Puigsagordi, and SMX: Sant Martí Xic.

Epoch	Age	Formation	Lithological units	Sedimentary regime
Eocene	Lower Priabonian	La Tossa Fm. (= Sant Martí Xic Fm.)	Collsuspina Limestone	Carbonate
			Transitional	Mixed siliciclastic-carbonate
			Centelles Sandstone	Siliciclastic

Fig. 4. Summary of the lithostratigraphic units of the La Tossa Formation and the dominant depositional regime.

longstanding controversy. It was originally considered to be lower Priabonian in age (Reguant, 1967; Reguant et al., 1987; Ferrer, 1967, 1971a, 1971b), subsequently reinterpreted as upper Bartonian (Papazzoni and Sirotti, 1995; Travé et al., 1999; Serra-Kiel et al., 2003a, 2003b), and later reassigned to the lower Priabonian (Cascella and Dinarès-Turell, 2009; Costa et al., 2013). According to Reguant (1967), Ferrer (1967, 1971a, 1971b), Barnolas et al. (1981), Papazzoni and Sirotti (1995), Romero (1996), Serra-Kiel et al. (1998, 2003a, 2003b), Travé et al. (1999), Romero et al. (1999) and Hottinger et al. (2001), the updated larger foraminiferal assemblage of the La Tossa Formation includes *Nummulites biedai* (Schaub), *N. chavannesi* (De la Harpe), *N. cyrenaicus* (Schaub), *N. garnieri* (De la Harpe), *N. hormoensis* (Nutall and Brighton), *N. incrassatus* (De la Harpe), *N. striatus* (Bruguière), *N. stellatus* (Roveda), *N. vicaryi* (d'Archiac and Haime), *Assilina schwageri* (Silvestri), *Operculina roselli* (Hottinger), *Heterostegina reticulata* Rütimeyer, *Discocyclina augustae augustae* (Weijden), *D. radians radians* (d'Archiac), *Asterocyclina stellaris* (Brünner), *Orbitoclypeus varians* (Kaufmann), *Pellatispira madaraszi* (Hantken), and *Biplanispira absurda* (Umgrove). This association corresponds to the Shallow Benthic zone SB 18, originally defined as upper Bartonian in age (Serra-Kiel et al., 1998). The reference stratigraphic sections used to define SB 18 (e.g., La Tossa in Igualada and Varignano in northern Italy) were reinterpreted as being of late Bartonian–early Priabonian age based on magnetostratigraphic studies (Cascella and Dinarès-Turell, 2009; Costa et al., 2013; Luciani et al., 2020). Consequently, SB 18 was divided either into two (SB 18a and 18b, Costa et al., 2013) or three subzones (18a, 18b and 18c, Less et al., 2011; Less and Özcan, 2012; Papazzoni et al., 2017). In both subdivisions, the 18a/18b boundary roughly corresponds to Bartonian–Priabonian boundary. Currently, the SB 18b/18c boundary is based solely on the range of biometrically defined subspecies of *Heterostegina reticulata*. The correlation of our biostratigraphical results (Acosta et al., in press; present study) with data from previous studies based on magnetostratigraphy, calcareous nannofossils, and planktic foraminifera from the Ebro Basin (Ferrer, 1967, 1971a, 1971b; Cascella and Dinarès-Turell, 2009; Costa et al., 2010, 2013), as well as with reference works on the GSSP (Agnini et al., 2011; Agnini et al., 2021) and studies addressing the Bartonian–Priabonian boundary and updates to the Shallow Benthic zonation

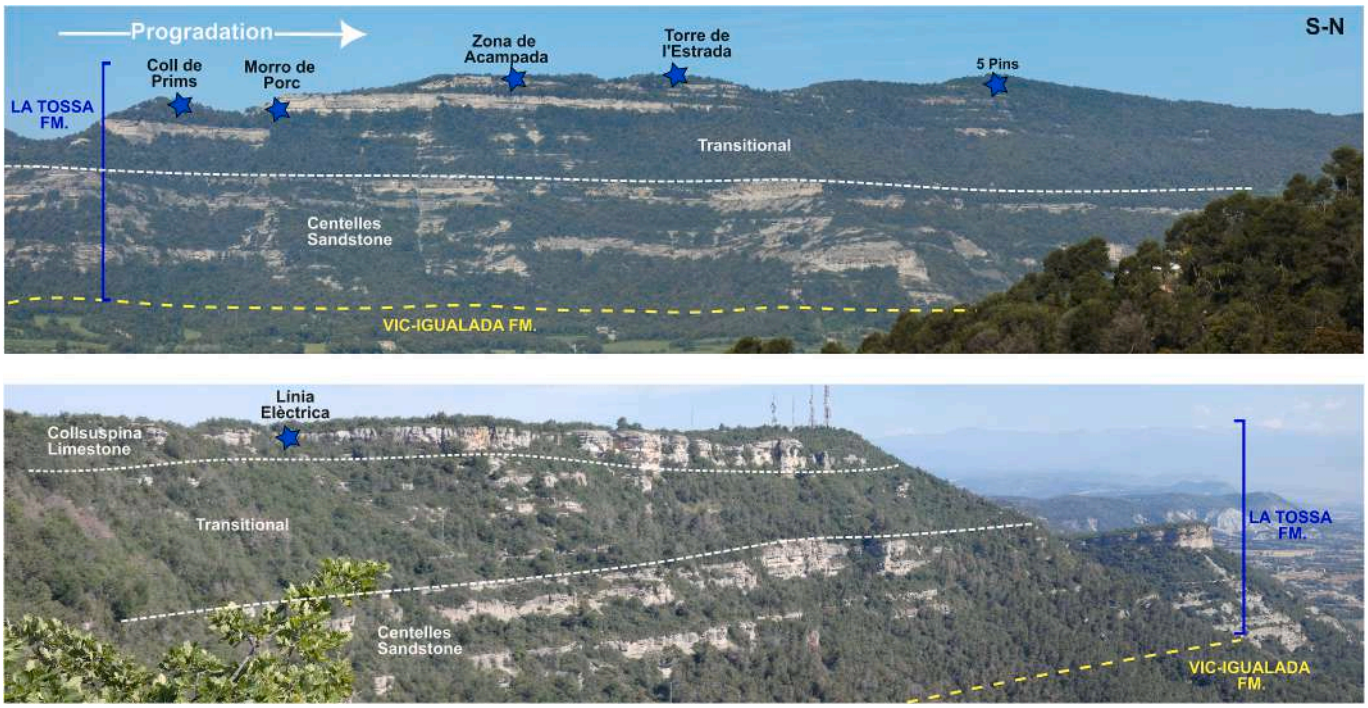


Fig. 5. Panoramic views of the study area. The stars indicate the approximate location of selected stratigraphic sections. The dashed lines mark the contact between the Centelles Sandstone, the transitional unit and the Collsuspina Limestone, whereas the yellow dashed line marks the contact between the La Tossa Formation and the Igualada Formation.

(Briguglio et al., 2026; Cotton et al., 2017; Luciani et al., 2020; Özcan et al., 2007; Özcan et al., 2018; Özcan et al., 2019; Less and Özcan, 2012; Papazzoni et al., 2017; Zakrevskaya et al., 2020), together with the lastest version of the Geological Time Scale (Gradstein et al., 2020), confirms a lower Priabonian age (SB 18b-c) for the La Tossa Fm. and its equivalent in the central Vic sub-basin, the Sant Martí Xic Formation (Figs. 3 and 4), with an estimated age of around 37 Ma.

3. Material and methods

Fourteen stratigraphic sections, up to 72 m thick, were logged and sampled to the west of Centelles. Particular attention was given to stratigraphic surfaces marking significant facies changes, fossil distribution and sedimentary structures. From south to north, the measured sections are: La Rovira (R), Coll de Prims (CP), Morro de Porc (MP), Zona d'Acampada (ZA), Pantà de Santa Maria (PSM), Maërl (MRL), Torre de l'Estrada (TE), 5 Pins (5P), Mirambell (MB), Via Ferrada-Puigsagordi (VF), Puigsagordi (PG), Línia Elèctrica (LE), La Creu (CRE), and Collsuspina (CLP) (Table 1; Figs. 5–8).

Table 1
List of stratigraphic sections arranged from south to north, showing their corresponding abbreviations (also used in sample numbering) and geographic coordinates (latitude and longitude in degrees, minutes, and seconds).

Section	Abbreviation	Coordinates
La Rovira	R	41°46′49.2" N, 2°11′57.1″ E
Coll de Prims	CP	41°46′57.5" N, 2°11′54.9″ E
Morro de Porc	MP	41°47′04.6" N, 2°,12′,11.9″E
Zona d'Acampada	ZA	41°47′19.4" N, 2°12′06.9″ E
Pantà de Santa Maria	PSM	41°47′18.1" N, 2°11′40.8″ E
Maërl	MRL	41°47′29.0" N, 2°12′09.8″E
Torre de l'Estrada	TE	41°47′37.6" N, 2°11′52.5″ E
5 Pins	5P	41°48′08.6" N, 2°11′26.1″ E
Mirambell	MB	41°48′16.3" N, 2°11′39.8″ E
Via Ferrada	VF	41°48′07.3" N, 2°12′12.0″ E
Puigsagordi	PG	41°48′17.4" N, 2°11′52.8″ E
Línia Elèctrica	LE	41°48′40.6" N, 2°11′54.8″ E
La Creu	CRE	41°49′10.4" N, 2°11′40.0″ E
Collsuspina	CLP	41°49′21.5" N, 2°11′35.0″ E

Facies-representative rock samples and isolated specimens were taken for palaeontological, biostratigraphic and microfacies analysis. Facies analysis, palaeoecological and depositional interpretations, and the taxonomic identification of larger foraminifera and coralline algae were based on the study of 344 thin sections and 108 isolated specimens, prepared at the Laboratory of Palaeontology of the Faculty of Earth Sciences of the University of Barcelona. Thin sections were examined under an optical microscope, whereas polished isolated specimens were analysed under a stereo microscope, using a digital camera attachment. The material is currently housed at the Department of Earth and Ocean Dynamics of the University of Barcelona.

The biostratigraphical assignment to Shallow Benthic biozones follows Serra-Kiel et al. (1998), Less and Özcan (2012), Costa et al. (2013), Papazzoni et al. (2017), Özcan et al. (2019), Zakrevskaya et al. (2020), and Briguglio et al. (2026). The carbonate textures follow the classifications by Dunham (1962) and Embry and Klovan (1971). The coral-bearing deposits were described and classified according to the coral reef growth fabric nomenclature proposed by Insalaco (1998). The coral buildup types were classified according to the nomenclature established by Riding (2002).

4. Results

4.1. Fossil assemblages

The skeletal assemblage of the lower Priabonian La Tossa Formation is mainly dominated by coralline algae and larger foraminifera. Scleractinian corals are also locally abundant, forming buildups. Additional skeletal components include encrusting foraminifera (acervulinids, *Planorbulina*, *Haddonia*, *Fabiania*, and victoriellids), small benthic foraminifera (including textulariids, miliolids and rotaliids), bryozoans, bivalves, gastropods, echinoids, solitary corals, and serpulids (Figs. 6–8).

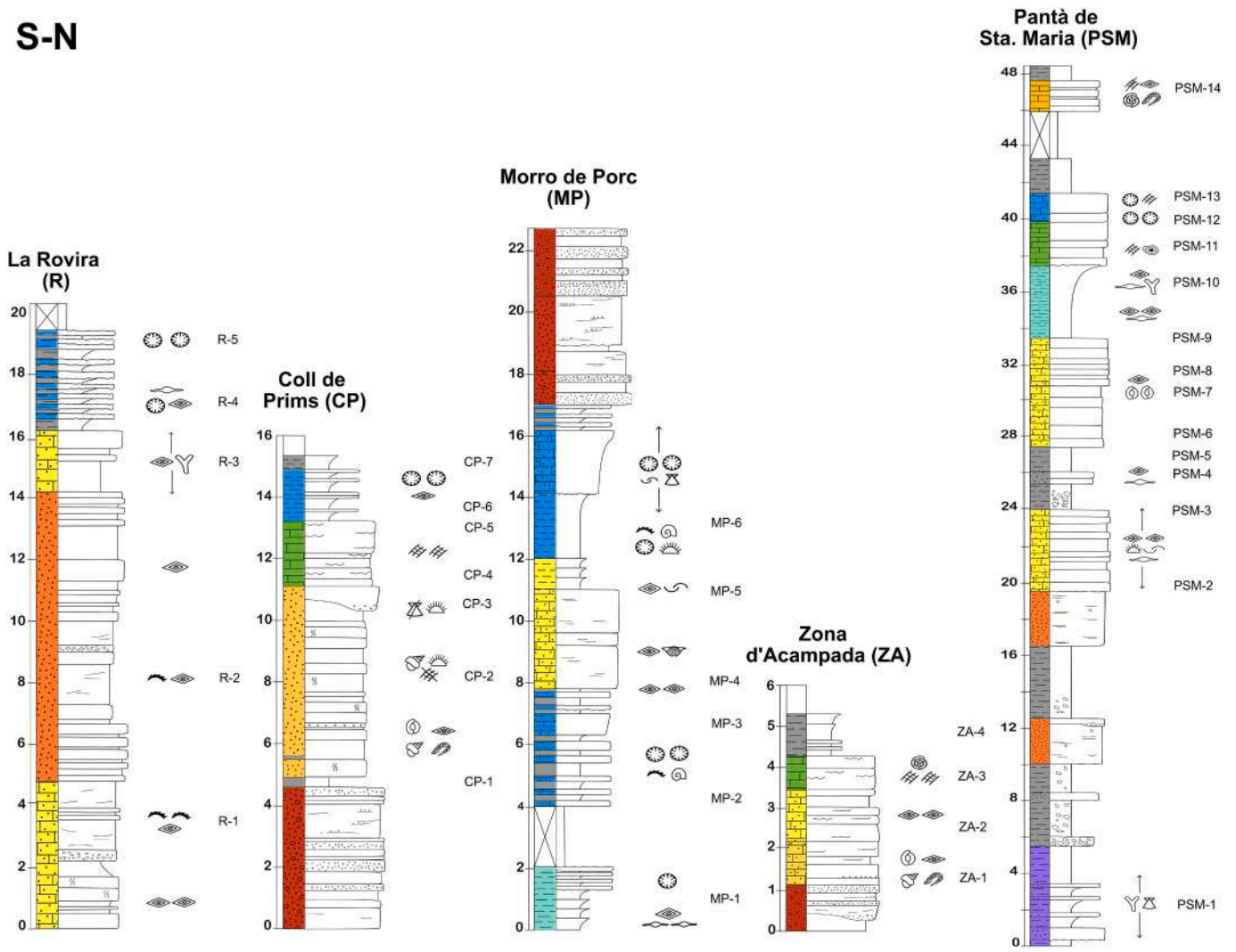


Fig. 6. Stratigraphic sections, fossil content, and sample positions recorded from south to north for the La Rovira (R), Coll de Prims (CP), Morro de Porc (MP), Zona d'Acampada (ZA), and Pantà de Santa Maria (PSM) sections. The location of each section is presented in Fig. 2. The key for this figure is provided in Fig. 8.

4.1.1. *Coralline algae*

Coralline algae occur as fragments, isolated unbroken branches, loose laminar thalli, or forming rhodoliths. They dominate specific facies types, such as maërl beds (sensu Jardim et al., 2025). In addition, coralline algae also exhibit in situ fruticose growth. The maërl algal assemblages are mostly dominated by members of the order Hapalidiales followed by representatives of the order Sporolithales (Figs. 9 and 10). The former includes branches of several morphospecies attributed to *Lithothamnion* (*L. ramosissimum* (Reuss) (Fig. 9A) and L. *vaughanii* (Howe) (Fig. 9B) among them), followed by encrusting forms of *Mesophyllum* sp. and slender branches of *Melyvonnea* sp. (Fig. 9C). Dimerous, thin encrusting plants displaying multiporate sporangial conceptacles are very rare (Fig. 9D). They show similarities with the undifferentiated species *Melobesia* sp. described by Aguirre et al. (2022) in Ypresian (early Eocene) carbonates at the Campo section (Southern Pyrenees). The Sporolithales is represented by encrusting-warty-fruticose growths of *Sporolithon lugeonii* (Pfender) and *Sporolithon* sp. (Figs. 9E and F). They occur as isolated branches, forming small rhodoliths or partially encrusting other organisms, such as corals. Members of the order Corallinales, represented by *Spongites* sp. (Fig. 10A) and *Neogoniolithon* sp., are scarce. Thin encrusting plants of *Lithoporella* cf. *minus*, although not abundant, are pervasively present attached to and intergrowing with other corallines and larger benthic foraminifer tests. Together with the non-geniculate coralline algae, numerous calcified intergenicula of articulated forms are dispersed in the matrix.

Rhodoliths (sensu Jardim et al., 2025) are mostly made up of encrusting-warty plants of *Lithothamnion* spp. and encrusting-fruticose thalli of *Sporolithon* spp. Thin, unistratose and multistratose encrusting growths of *Lithoporella* cf. *minus* are also very frequent. *Mesophyllum* sp. and dimerous plants with uniporate sporangial conceptacles, most likely attributable to the genus *Hydrolithon*, are minor components (Fig. 10B). Crusts of *Karpathia spherocellulosa* (Maslov) are also present (Fig. 10C). Accompanying coralline algae, encrusting growths of *Polystrata alba* (Pfender) (Fig. 10D) and scarce massive and nodular fragments of *Marinella lugeonii* (Pfender) also occur.

4.1.2. *Larger foraminifera*

Larger foraminifera are present in most facies and are predominantly represented by nummulitids including *Nummulites, Assilina, Heterostegina,* and orthophragmines such as *Discocyclina, Orbitoclypeus,* and *Asterocyclina.* Porcelaneous larger foraminifera are rare, represented by *Orbitolites, Glomalveolina* and *Rhabdorites* (Fig. 11). Identified benthic foraminifera at genus and/or species levels include *Nummulites biedai* (Fig. 11A), *N. chavannesi, N. cyrenaicus, N. garnieri, N. hormoensis* (Figs. 11B and C), *N. incrassatus, N. striatus, N. vicaryi, Assilina schwageri, Discocyclina* sp., *Orbitoclypeus varians varians* (Figs. 11D and E), *Asterocyclina stellata, A. stella* (Gümbel), *Asterigerina rotula* (Kaufmann) (Fig. 11F), *Acervulina linearis* (Hanzawa), *Gypsina* sp., *Solenomeris* sp.,

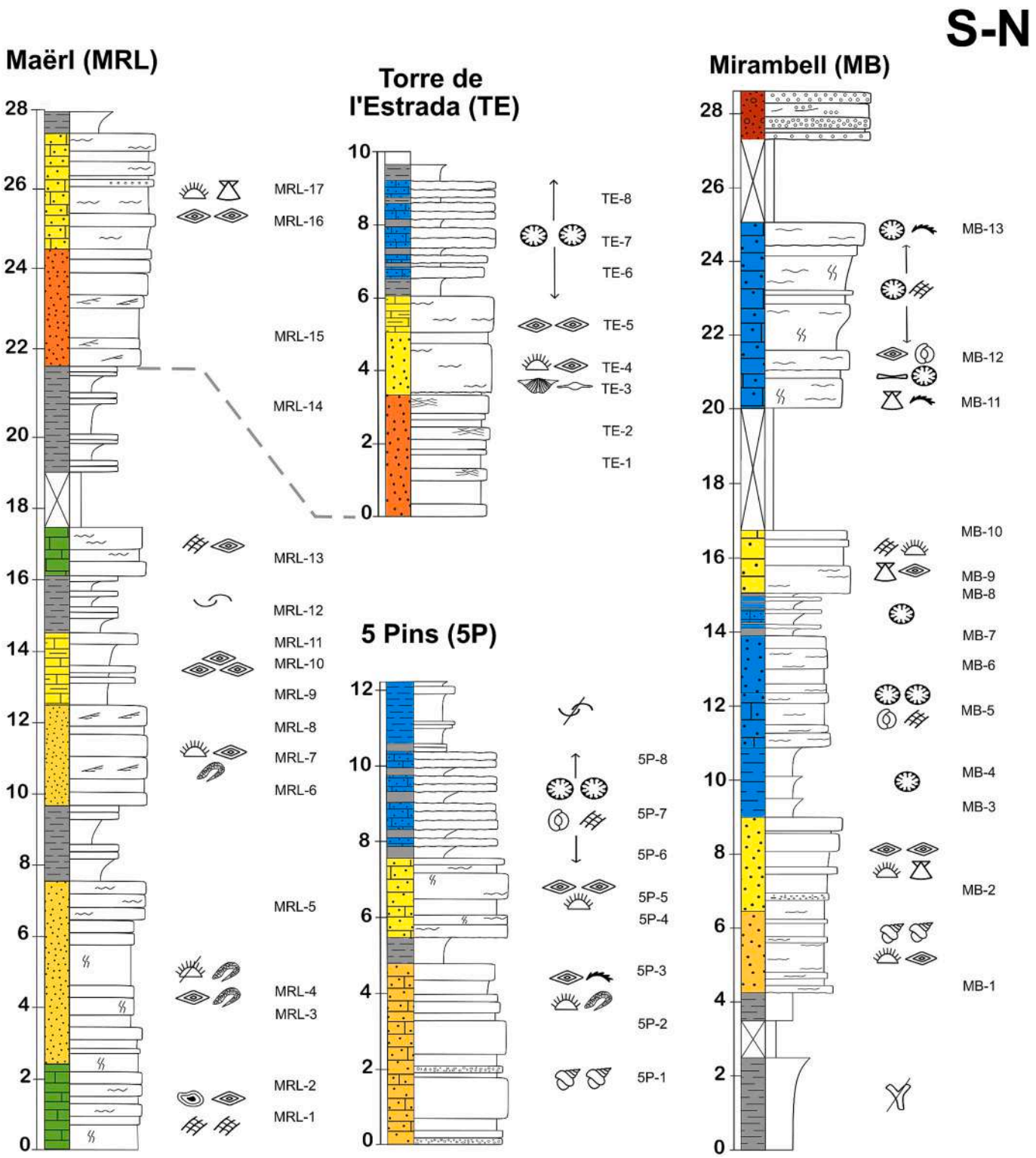


Fig. 7. Stratigraphic sections, fossil content, and sample positions from south to north for the Maërl (MRL), Torre de l'Estrada (TE), 5 Pins (5P), and Mirambell (MB) sections. The location of each section is presented in Fig. 2. The key for this figure is provided in Fig. 8.

Sphaerogypsina globulus (Reuss) (Fig. 11G), *Chapmanina gassinensis* (Silvestri) (Figs. 11H and I), *Fabiania cassis* (Oppenheim), *Gyroidinella magna* (Le Calvez), *Haddonia heissigi* (Hagn), *Halkyardia minima* (Liebus) (Figs. 11J and K), *Silvestriella tetraedra* (Gümbel) (Fig. 11L), *Schlosserina asterites* (Gümbel) (Fig. 11M), *Glomalveolina ungaroi* (Bassi and Loriga Broglio) (Fig. 11N), *Rhabdorites malatyaensis* (Sirel) (Fig. 11O), and *Orbitolites* sp. (Fig. 11P).

4.2. Facies analysis

The studied sedimentary succession consists of siliciclastic, mixed siliciclastic-carbonate and carbonate deposits. Based on an integrated analysis of compositional, textural, and palaeontological content, along with other sedimentological criteria, 9 distinct Facies types, including 7 subfacies, were differentiated (Table 2, Figs. 12–14).

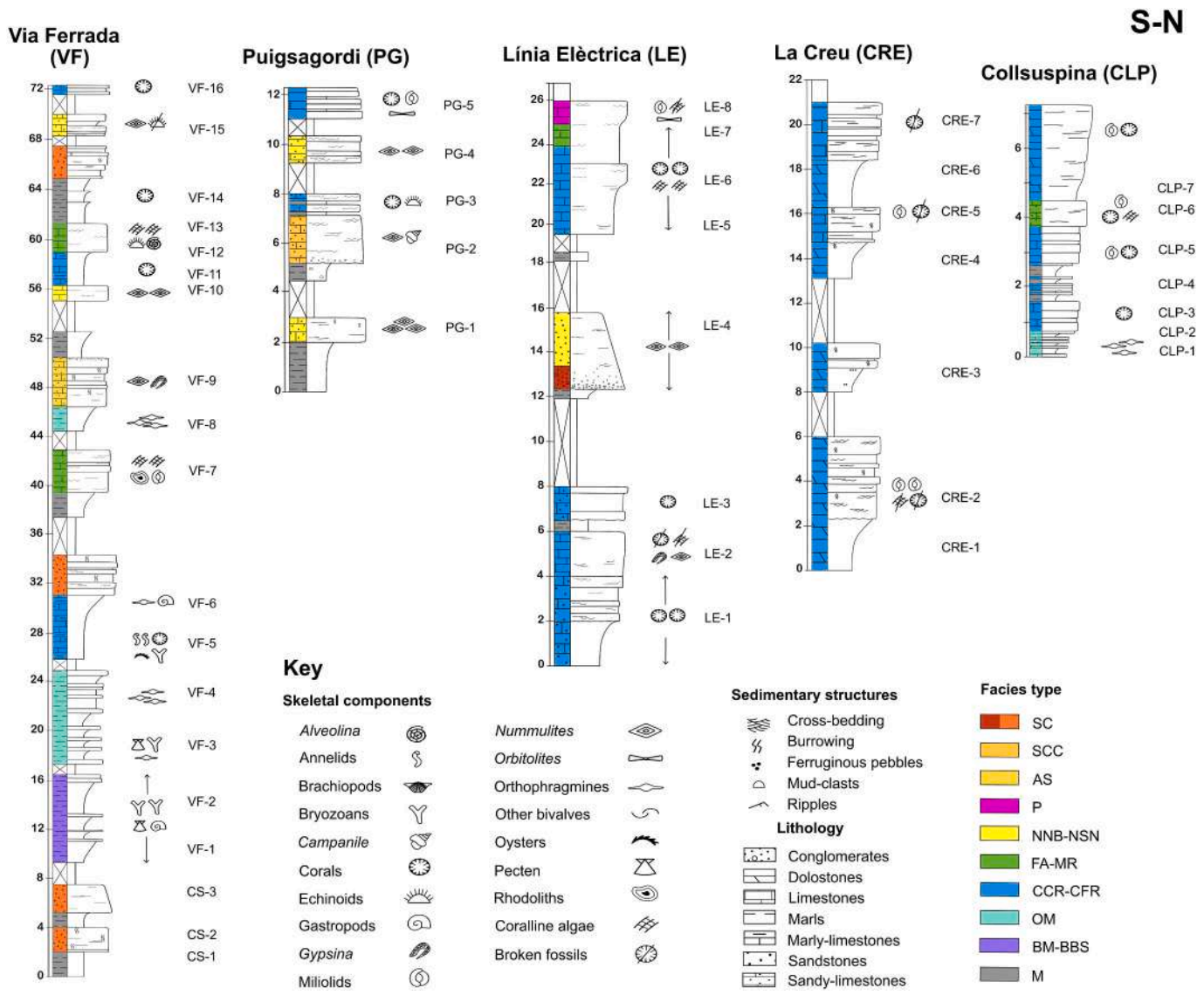


Fig. 8. Stratigraphic sections, fossil content, sample positions and legend including the facies types. From south to north Via Ferrada (VF), Puigsagordi (PG), Línia Elèctrica (LE), La Creu (CRE) and Collsuspina (CLP) sections. The location of each section is presented in Fig. 2. SC = Sandstone and Conglomerate facies, SCC = *Campanile* subfacies, AS = Acervulinid subfacies, P = Porcelaneous foraminifera, NNB = Large *Nummulites* and *Nummulites* bank subfacies, SSN = Small *Nummulites* subfacies, CCR = Cluster reef subfacies, CFR = Frame reef subfacies, FA = Foraminifera and coralline algae facies, MR = Maërl facies, OM = Orthophragmine facies, BM = Bryozoan facies, BBS = *Smittina* subfacies, and M = Marl facies.

4.2.1. Sandstone and conglomerate facies (SC)

This facies consists of gray to ochre, well-sorted and uniform, medium- to coarse-grained quartz sandstones, as well as polymictic clast-supported conglomerates (Figs. 12A and B). These lithologies are organised into 3 to 6 m-thick beds, forming general fining-upward successions. The sandstones exhibit tabular bedding and wavy laminations (Fig. 12B), locally displaying erosional bases and small channels. The siliciclastic beds generally lack well-developed sedimentary structures, although small-scale cross-bedding and bioturbation horizons with *Thalassinoides* are locally present, along with occasional occurrences of serpulids and small bivalves. Laterally, this facies grade into sandstones with acervulinids and in some sections, into sandstones bearing *Campanile* (e.g., Coll de Prims and Zona d'Acampada sections).

4.2.1.1. Campanile subfacies (SCC). The subfacies consists of medium- to coarse-grained quartz sandstones, locally interbedded with cm-scale microconglomerate layers, forming fining-upward successions. These sandstone layers are 0.5 to 2 m in thickness and exhibit a characteristic nodular bedding, distinguished by abundant *Campanile* gastropods (Fig. 12C), which can attain lengths of up to 30 cm, and by frequent bioturbated intervals containing *Thalassinoides*. The gastropods are arranged parallel to stratification but do not follow a preferential orientation. Locally some specimens show *Entobia* borings. Secondary components are bivalves, echinoids, non-articulated coralline algae fragments and scarce bryozoans. The associated foraminiferal assemblage is composed of small miliolids, a high abundance of *Gypsina, Acervulina linearis,* and *Fabiania*, with local occurrences of *Nummulites*. This facies shows a lateral and vertical change to the acervulinid-dominated subfacies.

4.2.1.2. Acervulinid subfacies (AS). This subfacies is formed by medium- to fine-grained, moderately to well-sorted quartz sandstones with abundant acervulinids (Fig. 12D). It is characterised by tabular beds, ranging from 3 to 5 m in thickness, that locally exhibit cross-stratification and lamination. Due to its high skeletal component content, it is classified as a sandy limestone with a grain-supported fabric. It

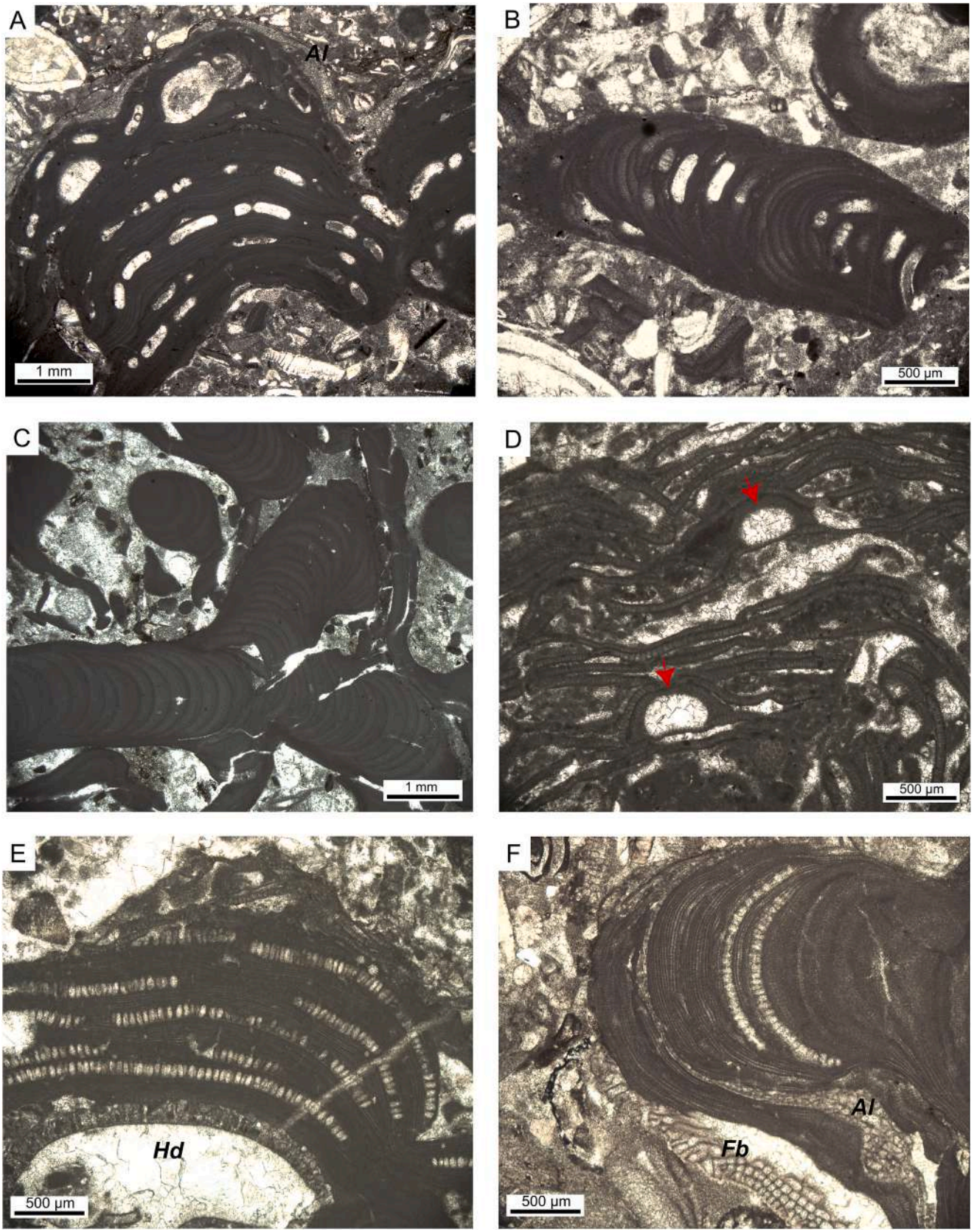


Fig. 9. Photomicrographs of the Foraminifera-Coralline algae and Maërl facies. (A) Branch of *Lithothamnion ramosissimum* with *Acervulina linearis*, sample PSM-13. (B) Branch of *Lithothamnion vaughani* displaying well-developed growth zonation, sample VF-7. (C) Fruticose growth forms of *Melyvonnea* sp., sample MRL-2. (D) Thin encrusting thalli of *Melobesia* sp. exhibiting multiporate sporangial conceptacles, sample PSM-11. (E) Encrusting growth forms of *Sporolithon* sp. and *Haddonia heissigi*, sample LE-3. (F) Encrusting growths of *Sporolithon* sp. intergrowing with *Acervulina linearis* and *Fabiania* sp., sample MRL-13. *(Al) Acervulina linearis*, *(Fb) Fabiania* sp., *(Hd) Haddonia heissigi*. See Figs. 6–8 for the stratigraphic position of the samples.

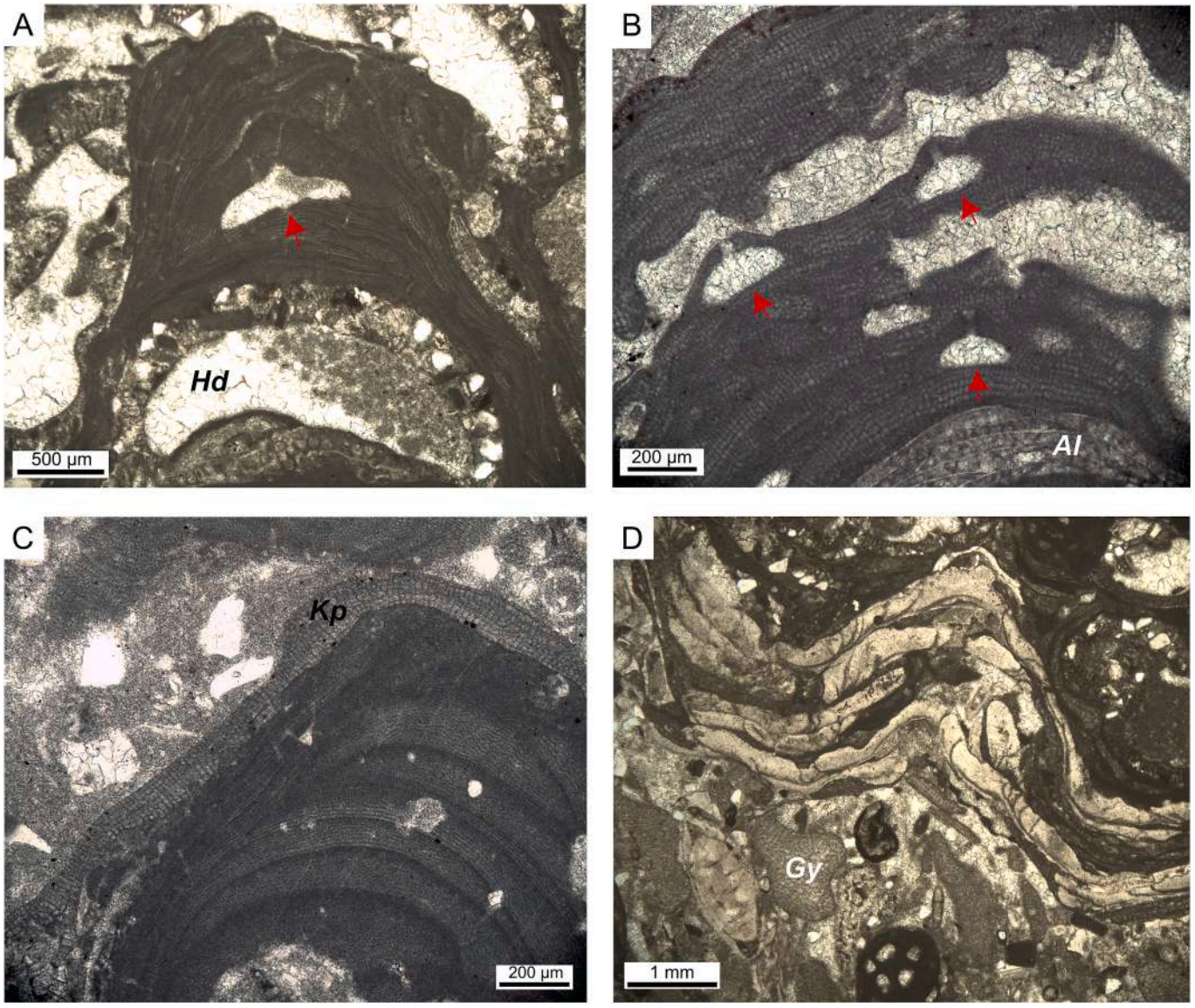


Fig. 10. Photomicrographs of the Foraminifera-Coralline algae and Maërl facies. (A) Detail of a uniporate conceptacle of *Spongites* sp. attached to the encrusting foraminifer *Haddonia heissigi*, sample MRL-1. (B) Encrusting thalli of *Hydrolithon* sp. exhibiting uniporate sporangial conceptacles, associated with the encrusting foraminifer *Acervulina linearis*, sample MRL-13. (C) Thin crustose thalli of *Karpathia spherocellulosa*, sample ZA-3. (D) Encrusting plants of peyssonneliacean algae *Polystrata alba* in association with *Gypsina* sp. and other larger foraminifera, sample MRL-13. *(Al) Acervulina linearis, (Gy) Gypsina* sp., *(Hd) Haddonia heissigi, (Kp) Karpathia.* See Figs. 6–8 for the stratigraphic position of the samples.

is dominated by encrusting foraminifera including *Acervulina*, *Solenomeris, Gypsina,* and victoriellids. Acervulinid foraminifera show cylindrical saddle and hook-shaped forms. Also present are small specimens of *Nummulites* and miliolids, along with fragments of geniculate coralline algae, bivalves, gastropods, echinoid spines, serpulids, and bryozoans. Similar facies have often been called "*Gypsina* facies" in the literature (e.g., Rasser, 1994; Morabito et al., 2024).

Additionally, within this facies type, packages of sandy limestones exhibiting cross-stratification have been observed, occurring in 2–3 m-thick beds. These beds display a packstone-grainstone texture and are characterised by abundant *Silvestriella tetraedra* (Fig. 12E), alongside encrusting foraminifera, including *Acervulina, Gypsina*, and victoriellids. Locally, *Asterigerina*, miliolids, and fragments of geniculate coralline algae, echinoids and bivalves, are also present. The acervulinid facies grades vertically into the small *Nummulites* (N-SN) subfacies (e.g., Maërl section), whereas laterally, toward a proximal direction transitions into the Sandstone and conglomerate Facies (SC) and the *Campanile* subfacies (SCC) (e.g., 5 Pins section).

4.2.2. Porcelaneous foraminifera Facies (P)

This facies is characterised by bioclastic limestones with packstone to grainstone textures, dominated by miliolids (Fig. 12F). It is distinguished by roughly nodular to locally tabular bedding, reaching thicknesses of up to 3 m. Skeletal components include fragments of bivalves, gastropods, echinoid plates and coral branches. The foraminiferal assemblage consists of miliolids, *Orbitolites, Rhabdorites*, *Nummulites, Asterigerina,* and encrusting foraminifera such as *Gypsina*, along with small rotaliids and textulariids. Geniculate coralline algae, dasycladacean algae and coralline detritus were also observed. This facies grades downward into Foraminifera-Coralline algae (FA) and into the coral-bearing frame-reef (C-FR) subfacies (e.g., Línia Elèctrica section).

4.2.3. Nummulites Facies (N)

Nummulites-bearing deposits occur with varying *Nummulites* abundances and in different sedimentary contexts (i.e., in situ versus reworked), forming distinct banks or occurring as resedimented siliciclastic-influenced accumulations. Two subfacies were recognised:

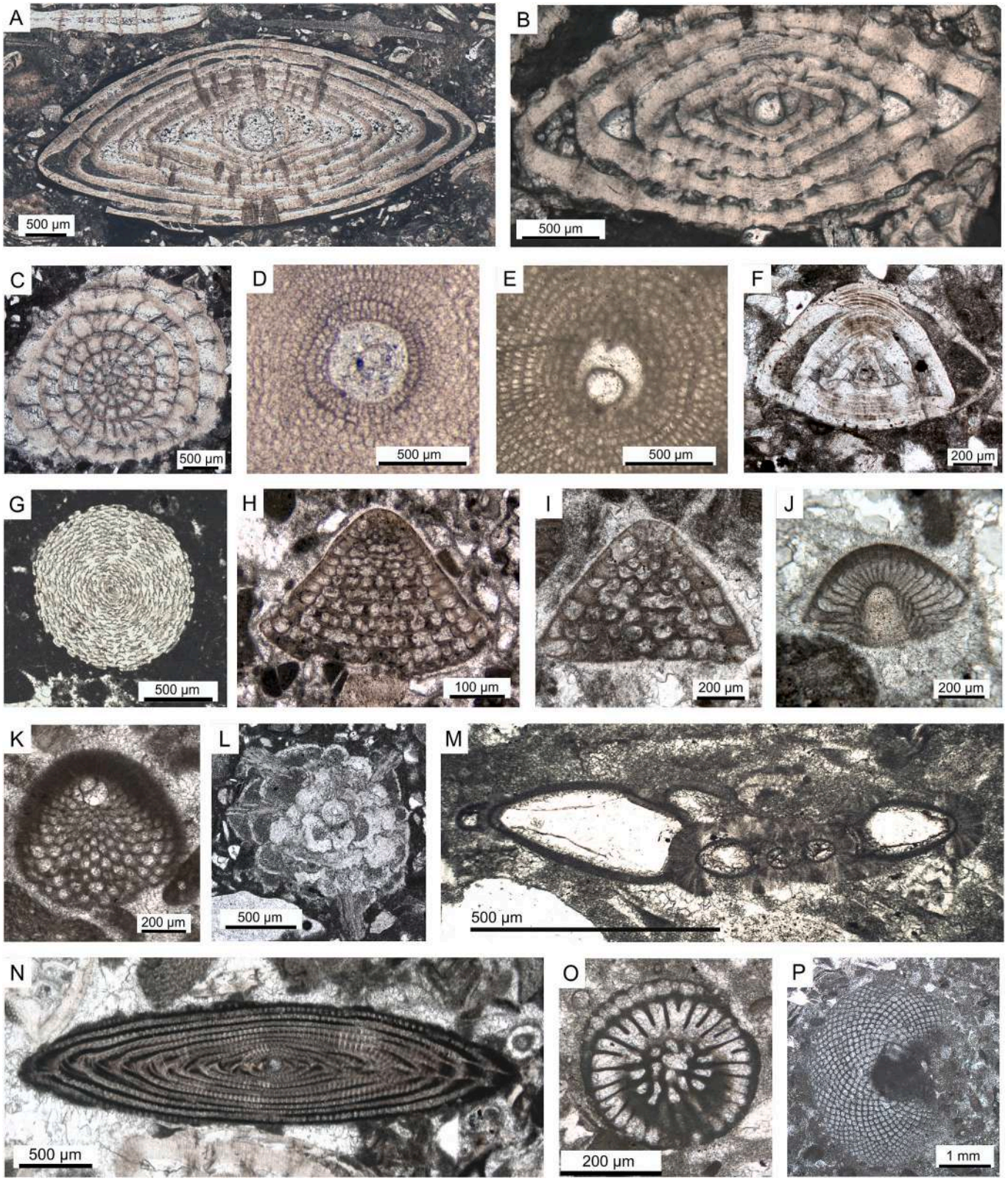


Fig. 11. Microphotographs of foraminifera present in the La Tossa Formation. (A) Axial section of *Nummulites biedai,* sample MRL-10. (B) Axial section of *Nummulites hormoensis,* sample TE-4. (C) Equatorial section of *Nummulites hormoensis,* sample PSM-3. (D) Equatorial section of *Orbitoclypeus varians varians*, sample TE-4. (E) Equatorial section of *Orbitoclypeus varians varians.,* sample MP-1. (F) *Asterigerina rotula,* sample TE-3. (G) Equatorial section of *Sphaerogypsina* sp., sample LE-2. (H) *Chapmanina gassinensis,* sample LE-5. (I) *Chapmanina gassinensis,* sample LE-5. (J) *Halkyardia minima,* sample LE-8. (K) *Halkyardia minima*, pseudo-equatorial section, sample LE-8. (L) Pseudo-equatorial section of *Silvestriella* sp., sample VF-13. (M) *Schlosserina asterites,* sample LE-8. (N) Axial section of *Glomalveolina ungaroi,* sample VF-13. (O) *Rhabdorites malatyaensis,* sample MB-13. (P) Tangential section of *Orbitolites* sp., sample PG-5. See Figs. 6–8 for the stratigraphic position of the samples.

4.2.3.1. Large Nummulites and Nummulites bank subfacies (N-NB). Two *Nummulites* banks have been identified in the Torre de l'Estrada and Puigsagordi sections (Figs. 7 and 8) (Acosta et al., in press). This subfacies is characterised by a rudstone texture in the central areas of the nummulitic assemblage, whereas a floatstone texture occurs along the periphery of the bank. Within the central area, the banks form marly limestone beds in the Torre de l'Estrada section (Fig. 7), and sandy limestone beds in the Puigsagordi section up to 1 m thick (Fig. 8). Notably, this facies lacks any observable sedimentary structure, and it typically exhibits a chaotic fabric of *Nummulites* tests (Fig. 12G). The central part of the banks is dominated by *Nummulites biedai* (54–65%), with variable proportions of *N. striatus* and *N. hormoensis*. The peripheral areas contain a more diverse assemblage including *N. incrassatus*, *N. chavannesi*, *N. cyrenaicus*, *N. vicaryi*, and *N. garnieri garnieri* (Acosta et al., in press). The benthic foraminiferal assemblage is further composed of *Assilina, Asterocyclina*, *Orbitoclypeus*, *Discocyclina*, *Acervulina*, *Asterigerina,* and *Gypsina*, as well as coral, bryozoans and echinoid fragments. These deposits change laterally to small *Nummulites* (N-SN) subfacies, whereas vertically pass into the cluster-reef (C-CR) subfacies (e.g., Torre de l'Estrada and Via Ferrada sections).

4.2.3.2. Small Nummulites subfacies (N-SN). The subfacies consists of siliciclastic-influenced limestones that display a nodular, wavy, and locally, cross-bedding, with packstone to grainstone textures dominated by small *Nummulites* (Fig. 12H). This subfacies forms beds up to 4 m-thick, in which the *Nummulites* tests are small, <5 mm in diameter, and in some sections (Morro de Porc, Pantà de Santa Maria; Fig. 6) they are imbricated. Other larger foraminifera present are *Assilina, Discocyclina, Orbitoclypeus* and *Glomalveolina*. Locally, *Fabiania, Halkyardia*, small rotaliids, and textulariids are present, along with fragments of coralline algae, echinoids, gastropods, and bivalves. The subfacies evolves vertically into the cluster-reef (C-CR) subfacies (e.g., Morro de Porc section).

4.2.4. Coral Facies (C)

This facies consists of scleractinian-rich deposits exhibiting floatstone, rudstone and boundstone textures. It has been subdivided into two subfacies based on the internal architecture and composition of the reefal buildups.

4.2.4.1. Cluster-reef subfacies (C-CR). The subfacies is mainly composed of sheet-like and branching coral colonies, exhibiting a loose and unbound growth fabric with a mixstone style. These coral-bearing deposits include a clay-marl matrix, and reach an approximate thickness of up to 3 m (Figs. 13A, C and F). The lithological contrast between the corals and the fine-grained matrix results in a distinctive nodular stratification. In this structure, the nodules correspond to individual coral colonies ranging from 5 to 30 cm in diameter. According to Taberner and Bosence (1995), *Astreopora, Cereiphyllia* and *Goniopora* coral genera are present in the Morro de Porc area (Figs. 2, 6 and 13A). The skeletal assemblage also includes larger foraminifera such as *Asterocyclina*, *Orbitoclypeus* and scarce *Nummulites.* Textulariid foraminifera, as well as serpulids, and bryozoans, characterised by branched cyclostomes forms, occur. Locally

Table 2
Summary table of the facies and subfacies types, including lithology, sedimentary features and components.

	Facies/Subfacies	Lithology and sedimentary features	Components
SC	Sandstone and conglomerate	Medium- to coarse-grained quartz sandstones, and polymictic clast-supported conglomerates. Tabular bedding and wavy laminations	Bioturbated horizons with *Thalassinoides*
SCC	*Campanile* subfacies	Medium- to coarse-grained quartz sandstones, interbedded with microconglomerate layers. Nodular bedding	Main components: *Campanile* gastropods. Other components: acervulinids, *Fabiania, Nummulites*, bivalves, echinoids, non-geniculated coralline algae, and bryozoans
AS	Acervulinid subfacies	Medium- to fine-grained quartz sandstones. Locally exhibit cross-stratification and lamination	Main components: *Acervulina, Solenomeris, Gypsina*, and victoriellids. Other components: *Nummulites*, miliolids, geniculate coralline algae, bivalves, gastropods, echinoids, serpulids and bryozoans
P	Porcelaneous foraminifera	Limestones with packstone to grainstone textures. Nodular to tabular bedding	Main components: miliolids, *Orbitolites*, *Rhabdorites*, *Nummulites, Asterigerina*, acervulinids. Other components: geniculate coralline algae and coralline detritus.
N-NB	Large *Nummulites* and *Nummulites* bank subfacies	Marly limestones to sandy limestones	Main components: *Nummulites biedai, N. striatus and N. hormoensis.* Other components: *N. cyrenaicus, N. chavannesi, N. garnieri garnieri, N. vicaryi, Assilina schwageri, Asterocyclina, Orbitoclypeus, Acervulina, Asterigerina, Gypsina,* corals, bryozoans and echinoids.
N-SN	Small *Nummulites* subfacies	Sandy limestones with packstone to grainstone textures. Nodular, wavy and locally cross-bedding	Main components: *Nummulites, Assilina, Discocyclina, Orbitoclypeus* and *Glomalveolina.* Other components: *Fabiania, Halkyardia*, small rotallids, textulariids, coralline algae, echinoids, gastropods and bivalves.
C-CR	Cluster-reef subfacies	Unbound growth fabric with a mixstone style	Main components: coral colonies, *Asterocyclina, Orbitoclypeus* and *Nummulites.* Other components: Textulariids, serpulids, and bryozoans.
C-FR	Frame-reef subfacies	Bound growth fabric with a mixstone style	Main components: coral colonies mainly poritids, and coralline algae. Other components: *Nummulites*, miliolids, bivalves, bryozoans and echinoids.
FA	Foraminifera- Coralline algae	Limestones with rudstone to bindstone texture	Main components: coralline algae branches, crusts and rhodoliths, coral colonies and encrusting foraminifera. Secondary components: Bryozoans, echinoids and bivalve fragments. Foraminifera: *Fabiania, Gyroidinella, Sphaerogypsina, Haddonia, Planorbulina, Gypsina,* victoriellids, small *Nummulites, Assilina, Chapmanina*, textulariids, and miliolids.
MR	Maërl	Limestones with a packstone texture	Main components: coralline algae branches, small rhodoliths, and encrusting foraminifera. Secondary components: *Nummulites*, miliolids, echinoids, bivalves and bryozoans.
OM	Orthophragmine	Marly-limestones with a packstone texture	Main components: *Discocyclina, Orbitoclypeus, Asterocyclina* and *Assilina.* Other components: *Nummulites*, *Heterostegina*, bivalves and bryozoans.
BM	Bryozoans	Greyish-blue marls	Main components: branching bryozoans. Other components: Bivalves, gastropods, solitary corals, orthophragmines, and *Nummulites.*
B-BS	*Smittina* subfacies	Marls	Main components: *Smittina.* Other components: Solitary corals, gastropods, oysters and pectinids.
M	Marl	Ochre marls to silts. Parallel laminations	*Kuphus*, colonial and solitary corals, and other small bivalves.

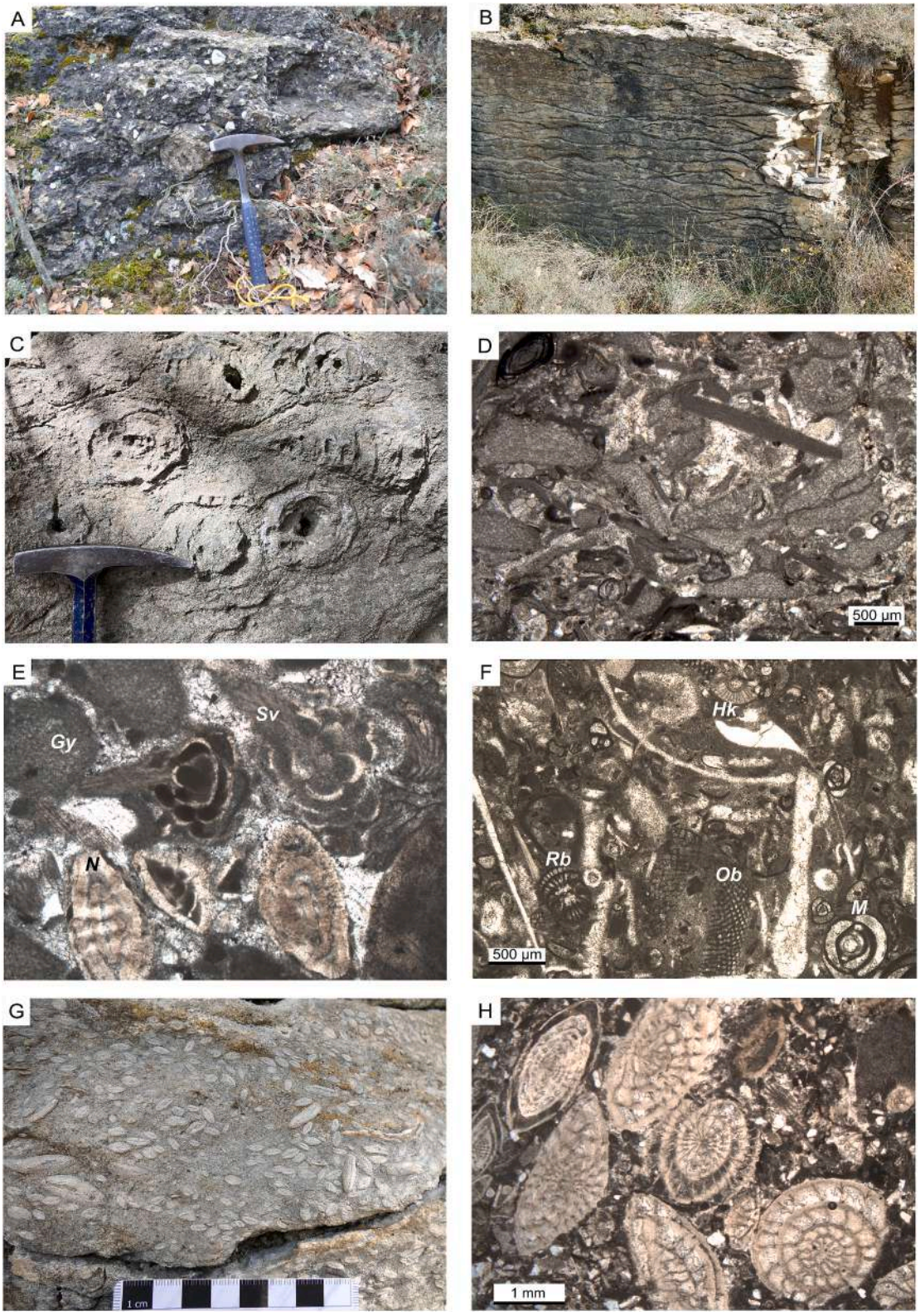


Fig. 12. Detailed view of the facies types. (A–B) Sandstone and conglomerate facies (SC) (A) Conglomerates exposed laterally to the Maërl section. (B) Nodular-wavy bedding in the sandstone facies at the 5 Pins section. (C) *Campanile* sandstone subfacies (SCC), south of the 5 Pins section. (D) Acervulinid and encrusting foraminifera subfacies (AS), packstone to grainstone texture, sample MRL-3. (E) *Silvestriella* specimens occurring in the acervulinids subfacies (AS), sample PSM-14. Grainstone texture with presence of *Nummulites* sp. and *Gypsina* sp., sample PSM-14. (F) Porcelaneous foraminifera facies (P), including miliolids, *Orbitolites*, *Halkyardia* and *Rhabdorites* specimens in a packstone to grainstone texture, sample MB-12. (G) Large *Nummulites* and *Nummulites* bank subfacies (N-NB) at Puigsagordi section; the dominant species is *N. biedai*. (H) Small *Nummulites* subfacies (N-SN), sample ZA-2. See Figs. 6–8 for the stratigraphic position of the samples. *(Gy) Gypsina*, *(Hk) Halkyardia*, *(M)* miliolids, *(N) Nummulites*, *(Ob) Orbitolites*, *(Rb) Rhabdorites*, *(Sv) Silvestriella*.

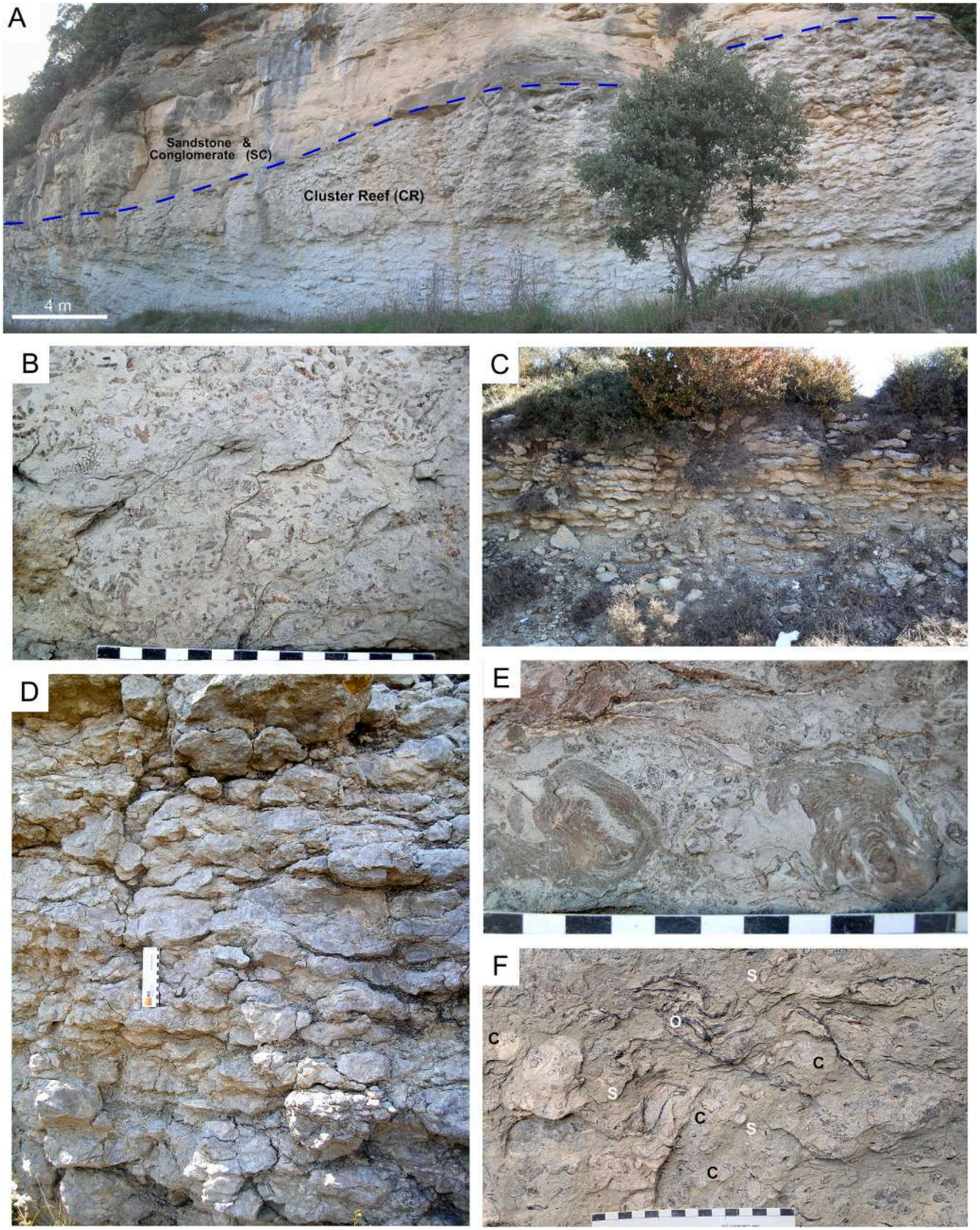


Fig. 13. General and detailed outcrop views of the Cluster-reef (C-CR) and Frame-reef (C-FR) subfacies. (A) Sandstone and conglomerate (SC) facies and their contact with the Cluster-reef facies marked by a dashed line at the Morro de Porc (MP) locality. (B) Close-up view of branching coral forms. (C) Cluster-reef buildup at the Torre de l'Estrada section. (D) Frame-reef subfacies (C-FR) at the Línia Elèctrica section. (E) Coral colonies (cf. *Actinacis*) embedded in a micritic matrix at the Línia Elèctrica frame reef. (F) Serpulids (S), corals (C), and ostreids (O) from the Via Ferrada section. Scale bars in cm.

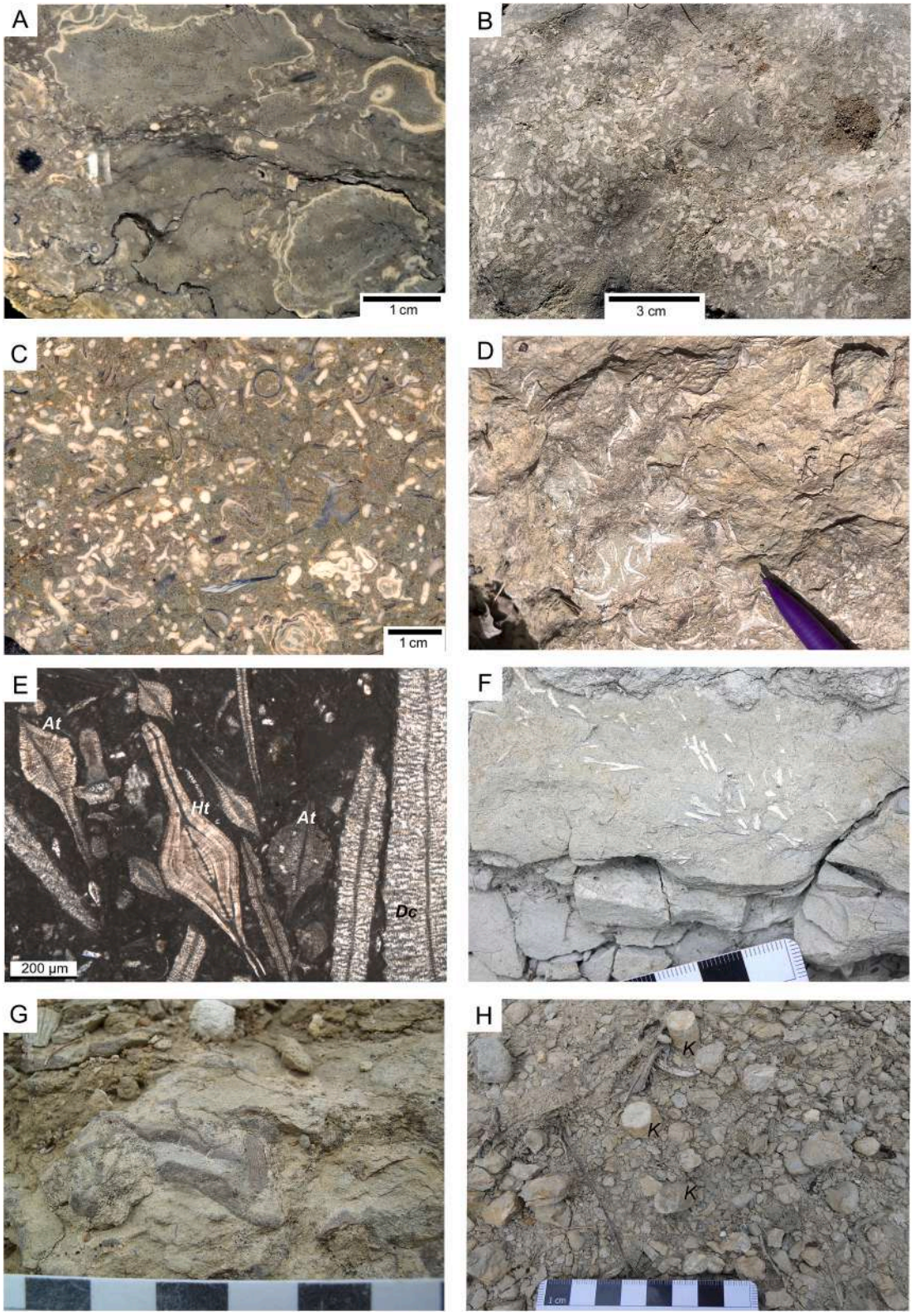


Fig. 14. Microphotographs and detailed outcrop views of facies types. (A) Foraminifera-Coralline algae facies (FA), showing crustose coralline algae white veneers growing on coral colonies at Torre de l'Estrada section. (B) Field photograph of Maërl facies at Via Ferrada section. (C) Polished slab showing Maërl facies with rhodoliths from the Via Ferrada section. (D) Orthophragmine marls (OM) exhibiting saddle-shape *Discocyclina* specimens at the Collsuspina section. (E) Orthophragmine facies (OM), with *Asterocyclina* (*At*), *Discocyclina* (*Dc*) and *Heterostegina* (*Ht*), sample CLP-1. (F) Bryozoan facies (BM), cyclostome branching colonies embedded in blue marls, at Via Ferrada section. (G) *Smittina* subfacies (B-BS) at Pantà de Santa Maria section. (H) *Kuphus*-bearing ochre marls. Note the preservation of *Kuphus* (*K*) specimens in life position, Torre de l'Estrada section. See Figs. 6–8 for the stratigraphic position of the samples.

(e.g., in the Via Ferrada section), corals are scarce and occur associated with serpulids and oysters, such as *Pycnodonte* (Fig. 13 F). Laterally, the cluster coral reef subfacies passes into marls (M) (e.g., Coll de Prims).

4.2.4.2. Frame-reef subfacies (C-FR). This subfacies is characterised by a diverse range of coral growth forms, up to 20 cm in diameter, which transition roughly upward from sheet-like and domal morphologies at the base of the buildups to branching forms at the top. The most common growth forms are branching colonies, mainly poritids (cf. *Actinacis*), which serve as substrates for coralline algal encrustations (Fig. 13E). Mancini et al. (2025) reported the occurrence of *Ellipsocoenia* and *Caulastrea* forming coral buildups in the Sant Martí Xic Formation in the Vic sub-basin. These coral reefs exhibit a more rigid and bound growth fabric (Fig. 13D) than that of the cluster-reef subfacies, giving rise to a mixstone that includes a micritic matrix. The frame-reef beds attain a thickness up to 6 to 8 m. Coralline algae are abundant, whereas the foraminiferal assemblage is diverse but generally sparse. Larger foraminifera, such as *Nummulites* and fragments of *Discocyclina* are present in minor quantities. Moreover, smaller benthic foraminifera include miliolids and textulariids. Brachiopods, echinoids, pectinids, bryozoans, and oysters, locally forming monospecific banks, as well as turritellid gastropods, are also present. Upwards, this subfacies evolves into porcelaneous foraminifera (P) and foraminifera-coralline algae (FA) facies (e.g., Línia Elèctrica) or is overlain by marls (M).

4.2.5. Foraminifera-Coralline algae Facies (FA)

This facies is constituted by coralline algal branches, as well as coral colonies, encrusted by coralline algae and foraminifera. The texture ranges from rudstone to bindstone, and the facies reaches an approximate thickness of 1.5 to 2 m. The coralline crusts grew mainly on coral colonies (Fig. 14A) but are also found encrusting other bioclastic components. Rhodoliths up to 4 cm in diameter are also common. They are embedded in a packstone-grainstone bioclastic matrix. Limestones are highly cemented precluding to dig isolated rhodoliths to describe their external morphology using ternary diagrams (see e.g., Bosence, 1976, 1983). In section, they are spheroidal to ellipsoidal in shape. Rhodoliths show distinct nuclei, made up mostly of coralline algal fragments and larger foraminifera, or are unnucleated. The inner arrangement of rhodoliths is characterised by encrusting, warty and fruticose plants intergrowing with encrusting benthic foraminifera, bryozoans and serpulids. Numerous primary voids are observed among algal thalli. Borings by lithophagid bivalves (*Gastrochaenolithes*) and sponges (*Entobia*) are frequent. The foraminiferal assemblage is dominated by encrusting forms, as well as by small nummulitids, miliolids, acervulinids, *Fabiania*, *Chapmanina*, rotaliids and small textulariids. Echinoid fragments, bivalves and bryozoans are scarce. Laterally, this facies transition into the maërl (MR) facies (e.g., Zona d'Acampada and Maërl sections).

4.2.6. Maërl Facies (MR)

This facies is characterised by the abundance of isolated branches of coralline algae embedded in a packstone bioclastic matrix (Fig. 14B and C). Algae occur as single branches or showing dichotomous divisions pristinely preserved. They reach up to 2.5 cm in length and 4 mm in diameter. The branches are often encrusted by laminar thalli of coralline algae and by encrusting foraminifera. Small rhodoliths, up to 1.5 cm in diameter, also occur. They can present a distinctive nucleus, mostly a coralline algal branch or a larger foraminifer. Sometimes, the nucleus is not obvious. Most rhodoliths are formed by the intergrow of coralline algae with encrusting foraminifera, bryozoans and serpulids. Coralline algae show laminar and encrusting growth forms with occasional warty and fruticose protuberances. The foraminiferal assemblage is represented by encrusting foraminifera such as *Acervulina, Gypsina, Solenomeris*, *Fabiania, Haddonia,* and victoriellids. *Nummulites,* miliolids, and textulariids were also observed. Echinoid fragments, bivalves, and bryozoans are minor constituents.

4.2.7. Orthophragmine Facies (OM)

This facies is characterised by the dominance of orthophragmines embedded within a silty-marly matrix, locally forming cm-thick limestone layers with a packstone texture (Figs. 14D and E). This facies exhibits a thickness ranging from 3 to 5 m in certain sections (Fig. 8). The fabric consists of densely packed orthophragmine tests (constituting over 70% of the rock) that, in some instances (Collsuspina and Via Ferrada sections; Fig. 8), are imbricated or show a preferred orientation parallel to the stratification. Orthophragmines identified include *Discocyclina*, *Asterocyclina* and *Orbitoclypeus*. Specimens of small *Nummulites,* and *Assilina* are also common, along with other rotaliids present in certain samples. Additionally, channelised structures and occasional slump deposits have been observed in certain sections (Fig. 8). The skeletal assemblage also includes fragments of bryozoans, pectinids, echinoids, and oysters. Vertically, this facies changes to the cluster-reef subfacies (e.g., Via Ferrada and Morro de Porc), whereas laterally, it transitions into the marl (M) facies.

4.2.8. Bryozoan facies (BM)

The Bryozoan Facies is characterised by a diverse bryozoan assemblage, dominated by branching cyclostomes along with robust, bilaminar cheilostome forms embedded within a marly matrix (Fig. 14F). It forms centimetre- to decimetre-thick marly beds exhibiting greyish-blue to ochre colorations. Other macrofossils include pectinids, gastropods, and rare solitary branching corals. The foraminiferal assemblage is mainly represented by orthophragmines, *Assilina* and sparse *Nummulites*; in some instances, smaller benthic rotaliid foraminifera are also observed.

4.2.8.1. Smittina subfacies (B-BS). A distinct subfacies is defined by the dominance of the bryozoan genus *Smittina* (Fig. 14G). These colonies can reach up to 3–5 cm in length and occur embedded within a marly matrix, forming packages up to 5 m in thickness. At the localities of Orís and Serratosa, in the northern part of the Vic sub-basin (Fig. 1B), specimens up to 20 cm in length have been documented (Serra-Kiel and Reguant, 1991). This subfacies is locally associated with orthophragmines and *Assilina*. However, distinct horizons have been identified in which foraminifera are absent, and bryozoans are the exclusive dominant component. Additional constituents include fragments of solitary corals, as well as occasional gastropods, oysters and pectinids. Together with the branching-bryozoan facies, this subfacies passes upwards into the marl (M) facies (Pantà de Santa Maria section) and the orthophragmine (OM) facies (Via Ferrada section).

4.2.9. Marl facies (M)

Ochre marls to silts facies, with a variable thickness of approximately 1 to 3 m. These deposits are roughly laminated in some sections (e.g., Zona d'Acampada; Figs. 5 and 6), whereas in the Pantà de Santa Maria section (Fig. 6) they are structureless. They lack fossil content.

In association with this facies, greyish-ochre marl deposits are documented in Maërl and Via Ferrada sections. They occur in beds 2 to 3 m thick, locally interbedded with centimetre-thick sandstone layers (Fig. 14H). Although the faunal content is generally scarce, specimens of *Kuphus* have been recorded, together with colonial and solitary corals preserved in life position, serpulids and other small bivalves.

4.3. Facies architecture

In the Centelles area, the La Tossa Formation records three distinct depositional regimes: i) a siliciclastic interval, constituted by the fossil-barren sandstone body of the Centelles Sandstone, ii) a mixed-siliciclastic-carbonate interval, documented as the transitional unit, and iii) a carbonate-dominated interval represented by the Collsuspina Limestone (Figs. 4 and 5). This study focuses on the mixed and carbonate-dominated intervals in order to constrain the evolution and

depositional dynamics of the upper part of the formation. To determine the facies architecture of this depositional system, seven representative stratigraphic logs have been selected along a south-to-north transect: Coll de Prims, Morro de Porc, Zona d'Acampada, Torre de l'Estrada-Maërl, Via Ferrada, Puigsagordi, and Línia Elèctrica (Fig. 15). The studied succession exhibits recurring lithological and facies associations that have been grouped into seven stratigraphic cycles (I-VII).

These stratigraphic cycles are defined on the basis of repetitive vertical stacking patterns rather than on regionally traceable sequence-stratigraphic surfaces. Typically, each cycle comprises a relatively carbonate-rich interval, followed by deposits showing greater siliciclastic influence (Fig. 15). The repeated stacking of these contrasting

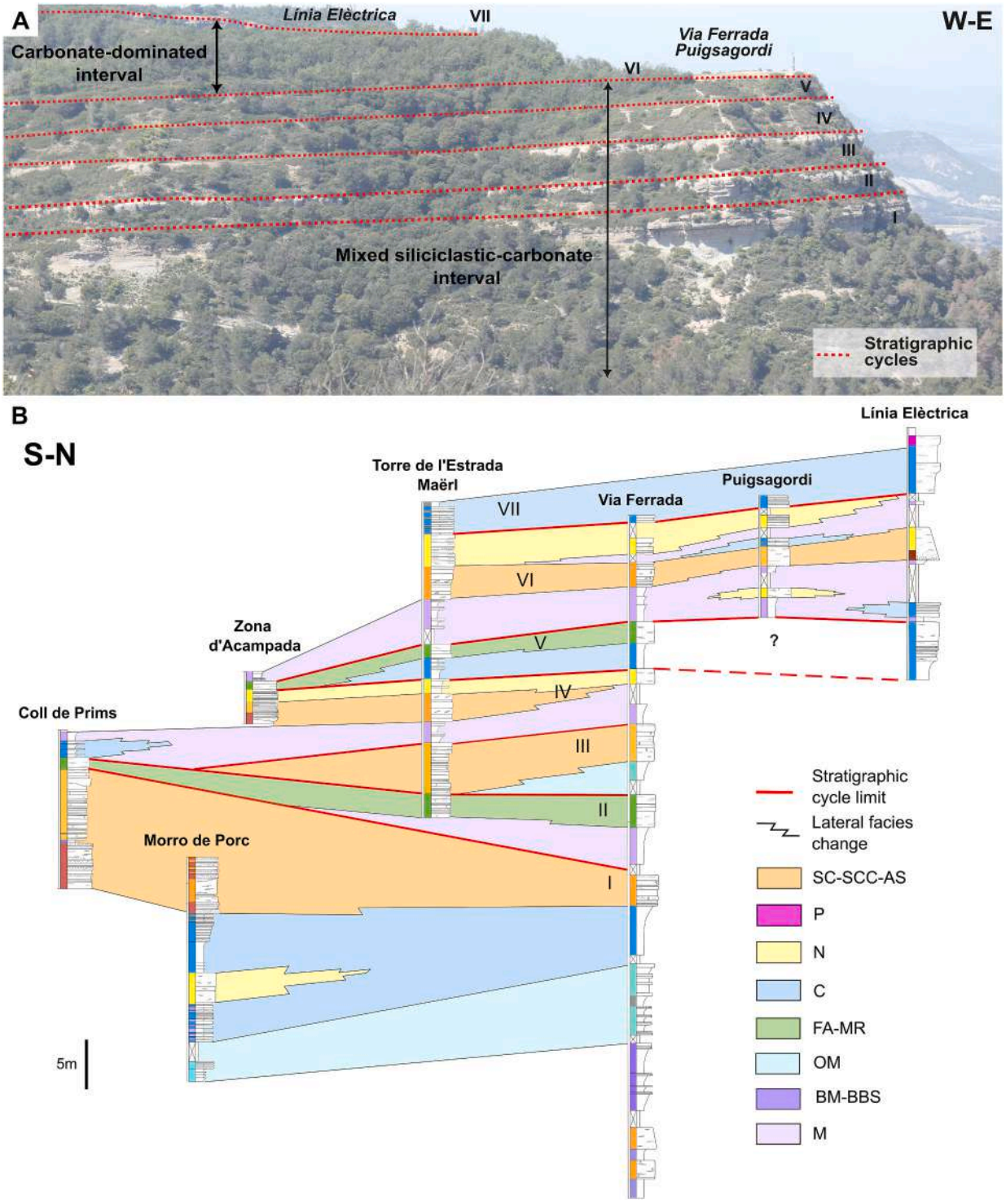


Fig. 15. A) West-to-east panoramic view of the Via Ferrada, Puigsagordi, and Línia Elèctrica sections, showing the distinction between the carbonate, and the mixed siliciclastic-carbonate intervals along with the seven stratigraphic cycles delineated by red dashed lines. (B) South-to-north correlation panel of the Coll de Prims, Morro de Porc, Zona d'Acampada, Maërl and Torre de l'Estrada, Via Ferrada, Puigsagordi, and Línia Elèctrica sections, showing the stratigraphic cycles and facies types. SC-SCC-AS = Sandstone and Conglomerate facies, *Campanile* subfacies and Acervulinid subfacies, N = *Nummulites* facies, C = Coral facies, FA-MR = Foraminifera-Coralline algae and Maërl facies, OM = Orthophragmine facies, BM-BBS = Bryozoan facies and *Smittina* subfacies, and M = Marl facies.

facies associations generate a distinctive lithological cyclicity throughout the Transitional interval of the La Tossa Formation. Accordingly, the term cycle is used here in a descriptive lithological and sedimentological sense to denote recurrent fluctuations in the ratio of carbonate production and terrigenous input during sedimentation, without implying a formal sequence-stratigraphic hierarchy.

The mixed siliciclastic-carbonate interval dominates the southern part of the study area, particularly in the Coll de Prims, Morro de Porc, Zona d'Acampada, Maërl, Torre de l'Estrada, and Via Ferrada sections (Figs. 2, and 6–8). This mixed domain occurs in stratigraphic cycles I, III, IV, and VI and is characterised by a facies belt containing at its base the distalmost facies, represented by marls (M) together with the cluster-reef subfacies (C-CR) in Coll de Prims section and the orthophragmine facies (OM) in the Morro de Porc and Via Ferrada sections. The Via Ferrada section exhibits the bryozoan facies (BM), and notably *Smittina*-bearing layers (B-BS) which reach thicknesses of up to 6 m (Figs. 6 and 8). In the Coll de Prims, Morro de Porc, and Via Ferrada sections, these facies progressively evolve into alternations of sandstone beds and clast-supported conglomerates (SC), which are overlain by the *Campanile* (SCC) and acervulinid (AS) subfacies (Fig. 15).

The stratigraphic cycle III shows the lateral evolution of these siliciclastic facies belt into the Marl facies (M), and their vertical transition into the small *Nummulites* subfacies (N-SN) in the Zona d'Acampada, Maërl and Via Ferrada sections. In the Torre de l'Estrada and Puigsagordi sections, *Nummulites* bank subfacies (N-NB) are locally developed (Figs. 7 and 8). The *Nummulites* (N) facies are vertically succeeded by nodular, coral-bearing sandy limestones that define a cluster-reef build-up in the stratigraphic cycle V, specifically at the Torre de l'Estrada section. Capping the coral beds, the Marl facies (M) were deposited, as observed in the Maërl section, where they do not exceed two metres in thickness. Locally, in the Pantà de Santa Maria and Torre de l'Estrada sections, the Foraminifera-Coralline algae facies (FA) occur at the base of the coral layers, constituting a relatively calcareous deposit characterised by low siliciclastic content and a sparse benthic foraminiferal assemblage. Within this facies belt, two episodes of Maërl (MR) facies are intercalated, corresponding to the stratigraphic cycles II and V. These two maërl levels extend from proximal zones, where they overlie the *Campanile* sandstones (SCC) in the Coll de Prims section, to distal zones in the Via Ferrada section, where they overlie the Orthophragmine facies (OM).

The carbonate deposits dominate the northern part of the area, specifically in the upper part of the Via Ferrada section, as well as in the Puigsagordi, Línia Elèctrica, La Creu and Collsuspina sections, where they constitute the stratigraphic cycle VII. In its most proximal domain, the sequence begins with Porcelaneous foraminifera-rich facies (P), which laterally grade into coral Frame-reef subfacies (C-FR), associated with Foraminifera-Coralline algae facies (FA). In the La Creu section (Fig. 8), the P, FR, and FA facies attain 6 to 8 m in thickness and are locally dolomitised, preserving a fabric-retentive texture in which skeletal components remain recognisable. In the Collsuspina section, these latter facies grade basinwards into marls and marly limestones rich in orthophragmines (OM), which vertically evolve into dm-thick gypsum layers belonging to the "Terminal Complex" (Travé, 1992; Travé et al., 1996), exposed along the road N-141c to Collsuspina (Fig. 2).

The palaeogeographic setting of the Centelles area corresponds to the northern flank of a palaeohigh (Taberner et al., 1999; Waltham et al., 2000). Here, the facies belts are narrower than in other parts of the basin, and lateral facies changes can be observed over distances of a few hundred metres. For example, the *Nummulites* banks extend for a few hundred metres in the Centelles area (Torre de l'Estrada and Puigsagordi sections), whereas in Sant Martí Xic, located in the central part of the sub-basin (Fig. 3), they reach lateral extents of about 3 km (Fig. 3; see Franquès, 1996; Acosta et al., in press).

5. Discussion

5.1. Depositional models and facies interpretation

The studied sedimentary succession exhibits a consistent regional strike and dip of 058/10 NW. No significant lateral thickness variations were observed, or were any geological bodies identified that could have functioned as high-relief topographic barriers separating a platform top from a slope. The lack of a marked slope break and the gradual lateral facies transitions suggest a low-gradient depositional profile (Fig. 16). Consequently, and given the presence of coarse siliciclastic deposits in the proximal areas, the studied mixed siliciclastic-carbonate system is interpreted as an attached homoclinal ramp. This interpretation aligns with established models and examples for Paleogene carbonate systems found in the literature (Bassi, 1998; Tomassetti et al., 2016; Rusciadelli and Shiner, 2018; Brandano and Tomassetti, 2020; Coletti et al., 2021; Briguglio et al., 2024; Gandolfi et al., 2025; Giraldo-Gómez et al., 2025).

Several schemes for classifying carbonate ramps have been proposed based on differing water depth criteria (Buxton and Pedley, 1989; Burchette and Wright, 1992; Somerville and Strogen, 1992). These classifications recognise two key interfaces; a fair-weather wave base (FWWB) and a storm wave base (SWB), where their boundaries vary according to the palaeogeography, palaeotopography, local hydrodynamic and climatic conditions, leaving identifiable sedimentary structures in the rock record. On this basis, Burchette and Wright (1992) proposed four carbonate ramp subdivisions: inner ramp, mid-ramp, outer-ramp and basin. These subdivisions carry significant sedimentological implications, as they require the recognition of the FWWB and SWB boundaries in the field through diagnostic sedimentary features. The rocks in the study area show little to no evidence of hydrodynamic structures precluding the use of these interfaces. Consequently, the classification model by Burchette and Wright (1992) is not considered suitable for the current study. Moreover, while this scheme relies on physical factors related to hydrodynamic energy and allows a relatively precise depth-based subdivision of the ramp, the distribution of the principal carbonate-producing organisms, such as hermatypic corals and larger foraminifera, is largely governed by light availability. As light penetration depends not only on water depth but also on water transparency, biological distributions cannot be directly linked to the hydrodynamic zonation proposed for carbonate ramps.

Different ramp zonation models for Eocene carbonate platforms have been proposed in the literature, correlating the distribution of larger foraminifera with water depth and photic conditions. A representative model is that of Hallock and Glenn (1986), which outlines a generalised distribution pattern for larger foraminifera. According to this model, flat and thin rotaliids including *Assilina, Operculina* and orthophragmines are indicative of lower photic zone assemblages. In contrast, thick and robust nummulitids and amphisteginids predominate in middle-platform environments, especially closer to the inner platform. In shallower, more restricted settings, miliolids, alveolinids and soritids become the dominant fauna (Greiner, 1969; Murray, 1973). In the Eocene of the Igualada sub-basin Romero et al. (2002) identified protected, barrier, and open platform settings, whereas Caus and Serra-Kiel (1984) proposed a subdivision consisting of a lagoon, a protected and restricted platform, a reef, and an open platform. Within these schemes, alveolinids, soritids and miliolids are characteristic of low-energy, restricted-platform settings. Acervulinids are associated with reefal and higher-energy environments (Romero et al., 2002), whereas *Nummulites* exhibit a broad environmental range, occurring from protected-platform to open platform settings, with *Nummulites* banks typically developing in intermediate environments. Orthophragmines, together with *Operculina, Assilina, Heterostegina*, and planktonic foraminifera, are generally regarded as indicators of open-platform conditions.

These interpretations should nevertheless be regarded as indicative, as the ecological distribution of larger foraminifera varies between carbonate platforms. Their depth distribution is mainly controlled by the

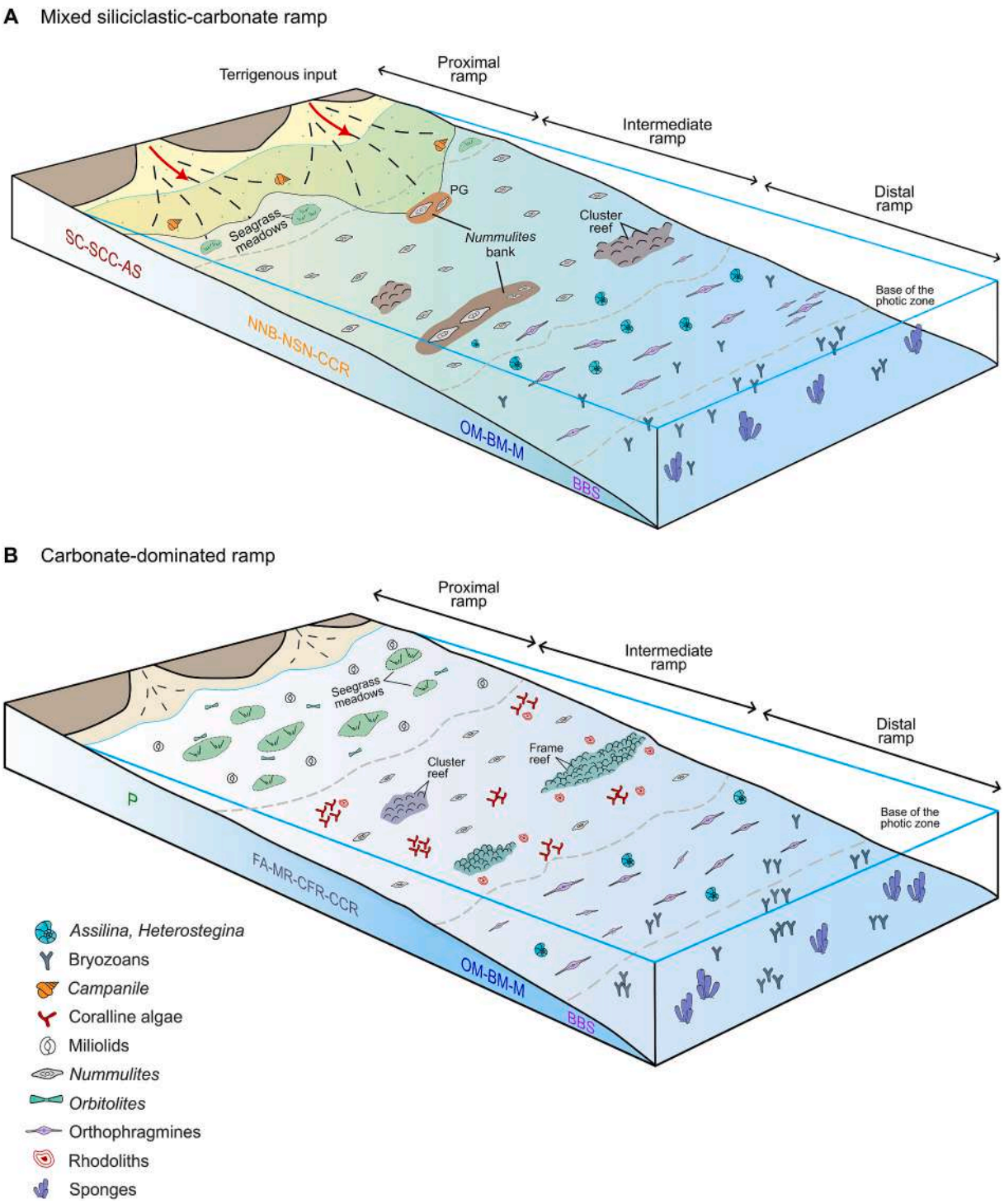


Fig. 16. (A) Not-to-scale palaeoenvironmental model for the mixed siliciclastic-carbonate ramp, including the proximal, intermediate, and distal zones of the ramp, as well as the lower limit of the photic zone. (PG) Puigsagordi, and (TE) Torre de l'Estrada *Nummulites* banks. (B) Not-to-scale palaeoenvironmental model for the carbonate-dominated ramp. SC-SCC-AS = Sandstone and conglomerate facies, *Campanile* and Acervulinid subfacies, NNB-NSN = Large *Nummulites* and *Nummulites* bank subfacies and Small *Nummulites* subfacies, CCR-CFR = Cluster reef and Frame reef subfacies, FA-MR = Foraminifera-Coralline algae and Maërl facies, OM = Orthophragmine facies, BBM-BBS = Bryozoan facies, and *Smittina* subfacies, and M = Marl facies.

light requirements of their algal symbionts (e.g., Reiss and Hottinger, 1984), as well as by substrate conditions and water turbidity. Consequently, the same species may occupy different depth ranges in different environmental settings, and thus, larger foraminiferal assemblages cannot always be translated directly into absolute water depths.

Romero and Caus (2000) developed a model for the depth distribution of Bartonian–Priabonian larger foraminiferal genera in the Igualada sub-basin. They divided the photic zone (up to 60 m depth) into an upper zone and a lower zone, each one further subdivided into upper and lower parts, where they located up to six assemblages of larger foraminifera. Similarly, Morsilli et al. (2012) and Pomar et al. (2017) used a zonation scheme of bathymetric zones related to light penetration, distinguishing the euphotic, mesophotic, oligophotic and aphotic zones. The transition from the euphotic to the oligophotic zone corresponds to depths at

which carbonate producers such as zooxanthellate corals and calcareous green algae disappear, giving way to an association dominated by coralline algae. Where skeletal components allow a finer bathymetric differentiation based on light conditions (e.g., in the case of corals), the mesophotic zone can also be distinguished. It is important to note that this zonation scheme may vary considerably as a function of water transparency and the adaptive traits of the mesophotic biota. For instance, according to Romero and Caus (2000), the photic zone in the Igualada area (Fig. 1) during the middle-late Eocene reached a depth of 60 m, whereas it extends to 130 m in the exceptionally transparent waters of the modern Gulf of Aqaba (Reiss and Hottinger, 1984).

Given this variability and the lack of conformity to a single or bathymetric model, together with the virtual absence of sedimentary structures or other indicators such as green algae, a purely spatial nomenclature has been adopted herein, subdividing the carbonate ramp into proximal, intermediate, and distal domains, regardless of physical parameters or sedimentary structures. This subdivision reflects the relative depositional depth of each facies with respect to the others, that is, whether a given facies was deposited in shallower or deeper conditions than adjacent ones, rather than absolute depth estimates. Each facies described above is hereafter ascribed to one of these three ramp environments based on lithology, fossil content, facies architecture (Fig. 15) and inferred relative water depth.

The alternation between mixed siliciclastic-carbonate and carbonate-dominated deposits resulted in two distinct depositional ramp models, each with a different facies architecture and spatial organisation. The mixed siliciclastic-carbonate-dominated model (Fig. 16A) reflects a ramp strongly conditioned by terrigenous input, which governs both the nature of the deposits and the distribution of carbonate producers. The carbonate-dominated model (Fig. 16B) developed under conditions of reduced siliciclastic supply, allowing carbonate production to prevail across the ramp from proximal to distal domains. These two models account for the lateral and vertical variability documented in the La Tossa Formation and offer an interpretive framework for the recurrent transitions between the two depositional regimes.

5.1.1. *Mixed siliciclastic-carbonate ramp*

The mixed siliciclastic-carbonate-dominated interval records deposition in a mixed siliciclastic-carbonate ramp system. Its most proximal domain is characterised by sandstone and conglomerate facies (SC), interpreted as fan-delta deposits (Fig. 16A). In this proximal setting, wave action effectively winnowed fine-grained material, while the remaining fraction was reworked and redistributed within a shoreface environment. The absence of sedimentary structures in the terrigenous layers may be attributed to a rapid deposition from mass-flow processes, which typically generate massive conglomerate and sandstone beds in fan-delta settings (e.g., Kazancı and Varol, 1990). In sandstones, the lack of visible cross-stratification or lamination may also result from textural homogeneity caused by a very uniform grain size.

Regarding the *Campanile* subfacies (SCC), Houbrick (1981) documented that members of the Campanilidae likely occupied an ecological niche in Tethyan marine ecosystems during the Palaeogene similar to that of extent Strombidae in contemporary habitats, acting as detritivores that fed on epiphytic algae inhabiting sandy patches at shallow depths (Figs. 12C, 16A). With respect to the sandstones rich in encrusting foraminifera (AS), acervulinids display a wide morphological diversity influenced by the substrate on which they are attached, often encrusting and adopting its shape (e.g., Ungaro, 1996). In particular, saddle- and hook-shaped forms are characteristic of shallow-marine settings associated with seagrass meadows and reefal barriers (Brasier, 1975; Tomassetti et al., 2016; Baceta and Mateu-Vicens, 2022; Morabito et al., 2024). Hook-shaped forms of gypsinids, as well as crustose coralline algae (Beavington-Penney and Racey, 2004; Mateu-Vicens et al., 2012) are commonly interpreted as having developed attached to seagrass leaves, thus providing evidence for the presence of vegetated substrates within the depositional system.

The intermediate ramp domain within this interval is recognisable from the Small *Nummulites* (N-SN) and the Large *Nummulites* and *Nummulites* banks (N-NB) subfacies. Nummulitids can be found at less than 30 m, but they predominate in mesophotic to oligophotic settings (> 30 m; see Hohenegger, 2005). The N-SN subfacies (Fig. 12H) represents a relatively high energy environment with a coarse substrate and terrigenous influence. The N-NB subfacies is characterised by the presence of large *Nummulites* species (*N. biedai, N. striatus*), which locally form banks (Torre de l'Estrada, Puigsagordi; Figs. 3 and 12G). The proportions of A- and B- forms, together with sedimentological and taphonomic features, indicate that these *Nummulites* banks represent autochthonous to slightly para-autochthonous deposits (Acosta et al., in press). *Nummulites* banks are commonly interpreted to have formed under optimal environmental conditions within intermediate to distal ramp settings (Hottinger, 1997; Bassi, 1998; Geel, 2000; Racey, 2001; Martín-Martín et al., 2021; Tosquella et al., 2022) (Fig. 16A). In the PG section, the *Nummulites* bank subfacies consists of a sandy limestone layer in which *Nummulites* are associated with *Acervulina linearis* and *Gypsina*, suggesting a relatively proximal-intermediate setting. In contrast, the *Nummulites* bank in the TE section is characterised by a marly-limestone assemblage with *Assilina* and orthophragmines, which indicates a distal-intermediate depositional environment (Acosta et al., in press).

The coral buildups observed in Centelles are dominated by *Actinacis* and small to medium-sized branched colonies (e.g. *Astreopora*) (Taberner and Bosence, 1995), which predominantly occur as cluster reefs assemblages (sensu Riding, 2002). This association may indicate deposition in deeper environments under moderate to high turbid waters (Sanders and Baron-Szabo, 2005; Lokier et al., 2009) (Fig. 16A). The abundance of clay and silt in the matrix, containing scattered orthophragmines and *Assilina*, together with the absence of other shallow-water components in the capping beds, likely place these buildups at relatively deep, low-energy settings within the intermediate to distal ramp domain. Comparable facies have been described in the Aínsa Basin, in the south-central Pyrenean zone (Morsilli et al., 2012), where reefal facies exhibit similar fossil associations. In that context, corals are embedded either in clayey or in a silty matrix and they also occur in the distal portions of deltaic systems.

The distal domain comprises the orthophragmine facies (OM), which indicates deposition in a relatively deep-water setting (Ćosović and Drobne, 1998; Tomassetti et al., 2016). Orthophragmines, in particular flat forms occurring in marls, are interpreted to inhabit in deeper waters, down to the limit of the photic zone (Fermont, 1982; Setiawan, 1983; Caus and Serra-Kiel, 1984; Teixell and Serra-Kiel, 1988; Geel, 2000; Hallock and Glenn, 1986; Less, 1987; Molina et al., 1988; Serra-Kiel et al., 1994; Racey, 2001). This interpretation is also indicated by the functional morphology of their tests (Ferràndez-Cañadell and Serra-Kiel, 1992) and is consistent with their association with flat nummulitids and planktic foraminifera. The dominance of flattened tests, together with the absence of coralline algae or proximal platform organisms suggest a deposition in a distal ramp setting (Fig. 16A).

The bryozoan facies (BM) is indicative of deeper and/or cooler environmental conditions (Rasser, 2000; Jaramillo-Vogel et al., 2016). The *Smittina* subfacies (B-BS) corresponds to the “Bryozoa protuberance facies” of Reguant et al. (1991), who interpreted it as the shallowest bryozoan facies, formed during intervals of low or no sedimentation. The absence of symbiotic-bearing organisms, such as larger foraminifera, suggests deposition below the photic zone. The vinculariiform (branching) bryozoan facies (Fig. 14F) is interpreted as representing a deeper depositional setting (Busquets et al., 1997). Farther north of Centelles, even deeper-water facies occur, including bryozoan mud mounds and hexactinellid sponges (Busquets et al., 1997; Pisera and Busquets, 2002; Serra-Kiel and Reguant, 1991; Serra-Kiel et al., 2003b; Reguant et al., 1991).

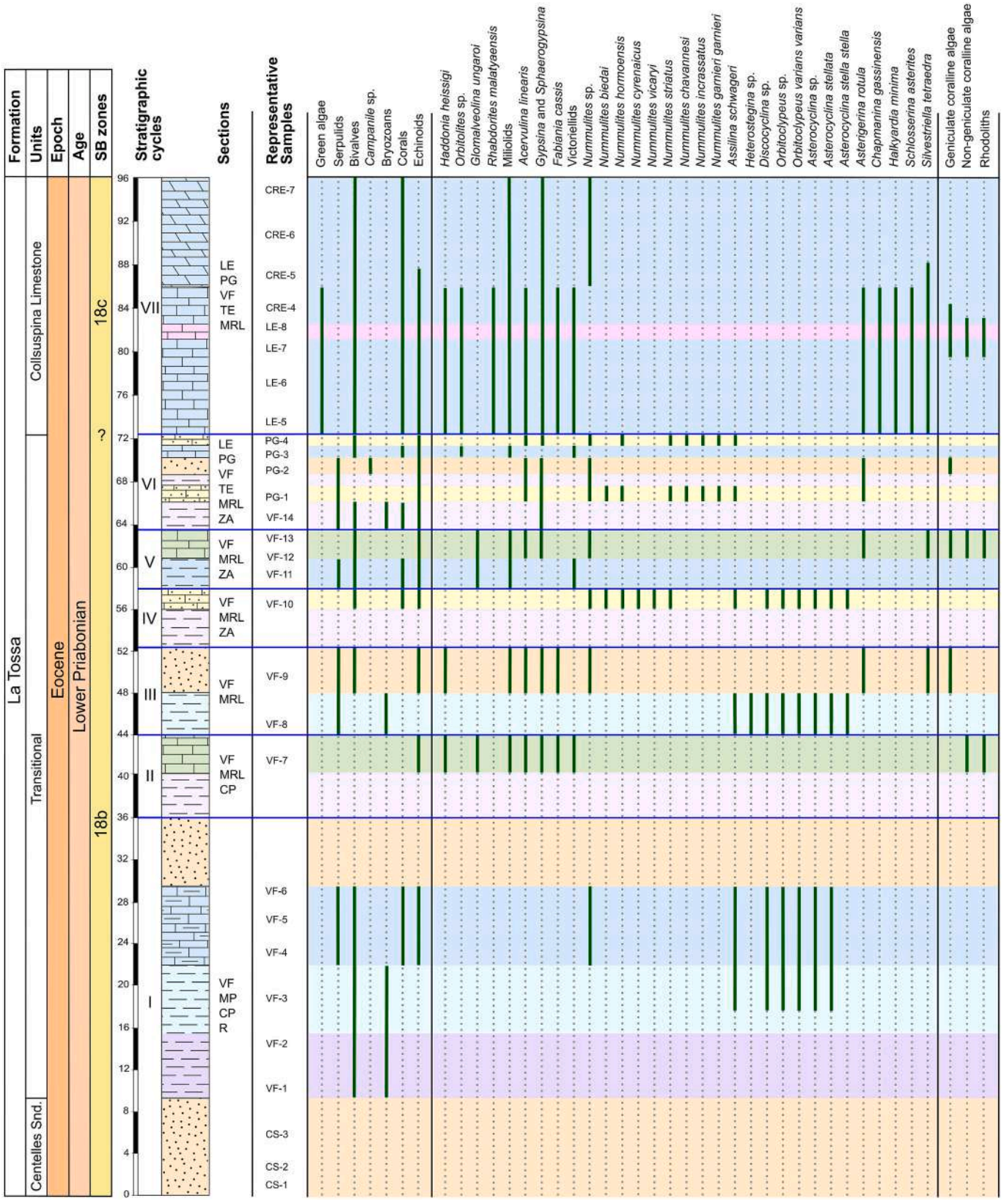


Fig. 17. Synthetic stratigraphic log of the studied succession displaying the stratigraphic cycles, with the distribution of the larger foraminifera, other key genera and species identified, and their correlation to the Shallow Benthic Zones (SB). See Fig. 8 for lithology key.

5.1.2. Carbonate-dominated ramp

The carbonate-dominated interval records deposition in a carbonate ramp system. The proximal domain of this ramp is characterised by abundant porcelaneous foraminifera including *Orbitolites*, *Glomalveolina*, *Rhabdorites*, miliolids, along with acervulinids, small rotaliids, and dasycladacean algae. The Porcelaneous foraminifera (P) facies indicates deposition in shallow-marine settings (Geel, 2000; Drobne et al., 2011; Tomassetti et al., 2016). Porcelaneous foraminifera are euryhaline organisms that inhabit in shallow marine waters (Brasier, 1975; Murray, 2006; Tomassetti et al., 2016). Similarly, dasycladaceans preferentially inhabited low latitude, shallow bays (Flügel, 1985; Aguirre and Riding, 2005; Aguirre et al., 2022). The occasional presence of geniculate coralline algae, which typically thrive in relatively high-energy intertidal settings (Scheibner et al., 2007; Brandano, 2017), further supports this interpretation. The occurrence of *Orbitolites* (Fig. 16B), an epiphytic foraminifer whose living relatives, *Sorites* and *Marginopora*, are specialised seagrass dwellers (Brasier, 1975; Beavington-Penney and Racey, 2004; Tomassetti et al., 2016), indicates tropical to temperate marine conditions characterised by the presence of marine vegetation, most likely seagrass meadows (Johnson, 1961; Brasier, 1975; Hottinger, 1997). Additional support for this interpretation is provided by the abundance of sirenian remains in the Vic and Igualada sub-basins (e.g., Pilleri et al., 1989; Balaguer and Alba, 2016), as well as in the Pamplona and Aínsa basins (Astibia et al., 2005, 2010). Together, these observations support the presence of seagrass meadows across parts of the South Pyrenean foreland basin during the Bartonian and early Priabonian.

The intermediate ramp environment exhibits the Maërl facies (MR), characterised by branches of unattached coralline algae. This setting is recognised by a high diversified coralline algal assemblage that includes members of the orders Hapalidiales, Sporolithales, and Corallinales. This facies generally lies below the deepest extent of seagrass meadows in both temperate and tropical settings (Nebelsick et al., 2005; Basso et al., 2008; Brandano and Tomassetti, 2020). The distal zones of the intermediate ramp are distinguished by thin crusts composed of coralline algae alternating with encrusting foraminiferal associations (FA). The occurrence of rhodoliths composed predominantly of Hapalidiales, Sporolithales, along with peyssonneliaceans, indicates relatively deep-water environments on the order of several tens of metres (Adey and Macintyre, 1973; Adey, 1979; Aguirre et al., 2000; Braga and Aguirre, 2001; Braga and Bassi, 2007; Aguirre et al., 2020; Aguirre et al., 2022). The fine-grained matrix and the good preservation of the rhodoliths, as well as the foraminiferal tests, with no evidence of significant reworking suggest a middle to intermediate ramp setting (Aguirre et al., 2022).

Contrarily to the mixed siliciclastic-carbonate interval (Fig. 16A), in the carbonate regime the coral facies form a denser and more compact buildup, characteristic of a "frame-reef" (FR) structure sensu Riding (2002) (Fig. 16B). The corals are preserved in life position and the presence of encrusting foraminifera, and *Nummulites* within the matrix suggest that this subfacies developed under meso-oligophotic conditions, in an intermediate zone of the carbonate ramp (Morsilli et al., 2012; Pomar et al., 2017; Serra-Kiel et al., 2003b).

5.2. Biostratigraphy

The benthic foraminiferal assemblage determined in the La Tossa Formation includes *Nummulites biedai*, *N. hormoensis,* and *Glomalveolina ungaroi.* Additional diagnostic taxa include *N. cyrenaicus, N. chavannesi, N. garnieri garnieri, N. incrassatus*, *N. striatus, N. vicaryi, Assilina schwageri, Orbitoclypeus varians varians, A, Asterocyclina stella stella,* and *A. stellata buekkensis,* along with the occurrence of *Chapmanina gassinensis, Rhabdorites malatyaensis, Schlosserina asterites*, and *Silvestriella tetraedra* (Fig. 17). The stratigraphic ranges of the identified species allow to correlate this interval with the lowermost Priabonian, corresponding to the upper part of the Shallow Benthic zone SB 18, specifically subzones 18b (Costa et al., 2013) or 18b-c (Less et al., 2011; Less and Özcan, 2012; Papazzoni et al., 2017; Briguglio et al., 2026).

This biostratigraphic interpretation is further supported by the presence of *Heterostegina reticulata tronensis* Less, Özcan, Papazzoni and Stockar in La Trona section, at the base of the Sant Martí Xic Formation in the Vic sub-basin (Less et al., 2008), and of *H. reticulata multifida* (Bieda) in the Puig Aguilera section in the Igualada sub-basin (Romero et al., 1999; Less et al., 2008). These subspecies are diagnostic of the lower part of SB 18b and the basal part of 18c, respectively (Less et al., 2008; Less et al., 2011; Less and Özcan, 2012).

5.3. Palaeoclimatic framework and external controls

The upward successive three different depositional regimes recorded were likely controlled by a combination of local and global factors, resulting from the interplay between allogenic controls, such as climate and eustatic sea-level fluctuations, and autogenic processes, including subsidence, delta-lobe switching, carbonate factory dynamics, and sediment supply (e.g., Strasser et al., 1999).

A review of the Priabonian interval, and specifically magnetochron C17n.1n in which the studied succession is situated (Fig. 18), indicates that major global climatic and eustatic forcing may have influenced its genesis. Progressive cooling in the Southern Hemisphere likely promoted transient Antarctic ice sheets and was associated with a major eustatic sea-level fall (Scher et al., 2014; Carter et al., 2017). In contrast, lower-latitude regions remained relatively warm, probably due to changes in ocean–atmosphere circulation and reduced poleward heat transport (Tremblin et al., 2016). Consistent with this, pCO_2 values reported by Zhang et al. (2013) from equatorial western Atlantic indicate relatively high levels coeval with the deposition of the La Tossa Formation (Fig. 18).

In agreement with this climatic framework, no clear evidence of significant cooling is recorded in the studied succession. Cooling events during the Priabonian have been mainly documented in the Southern Hemisphere through $\delta^{18}O$ isotopic analyses of bulk sediment (e.g., Scher et al., 2014) and benthic foraminiferal tests (e.g., Lear et al., 2008), as well as changes in calcareous nannoplankton assemblages (e.g., Persico and Villa, 2004). In lower-latitude carbonate platform proximal settings, cooling episodes have been linked to the widespread development of bryozoan limestones in rock-forming abundances, such as those described in northern Italy and associated with the Oi-1 glaciation event and the onset of permanent Antarctic ice sheets (e.g., Jaramillo-Vogel et al., 2016). However, such indicators are absent from the La Tossa Formation, which is instead dominated by invertebrates hosting photosymbionts, such as corals and hyaline larger foraminifera (Figs. 6–17), indicative of warm, tropical to subtropical conditions (James, 1997; Schlager, 2003; Reijmer, 2021).

Two laterally continuous beds of coralline algal (maërl) facies occur within the La Tossa Formation, at the top of stratigraphic cycles I and IV (Fig. 15), represented by samples VF-7 and VF-13 (Figs. 6, 7, and 14D). This facies association (MR) is dominated by coralline algae with only rare miliolid and acervulinid foraminifera, echinoid fragments, and bivalves. The absence of skeletal grains characteristic of a shallow warm-water carbonate factory (i.e., the photozoan association sensu James, 1997), such as abundant nummulitids, orthophragmines, green algae, and corals, may suggest cooler conditions, potentially linked to short-lived cooling events such as the PrOM (Fig. 18; Scher et al., 2014). However, maërl beds occur worldwide across a broad range of latitudes and temperatures (e.g., Aguirre et al., 2017; Tuya et al., 2023; Aguirre and Braga, 2024), and their presence alone is not diagnostic of temperate- or cool-water settings. The identified maërl-forming coralline algae assemblages are dominated by Hapalidiales (Figs. 9A, B and D), a group commonly associated with temperate to cool waters (Harvey et al., 2003). Nevertheless, the subordinate presence of Sporolithales (Figs. 9E and F), which are generally more abundant in warmer temperate settings (Aguirre et al., 2000), would argue against a distinctly cooler regime.

Similarly, no clear evidence supports a major regression during deposition of the La Tossa Formation (Figs. 6–8 and 17). The preserved succession is stacked in a prograding pattern (Figs. 5 and 15), characteristic of a sustained balance between accommodation and sediment accumulation (Catuneanu et al., 2011). The absence of subaerial exposure surfaces, including erosion features or palaeokarst development (e.g., Esteban and Klappa, 1983; Catuneanu et al., 2011), together with the lack of a basinward shift of shallow-water facies toward depocentral areas of the Vic sub-basin (Fig. 1B; see e.g., Taberner, 1984) indicate a relatively sea-level stand during the Priabonian. A major regression in this sector of the South Pyrenean foreland basin occurred only later, above the Collsuspina Limestone (late part of magnetochron C17n.1n), marked by the development of stromatolitic carbonates interbedded with evaporitic facies of the "Terminal Complex" (Travé, 1992; Travé et al., 1996), followed by the evaporite deposits of the Cardona Formation (Puigdefàbregas et al., 1986) and the overlying continental deposits of the Artés Formation (Ferrer et al., 1968) (Fig. 3). Nevertheless, an overall Priabonian regressive trend may have been locally counterbalanced by tectonic foreland subsidence associated with the emplacement of the Catalan Coastal Ranges and the Pyrenees (López-Blanco et al., 2000; López-Blanco, 2002; Gómez-Paccard et al., 2011; Fig. 1).

Within this warm background, however, Priabonian floral records from the Ebro Basin and Iberia document a progressive trend toward increased aridity (Cavagnetto and Anadón, 1996; Barrón et al., 2010). According to Barrón et al. (2010), tropical forests across Iberia were replaced during the earliest Priabonian by evergreen, drought-tolerant (sclerophyllous) vegetation. Similar conclusions were reported from southern France (Suc et al., 2025) and Germany (Moraweck et al., 2015). Clumped isotope (Δ47) palaeotemperatures from pedogenic carbonates in the Çiçekdağı Basin (Turkey) also indicate warming during the lower-middle Priabonian (*c.* 37 Ma), and a progressive shift toward more arid conditions that culminated at the EOT (Botté et al., 2026). Although European aridity around the EOT has often been linked to Alpine uplift (Kocsis et al., 2014), evidence indicates that relatively dry conditions and increased climatic seasonality were already established during the Priabonian (Pound and Salzmann, 2017). Isotopic data from the Priabonian continental Artés Formation in the Ebro Basin (Fig. 3) indicate limited climatic change across the Eocene–Oligocene boundary (Sheldon et al., 2012), whereas a major shift toward more arid vegetation, occurred earlier, as constrained by Costa et al. (2011). Based on palaeosol-derived palaeoprecipitation estimates, Sheldon and Retallack (2004) document a long-term trend toward increasing aridity in North America across the EOT and into the early Oligocene. Comparable trends have been documented in Asia during magnetochron C17n.1n (Bosboom et al., 2013, 2014), broadly coeval with the La Tossa Formation (Fig. 18).

Although warming and relatively high pCO_2 conditions are commonly associated with intensified hydrological cycling (Held and Soden, 2006), this relationship is not straightforward at low to mid latitudes. Tremblin et al. (2016) documented progressive tropical warming in the equatorial Atlantic initiated *c.* 4 My prior to the EOT, interpreted as the result of heat accumulation at lower latitudes within a progressively isolated South Atlantic gyre. This redistribution of heat contributed to enhanced Southern Hemisphere cooling and the development of a stronger meridional temperature gradient, favouring the onset of Antarctic glaciation. At ~33°N, the study area was located at subtropical latitudes, where the combined effects of a strengthened meridional gradient and increasing climatic seasonality may have

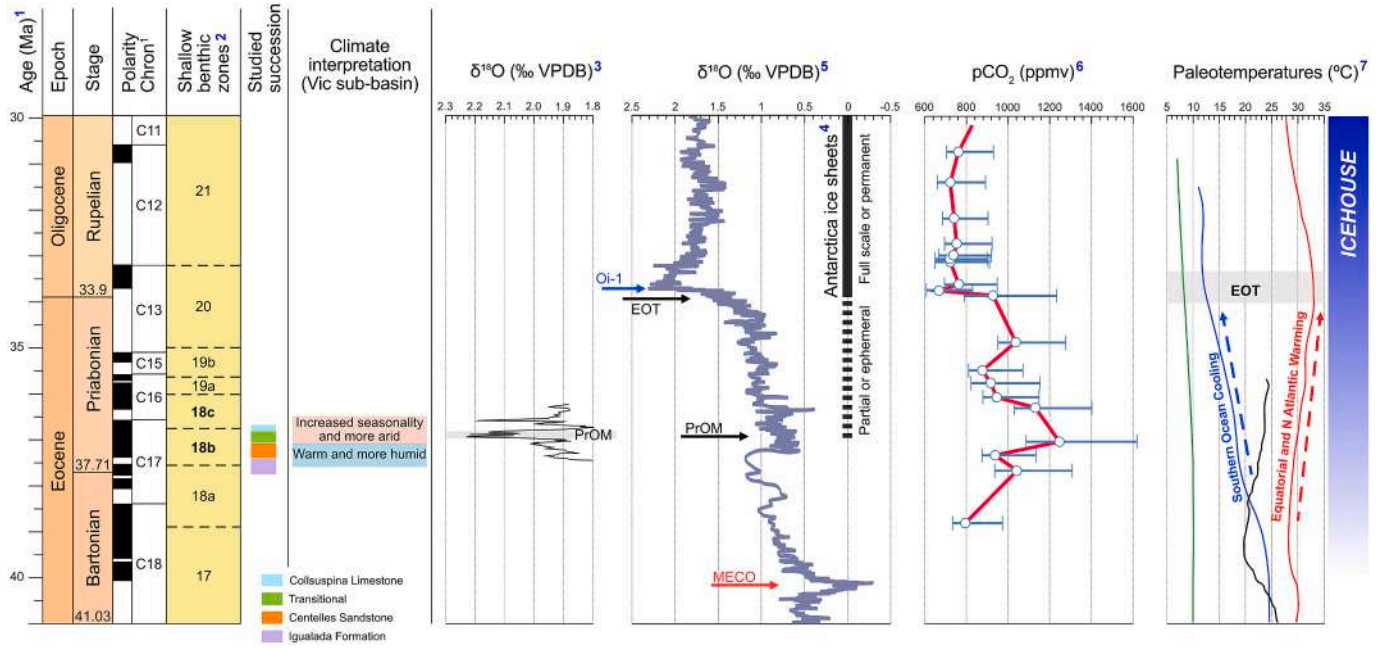


Fig. 18. Tentative correlation between the studied low-latitude shallow-water succession and its palaeoclimatic interpretation with the main Bartonian to Rupelian climatic events, alongside published $\delta^{18}O$, atmospheric pCO_2, and palaeotemperature records. 1) Numerical ages and polarity chrons follow Gradstein et al. (2020). 2) Shallow benthic foraminiferal subzones correlated to the magnetochronostratigraphic framework are modified from Briguglio et al. (2026). 3) The $\delta^{18}O$ curve illustrating the Priabonian Oxygen Isotope Maximum (PrOM) is taken from Scher et al. (2014) and is based on benthic foraminiferal $\delta^{18}O$ measurements from ODP Site 738 (offshore eastern Antarctica). 4) The occurrence of partial or ephemeral, and full-scale or permanent, Antarctic ice sheets follows Zachos et al. (2001, 2008). 5) The $\delta^{18}O$ curve is taken from Gradstein et al. (2020) and incorporates data from Cramer et al. (2009). 6) The pCO_2 estimates for the late Bartonian–Rupelian interval are taken from Zhang et al. (2013) and are based on measurements from calcareous nannofossils (coccolithophores) recovered at ODP Site 925 (equatorial western Atlantic). 7) The palaeotemperature curves for the studied interval, including the onset of Icehouse conditions, are taken from Tremblin et al. (2016), which compile equatorial surface water palaeotemperatures from ODP Sites 925 and 929 (red line), high-latitude bottom water palaeotemperatures from Lear et al. (2000) (green line), austral high-latitude surface water palaeotemperatures from Plancq et al. (2014) and Inglis et al. (2015), and boreal high-latitude surface water palaeotemperatures from Subarctic ODP Site 913 reported in Inglis et al. (2015). The coeval Southern Ocean cooling trend leading to Antarctic glaciation, and the concurrent equatorial and North Atlantic warming identified by Tremblin et al. (2016), are also indicated.

reduced effective precipitation. Taken together, these mechanisms discussed by Tremblin et al. (2016) provide a coherent framework to explain the progressive aridification in Iberia, and particularly in the Ebro Basin, during the Priabonian, despite the persistence of elevated pCO_2 levels and warmth at lower latitudes.

5.4. Siliciclastic supply and ecological response

Siliciclastic supply to the Centelles Sandstone and the transitional interval of the La Tossa Formation was sourced from the Catalan Coastal Ranges (Fig. 1). Conglomeratic systems extended into the marine proximal sectors of the Centelles mixed siliciclastic-carbonate system (i.e., the La Rovira, Coll de Prims, and Morro de Porc sections; Figs. 6, 12A, 13A and 15). Nevertheless, siliciclastic input mainly consisted of finer-grained material (Fig. 12B) delivered episodically by alluvial systems during periods of increased discharge (e.g., López-Blanco et al., 2000; López-Blanco, 2002).

The relationship between rainfall and siliciclastic export to shallow-marine platforms is not straightforward (e.g., Langbein and Schumm, 1958). During relatively warm and humid intervals, dense vegetation cover in the Catalan Coastal Ranges (Fig. 1) would have reduced erosion, buffering terrigenous input to the platform. Nevertheless, high-intensity seasonal rainfall events could have periodically overwhelmed this vegetative barrier, generating discrete siliciclastic pulses capable of reaching the Centelles platform (Fig. 1). Conversely, during more arid intervals, reduced vegetation cover may have facilitated surface runoff, yet overall discharge and sediment transport capacity were substantially diminished, limiting siliciclastic supply to low-volume, infrequent events unlikely to leave a significant stratigraphic record. The scarcity of siliciclastic input in the Collsuspina Limestone (Figs. 3–5, 15 and 17) is therefore most consistent with a progressive reduction in precipitation and hydrological activity in the catchment area, in agreement with palaeoclimatic reconstructions during the Priabonian from Iberia (Barrón et al., 2010) and the Ebro Basin (Cavagnetto and Anadón, 1996). The Transitional mixed siliciclastic-carbonate interval and the overlying Collsuspina Limestone of the La Tossa Formation (Figs. 5, 17 and 18) may therefore record the onset of the long-term aridification trend that culminated at the EOT, or alternatively a transient phase of increased aridity.

This overall evolution toward semiarid conditions in the Ebro Basin, however, would have been punctuated by higher-frequency oscillations between siliciclastic and carbonate deposition during the transitional interval, giving rise to cycles I to VII (Figs. 5 and 15), which may reflect orbitally paced variations in precipitation, similar to those documented in EOT floras of the Ebro Basin by Tosal et al. (2018, 2019). In this context, increased climatic seasonality during the Late Eocene has also been reported elsewhere in Europe, including Germany (Moraweck et al., 2015) and France (Suc et al., 2025), based on floral evidence.

The reduced siliciclastic supply up-section (Figs. 5, 17) may also reflect a decline in source-area relief, which would have lowered erosion rates and transport capacity (e.g., Ahnert, 1970). The uppermost conglomerate deposits preserved in the nearby Montserrat Massif (Fig. 1B) yield an age of *c*. 37.2 Ma within the magnetochron C17n.1n (López-Blanco et al., 2000). Therefore, a transition from active conglomeratic systems (*c*. 37.2 Ma) to reduced siliciclastic input in the La Tossa Formation (*c*. 37 Ma) over such a short interval (within magnetochron C17n.1n) is unlikely to result from a rapid loss of topography alone.

Fossil assemblages and sedimentological patterns closely track these changes in siliciclastic supply. Facies dominated by orthophragmines and *Nummulites* occur within the transitional mixed siliciclastic-carbonate interval of the La Tossa Formation (Figs. 5–8, 15 and 17), reflecting periods of enhanced terrigenous input, likely associated with migrating delta lobes during relatively humid intervals (Morsilli et al., 2012; Mancini et al., 2025). These hyaline larger foraminifera (Figs. 11A–E, 12G–H and 14D–E), among the most siliciclastic-tolerant carbonate producers, were able to thrive despite sustained sediment influx (Lokier et al., 2009), but are notably absent from the carbonate-dominated Collsuspina Limestone (Fig. 17).

Coral assemblages within the studied succession (Fig. 13) record comparable variations in terrigenous influx, suggesting they developed under relatively turbid, low-light settings similar to modern deltaic-influenced, coral reefs along the eastern coast of Borneo (Wilson, 2012). In this regard, Mancini et al. (2025) and Morsilli et al. (2012) studied a coeval, analogous coral buildups in the Sant Martí Xic Formation (Fig. 3) in the northern Vic sub-basin and in the Aínsa-Jaca piggyback basin. Developing within a mixed siliciclastic-carbonate succession, they concluded that these corals grew in the mesophotic zone of a deltaic system, subject to light fluctuations during periods of low siliciclastic input. In contrast, the Maërl and Foraminifera-Coralline algae facies beds within the transitional mixed siliciclastic-carbonate interval (Figs. 6–8 and 17) reflect episodic drops in terrigenous influx and enhanced water clarity. Because coralline algae are highly sensitive to siliciclastic smothering (Aguirre et al., 2017), their development within this mixed interval marks sustained phases of reduced runoff.

Overall, the upward transition from siliciclastic-influenced facies dominated by nummulitids and orthophragmines to carbonate-dominated assemblages rich in miliolids and corals (Fig. 17), records a progressive decline in continental supply. This ecological turnover marks the stabilization of a clearer, more oligotrophic carbonate platform (i.e., the Collsuspina Limestone; Figs. 5, 15 and 17), driven by a regional climatic shift toward increased aridity and pronounced seasonality, which mirrors terrestrial Priabonian palaeobotanical records across the Iberian Peninsula (Barrón et al., 2010).

6. Conclusions

The larger foraminiferal assemblage identified within the lower Priabonian mixed carbonate–siliciclastic succession of the La Tossa Formation in the Vic sub-basin comprises biostratigraphically significant taxa such as *Nummulites biedai*, *N. hormoensis*, *N. striatus*, *Assilina schwageri*, *Glomalveolina ungaroi*, and *Rhabdorites malatyaensis*, among others. According to the current larger foraminiferal biozonation (Briguglio et al., 2026) and the Geological Time Scale (Gradstein et al., 2020), this assemblage assigns the studied stratigraphic interval to Shallow Benthic zone 18b-18c, within polarity chron C17n.1n at ~37 Ma. Deposition of the La Tossa Formation partially overlapped with the Priabonian Oxygen Isotope Maximum (PrOM), a transient glacial episode linked to ice-sheet growth in East Antarctica (Scher et al., 2014), whereas warmer conditions persisted in equatorial to subtropical regions (Tremblin et al., 2016), including the South Pyrenean foreland basin.

The vertical evolution of larger foraminifera and coralline algae, documented at both genus and species levels, shows no clear shift toward either warmer or cooler water conditions, nor any major change in accommodation (i.e., relative sea-level fluctuations). The lithological record of the La Tossa Formation, however, tells a different story: there is a marked upward transition from a siliciclastic-dominated lower interval, represented by the Centelles Sandstone unit, to a transitional interval of mixed carbonate–siliciclastic and cyclic deposits, and then to the carbonate-dominated Collsuspina Limestone, showing a progressive reduction in siliciclastic input.

Although the Priabonian Stage is generally described in the literature as a time of progressive cooling and major regression, neither signal is evident in the studied succession. Instead, the lithological evolution points to changing climatic conditions, from a warmer and more humid regime during deposition of the lower siliciclastic interval to more arid and seasonally variable conditions during deposition of the transitional and carbonate-dominated parts of the La Tossa Formation. This increase in aridity and seasonality in the south-eastern Pyrenean foreland basin during the early Priabonian is interpreted as the result of a large-scale reorganisation of atmospheric circulation, potentially driven by

Southern Hemisphere cooling and/or by enhanced equatorial warming. The latter scenario would have intensified tropical convection and redistributed moisture toward higher latitudes, thereby reducing relative humidity in subtropical regions, expanding the subtropical dry belts, and ultimately promoting the progressive decline in terrigenous supply recorded by the La Tossa Formation.

CRediT authorship contribution statement

Laura Acosta: Writing – original draft, Validation, Methodology, Investigation, Formal analysis, Data curation, Conceptualization. **Carles Ferràndez-Cañadell:** Writing – original draft, Visualization, Validation, Supervision, Methodology, Investigation, Formal analysis, Data curation, Conceptualization. **Julio Aguirre:** Writing – original draft, Validation, Supervision, Methodology, Investigation, Formal analysis, Conceptualization. **Alessandro Mancini:** Writing – review & editing, Visualization, Validation, Methodology, Investigation, Formal analysis, Conceptualization. **Telm Bover-Arnal:** Writing – original draft, Visualization, Validation, Supervision, Resources, Project administration, Methodology, Investigation, Funding acquisition, Formal analysis, Data curation, Conceptualization.

Declaration of competing interest

The authors declare that they have no known competing financial interests or personal relationships that could have appeared to influence the work reported in this paper.

Acknowledgements

The LCA research is supported by the Generalitat de Catalunya through the 2024 FI Joan Oró predoctoral grant (00194). The study was funded by the Grup de Recerca Reconegut per la Generalitat de Catalunya 2021 SGR-Cat 00349 “Geologia Sedimentària”, and the I + D + i research projects IBERCAFO (PID2024-159218NB-I00) and IBERINSULA (PID2020-113912GB-I00), funded by MCIN/AEI/10.13039/501100011033 and the European Regional Development Fund (ERDF). We are grateful to Alejandro Gallardo and Climent Roda for their assistance with sample preparation and excellent work in preparing the thin sections. We sincerely thank the reviewers and the editor, Laura Tomassetti, for their thoughtful comments and suggestions that have contributed substantially to improve the manuscript.

Data availability

No data was used for the research described in the article.

References

Acosta, L., Ferràndez-Cañadell, C., Tosquella, J., Bover-Arnal, T., in press. Early Priabonian *Nummulites* banks from the southeastern Pyrenean foreland basin (Central Catalonia), with notes on what defines a *Nummulites* bank. Paläontologische Zeitschrift, doi:https://doi.org/10.1007/s12542-026-00809-5.

Adey, W.H., 1979. Crustose coralline algae as microenvironmental indicators in the tertiary. In: Gray, J., Boucot, A.J. (Eds.), Historical Biogeography, Plate Tectonics and the Changing Environment. Oregon State University Press, Corvallis, pp. 459–464.

Adey, W.H., Macintyre, I.G., 1973. Crustose coralline algae: a re-evaluation in the geological sciences. Geological Society of America Bulletin 84, 883–904. https://doi.org/10.1130/0016-7606(1973)84<883:CCAARI>2.0.CO;2.

Agnini, C., Fornaciari, E., Giusberti, L., Grandesso, P., Lanci, L., Luciani, V., Muttoni, G., Pälike, H., Rio, D., Spofforth, D.J.A., Stefani, C., 2011. Integrated biomagnetostratigraphy of the Alano section (NE Italy): a proposal for defining the middle-late Eocene boundary. Geological Society of America Bulletin 123, 841–872. https://doi.org/10.1130/B30158.1.

Agnini, C., Backman, J., Boscolo-Galazzo, F., Condon, D.J., Fornaciari, E., Galeotti, S., Luca Giusberti, L., Grandesso, P., Lanci, L., Luciani, V., Monechi, S., Muttoni, G., Pälike, H., Pampaloni, M.L., Papazzoni, C.A., Pearson, P.N., Pignatti, J., Premoli Silva, I., Raffi, I., Rio, D., Rook, L., Sahy, D., Spofforth, D.J.A., Stefani, C., Wade, B.S., 2021. Proposal for the Global Boundary Stratotype Section and Point (GSSP) for the Priabonian Stage (Eocene) at the Alano section (Italy). Episodes 44, 151–173. https://doi.org/10.18814/epiiugs/2020/020074.

Aguirre, J., Braga, J.C., 2024. Rhodolith beds in a shifting world: a palaeontological perspective. Aquatic Conservation: Marine and Freshwater Ecosystems 34. https://doi.org/10.1002/aqc.70015, 2024.

Aguirre, J., Riding, R., 2005. Dasycladalean algal biodiversity compared with global variations in temperature and sea level over the past 350 Myr. Palaios 20, 581–588.

Aguirre, J., Riding, R., Braga, J.C., 2000. Diversity of coralline red algae: origination and extinction patterns from the early cretaceous to the Pleistocene. Paleobiology 26, 651–667.

Aguirre, J., Braga, J.C., Bassi, D., 2017. Rhodoliths and rhodolith beds in the rock record. In: Riosmena-Rodríguez, R., Nelson, W., Aguirre, J. (Eds.), Rhodolith/Maërl Beds: a Global Perspective, Coastal Research Library, 15. Springer, Cham, pp. 105–138. https://doi.org/10.1007/978-3-319-29315-8_5.

Aguirre, J., Braga, J.C., Pujalte, V., Orue-Etxebarria, X., Salazar-Ortiz, E., Rincón-Martínez, D., Abad, M., Pérez-Valera, F., 2020. Middle Eocene rhodoliths from tropical and mid-latitude regions. Diversity 12, 117. https://doi.org/10.3390/d12030117.

Aguirre, J., Baceta, J.I., Braga, J.C., 2022. Coralline algae at the Paleocene/Eocene thermal Maximum in the Southern Pyrenees (N Spain). Frontiers in Marine Science 9. https://doi.org/10.3389/fmars.2022.899877.

Ahnert, F., 1970. Functional relationships between denudation, relief, and uplift in large mid-latitude drainage basins. American Journal of Science 268, 243–263.

Akhmetiev, M.A., Gavrilov, Y.O., Zaporozhets, N.I., 2017. Events at the turn of the Eocene and Oligocene in the Central Eurasia Region (middle latitudes). Doklady Earth Sciences 473, 273–276. https://doi.org/10.1134/S1028334X17030199.

Allen, M.B., Armstrong, H.A., 2008. Arabia–Eurasia collision and the forcing of mid-Cenozoic global cooling. Palaeogeography, Palaeoclimatology, Palaeoecology 265, 52–58. https://doi.org/10.1016/j.palaeo.2008.04.021.

Alonso-Zarza, A.M., Armenteros, A., Braga, J.C., Muñoz, A., Pujalte, V., Ramos, E., Aguirre, J., Alonso-Gavilán, G., Arenas, C., Baceta, J.I., Carballeira, J., Calvo, J.P., Corrochano, A., Fornós, J.J., González, A., Luzón, A., Martín, J.M., Pardo, G., Payros, A., Perez, A., Pomar, L., Rodríguez, J.M., Villena, J., 2002. Tertiary. In: Gibbons, W., Moreno, T. (Eds.), The Geology of Spain. Geological Society, London, pp. 293–334.

Anadón, P., 1978. El Paleógeno continental anterior a la transgresión “Biarritziense” (Eoceno medio) entre los ríos Gaià y Ripoll (Provincias de Tarragona y Barcelona). PhD Thesis, University of Barcelona, 267 pp.

Anadón, P., Feist, M., 1981. Charophytes et biostratigraphie du Paléogène inférieur du bassin de l’Ebre oriental. Palaeontographica. Abteilung B, Paläobotanik-Paläophytologie 178, 143–168.

Anadón, P., Feist, M., Hartenberger, J.L., Müller, C., Villalta-Comella, J., 1983. Un exemple de corrélation biostratigraphique entre échelles marines et continentales dans l’Éocène: la coupe de Pontils (bassin de l’Ebre, Espagne). Bulletin de la Société Géologique de France 25, 747–755.

Anadón, P., Cabrera, L., Roca, E., 1989a. Contexto estructural y paleogeografico de los sistemas lacustres cenozoicos de España. Acta Geologica Hispánica 24, 167–184.

Anadón, P., Cabrera, L., Colldeforns, B., Sáez, A., 1989b. Los sistemas lacustres del Eoceno superior y Oligoceno del sector oriental de la Cuenca del Ebro. Acta Geologica Hispánica 24, 205–230.

Anagnostou, E., John, E.H., Edgar, K.M., Foster, G.L., Ridgwell, A., Inglis, G.N., Pancost, R.D., Lunt, D.J., Pearson, P.N., 2016. Changing atmospheric CO_2 concentration was the primary driver of early Cenozoic climate. Nature 533, 380–384. https://doi.org/10.1038/nature17423.

Astibia, H., Payros, A., Pereda-Suberbiola, X., Elorza, J., Berreteaga, A., Etxebarria, N., Badiola, A., Tosquella, J., 2005. Sedimentology and taphonomy of sirenian remains from the Middle Eocene of the Pamplona Basin (Navarre, Western Pyrenees). Facies 50, 463–475. https://doi.org/10.1007/s10347-004-0026-5.

Astibia, H., Bardet, N., Pereda-Suberbiola, X., Payros, A., de Buffrénil, V., Elorza, J., Tosquella, J., Berreteaga, A., Badiola, A., 2010. New fossils of Sirenia from the Middle Eocene of Navarre (Western Pyrenees): the oldest west European sea cow record. Geological Magazine 147, 665–673. https://doi.org/10.1017/S0016756810000130.

Baceta, J.I., Mateu-Vicens, G., 2022. Seagrass development in terrigenous-influenced inner ramp settings during the middle Eocene (Urbasa–Andia Plateau, Western Pyrenees, North Spain). Sedimentology 69, 301–344. https://doi.org/10.1111/sed.12937.

Balaguer, J., Alba, D.M., 2016. A new dugong species (Sirenia, Dugongidae) from the Eocene of Catalonia (NE Iberian Peninsula). Comptes Rendus Palevol 15, 489–500. https://doi.org/10.1016/j.crpv.2015.10.002.

Barnolas, A., 1992. Evolución sedimentaria de la Cuenca Surpirenaica Oriental durante el Eoceno. Acta Geologica Hispánica 27, 15–31.

Barnolas, A., Busquets, P., Serra-Kiel, J., 1981. Características sedimentológicas de la terminación del ciclo marino del Eoceno superior en el sector oriental de la Depresión del Ebro (Catalunya, N.E. de España). Acta Geologica Hispánica 16, 215–221.

Barnolas, A., Larrasoaña, J.C., Pujalte Navarro, V., Schmitz, B., Sierro, F.J., Mata, M.P., van den Berg, B.C.J., Pérez-Asensio, J.N., Salazar, Á., Salvany, J.M., Ledesma, S., García-Castellanos, D., Civis, J., Cunha, P.P., 2019. Alpine Foreland Basins. In: Quesada, C., Oliveiras, J.T. (Eds.), The Geology of Iberia: A Geodynamic Approach, Regional Geology Reviews. Springer International Publishing, Cham, pp. 7–59. https://doi.org/10.1007/978-3-030-11190-8_2.

Barrón, E., Rivas-Carballo, R., Postigo-Mijarra, J.M., Alcalde-Olivares, C., Vieira, M., Castro, L., Pais, J., Valle-Hernández, M., 2010. Cenozoic vegetation Iberian Peninsula: a synthesis. Review of Palaeobotany and Palynology 162, 382–402. https://doi.org/10.1016/j.revpalbo.2009.11.007.

Bassi, D., 1998. Coralline algal facies and their palaeoenvironments in the late Eocene of Northern Italy (Calcare di Nago, Trento). Sedimentary Geology 118, 237–256.
Bassi, D., 2005. Larger foraminiferal and coralline algal facies in an Upper Eocene storm-influenced, shallow-water carbonate platform (Colli Berici, North-Eastern Italy). Palaeogeography, Palaeoclimatology, Palaeoecology 226, 17–35.
Basso, D., Vrsaljko, D., Grgasović, T., 2008. The coralline flora of a Miocene maërl: the Croatian "Litavac". Geologia Croatica 61, 333–340. https://doi.org/10.4154/gc.2008.25.
Beaumont, C., Muñoz, J.A., Hamilton, J., Fullsack, P., 2000. Factors controlling the Alpine evolution of the Central Pyrenees inferred from the comparison of observations and geodynamical models. Journal of Geophysical Research 105, 8121–8145. https://doi.org/10.1029/1999JB900390.
Beavington-Penney, S.J., Racey, A., 2004. Ecology of extant nummulitids and other larger benthic foraminifera: applications in palaeoenvironmental analysis. Earth-Science Reviews 67, 219–265. https://doi.org/10.1016/j.earscirev.2004.02.005.
Benedetti, A., Papazzoni, C.A., Bosellini, F.R., 2024. Unparallel resilience of shallow-water tropical calcifiers (foraminifera and scleractinian reef corals) during the early Paleogene global warming intervals. Palaeogeography, Palaeoclimatology, Palaeoecology 651, 112393. https://doi.org/10.1016/j.palaeo.2024.112393.
Bosboom, R., Dupont-Nivet, G., Grothe, A., Brinkhuis, H., Villa, G., Mandic, O., Stoica, M., Huang, W., Yang, W., Guo, Z., Krijgsman, W., 2013. Linking Tarim Basin sea retreat (West China) and Asian aridification in the late Eocene. Basin Research 26, 621–640. https://doi.org/10.1111/bre.12054.
Bosboom, R.E., Abels, H.A., Hoorn, C., van den Berg, B.C.J., Guo, Z., Dupont-Nivet, G., 2014. Aridification in continental Asia after the Middle Eocene Climatic Optimum (MECO). Earth and Planetary Science Letters 389, 34–42. https://doi.org/10.1016/j.epsl.2013.12.014.
Bosence, D.W.J., 1983. Description and classification of Rhodoliths (Rhodoids, Rhodolites). In: Peryt, T.M. (Ed.), Coated Grains. Springer-Verlag, Berlin, pp. 217–224.
Bosence, D.W.J., 1976. Ecological studies on two unattached coralline algae from Western Ireland. Palaeontology 19, 365–395.
Botté, P., Licht, A., Jourdan, A.-L., Montheil, L., Demory, F., Kaya, M., Ocakoğlu, F., Akkiraz, M.S., İbilioğlu, D., Coster, P., Métais, G., Raynaud, B., Beard, K.C., 2026. Climate changes in Anatolia across the late Eocene and the Eocene–Oligocene transition: successive warming and cooling, aridification, and implications for the westward dispersal of Asian terrestrial mammals. EGUsphere. https://doi.org/10.5194/egusphere-2025-6383 [preprint].
Braga, J.C., Aguirre, J., 2001. Coralline algal assemblages in upper Neogene reef and temperate carbonates in southern Spain. Palaeogeography, Palaeoclimatology, Palaeoecology 175, 27–41. https://doi.org/10.1016/S0031-0182(01)00384-4.
Braga, J.C., Bassi, D., 2007. Neogene history of *Sporolithon* Heydrich (Corallinales, Rhodophyta) in the Mediterranean region. Palaeogeography, Palaeoclimatology, Palaeoecology 243, 205–220. https://doi.org/10.1016/j.palaeo.2006.07.014.
Brandano, M., 2017. Oligocene Rhodolith beds in the Central Mediterranean area. In: Riosmena-Rodríguez, R., Nelson, W., Aguirre, J. (Eds.), Rhodolith/Maërl Beds: A Global Perspective: Coastal Research Library, vol. 15. Springer International Publishing, pp. 195–219.
Brandano, M., Tomassetti, L., 2020. MECO and Alpine orogenesis: constraints for facies evolution of the Bartonian nummulitic and Solenomeris limestone in the Argentina Valley (Ligurian Alps). Sedimentology 69, 24–46. https://doi.org/10.1111/sed.12829.
Brasier, M.D., 1975. The ecology and distribution of recent foraminifera from the reefs and shoals around Barbuda, West Indies. Journal of Foraminiferal Research 5, 193–210.
Briguglio, A., Giraldo-Gómez, V.M., Baucon, A., Benedetti, A., Papazzoni, C.A., Pignatti, J., Wolfgring, E., Piazza, M., 2024. A middle Eocene shallow-water drowning ramp in NW Italy: from shoreface conglomerates to distal marls. Newsletters on Stratigraphy 57, 37–63. https://doi.org/10.1127/nos/2023/0784.
Briguglio, A., Benedetti, A., Papazzoni, C.A., 2026. A compendium of updated Shallow Benthic zones for the Paleogene and the Miocene. Micropaleontology 72, 329–336. https://doi.org/10.47894/mpal.72.4.02.
Buffan, L., Condamine, F.L., Stutz, N.S., Pujos, F., Antoine, P.-O., Marivaux, L., 2025. The fate of South America's endemic mammalian fauna in response to the most dramatic Cenozoic climate disruption. Proceedings of the National Academy of Sciences of the United States of America 122, e2419520122. https://doi.org/10.1073/pnas.2419520122.
Burbank, D.W., Puigdefàbregas, C., Muñoz, J.A., 1992. The chronology of the Eocene tectonic and stratigraphic development of the eastern Pyrenean foreland basin, Northeast Spain. Geological Society of America Bulletin 104, 1101–1120. https://doi.org/10.1130/00167606(1992)104<1101:TCOTET>2.3.CO;2.
Burchette, T.P., Wright, V.P., 1992. Carbonate ramp depositional systems. Sedimentary Geology 79, 3–57.
Busquets, P., Pisera, A., Reguant, S., Serra-Kiel, J., 1997. Biofacies of the outer continental shelf in the Bartonian of the eastern part of the Ebro Basin (NE Spain). Boletín de la Real Sociedad Española de Historia Natural (Sección Geológica) 92, 249–256.
Buxton, M.W.N., Pedley, H.M., 1989. A standardized model for Tethyan Tertiary carbonate ramps. Journal of the Geological Society, London 146, 746–748.
Carter, A., Riley, T.R., Hillenbrand, C.-D., Rittner, M., 2017. Widespread Antarctic glaciation during the late Eocene. Earth and Planetary Science Letters 458, 49–57. https://doi.org/10.1016/j.epsl.2016.10.045.
Cascella, A., Dinarès-Turell, J., 2009. Integrated calcareous nannofossil biostratigraphy and magnetostratigraphy from the uppermost marine Eocene deposits of the southeastern Pyrenean foreland basin: evidences for marine Priabonian deposition. Geologica Acta 7, 281–296. https://doi.org/10.1344/105.000000282.
Catuneanu, O., Galloway, W.E., Kendall, C.G.St.C., Miall, A.D., Posamentier, H.W., Strasser, A., Tucker, M.E., 2011. Sequence stratigraphy: methodology and nomenclature. Newsletters on Stratigraphy 44, 173–245. https://doi.org/10.1127/0078-0421/2011/0011.
Caus, E., Serra-Kiel, J., 1984. Distribución ambiental de los macroforaminíferos: Cretácico superior y Eoceno, Tomo 1. I Congreso Español de Geología, Segovia, pp. 399–406, 9-14 de abril de 1984.
Cavagnetto, C., Anadón, P., 1996. Preliminary palynological data on floristic and climatic changes during the Middle Eocene-early Oligocene of the eastern Ebro Basin, Northeast Spain. Review of Palaeobotany and Palynology 92, 281–305. https://doi.org/10.1016/0034-6667(95)00096-8.
Coletti, G., Mariani, L., Garzanti, E., Consani, S., Bosio, G., Vezzoli, G., Basso, D., 2021. Skeletal assemblages and terrigenous input in the Eocene carbonate systems of the Nummulitic Limestone (NW Europe). Sedimentary Geology 425, 106005. https://doi.org/10.1016/j.sedgeo.2021.106005.
Colom, G., Via, L., Reguant, S., 1970. Hallazgo de *Harrisichara lineata* Grambast en el yacimiento del Parés (Sant Boi del Lluçanés, Vic). Acta Geologica Hispánica 5, 65–66.
Corliss, B.H., 1981. Deep-sea benthonic foraminiferal faunal turnover near the Eocene/Oligocene boundary. Marine Micropaleontology 6, 367–384. https://doi.org/10.1016/0377-8398(81)90007-4.
Ćosović, V., Drobne, K., 1998. Lutetian Orthophragminae from the Istrian Peninsula (Adriatic Sea, Croatia and Slovenia). In: Hottinger, L., Drobne, K. (Eds.), Paleogene Shallow Benthos of the Tethys, Dela-Opera SAZU 4. Razred, 34, pp. 173–181.
Costa, E., Garcés, M., López-Blanco, M., Beamud, E., Gómez-Paccard, M., Larrasoaña, J.C., 2010. Closing and continentalization of the south Pyrenean foreland basin (NE Spain): magnetochronological constraints. Basin Research 22, 904–917. https://doi.org/10.1111/j.1365-2117.2009.00452.
Costa, E., Garcés, M., Sáez, A., Cabrera, L., López-Blanco, M., 2011. The age of the "Grande Coupure" mammal turnover: new constraints from the Eocene–Oligocene record of the Eastern Ebro Basin (NE Spain). Palaeogeography, Palaeoclimatology, Palaeoecology 301, 97–107. https://doi.org/10.1016/j.palaeo.2011.01.005.
Costa, E., Garcés, M., López-Blanco, M., Serra-Kiel, J., Bernaola, G., Cabrera, L., Beamud, E., 2013. The Bartonian-Priabonian marine record of the eastern south Pyrenean foreland basin (NE Spain): a new calibration of the larger foraminifers and calcareous nannofossil biozonation. Geologica Acta 11, 177–193. https://doi.org/10.1344/105.000001779.
Cotton, L.J., Zakrevskaya, E.Y., van der Boon, A., Asatryan, G., Hayrapetyan, F., Israyelyan, A., Krijgsman, W., Less, G., Monechi, S., Papazzoni, C.A., Pearson, P.N., Razumovskiy, A., Renema, W., Shcherbinina, E., Wade, B.S., 2017. Integrated stratigraphy of the Priabonian (upper Eocene) Urtsadzor section, Armenia. Newsletters on Stratigraphy 50, 269–295. https://doi.org/10.1127/nos/2016/0313.
Cramer, B.S., Toggweiler, J.R., Wright, J.D., Katz, M.E., Miller, K.G., 2009. Ocean overturning since the Late Cretaceous: inferences from a new benthic foraminiferal isotope compilation. Paleoceanography 24, PA4216. https://doi.org/10.1029/2008PA001683.
De Lira Mota, M.A., Dunkley Jones, T., Sulaiman, N., Edgar, K.M., Yamaguchi, T., Leng, M.J., Adloff, M., Greene, S.E., Norris, R., Warren, B., Duffy, G., Farrant, J., Murayama, M., Hall, J., Bendle, J., 2023. Multi-proxy evidence for sea level fall at the onset of the Eocene–Oligocene transition. Nature Communications 14, 4748. https://doi.org/10.1038/s41467-023-39806-6.
Del Santo, G., García-Sansegundo, J., Sarasa, L., Torrebadella, J., 2000. Estratigrafía y estructura del Terciario en el sector oriental de la Cuenca del Ebro entre Solsona y Manresa (NE de España). Revista de la Sociedad Geológica de España 13, 265–278.
Dimou, V.-G., Koukousioura, O., Less, G., Triantaphyllou, M.V., Dimiza, M.D., Syrides, G., Langer, M.R., 2024. Microfacies and species richness analysis of upper Bartonian and Priabonian carbonate shelf deposits from the Thrace Basin (Tethyan Ocean, Greece): paleoenvironmental evolution and species-richness hotspot revealed. Marine and Petroleum Geology 170, 107126. https://doi.org/10.1016/j.marpetgeo.2024.107126.
Drobne, K., Ćosović, V., Moro, A., Bucković, D., 2011. The role of the Palaeogene Adriatic Carbonate Platform in the spatial distribution of alveolinids. Turkish Journal of Earth Sciences 20, 721–751.
Dunham, R.J., 1962. Classification of carbonate rocks according to depositional texture. In: Ham, W.E. (Ed.), Classification of Carbonate Rocks, 1. American Association of Petroleum Geologist, pp. 108–121. Memoire.
Embry, A.F., Klovan, J.E., 1971. A late Devonian reef tract on Northeastern Banks Island, NWT. Bulletin of Canadian Petroleum Geology 19, 730–781.
Erkızan, L.S., Less, G., Papazzoni, C.A., 2025. Early Priabonian larger benthic foraminifera in the vicinity of Verona (N Italy). Geosciences 15, 334. https://doi.org/10.3390/geosciences15090334.
Esteban, M., Klappa, C.F., 1983. Subaerial exposure environment. In: Scholle, P.A., Bebout, D.G., Moore, C.H. (Eds.), Carbonate Depositional Environments, 33. AAPG Memoir, pp. 1–54.
Fermont, W.J.J., 1982. Discocyclinidae from Ein Avedat (Israel). Utrecht Micropaleontological Bulletin 27, 1–173.
Ferràndez-Cañadell, C., Serra-Kiel, J., 1992. Morphostructure and paleobiology of *Discocyclina* Gümbel, 1870. Journal of Foraminiferal Research 22, 147–165. https://doi.org/10.2113/gsjfr.22.2.147.
Ferrer, J., 1967. Le Paléocene et l'Eocene des Cordilleres côtieres de la Catalogne (Espagne). Eclogae Geologicae Helvetiae 60, 567–576.
Ferrer, J., 1971a. El Paleoceno y Eoceno del borde sur-oriental de la Depresión del Ebro (Cataluña). Mémoires Suisses de Paléontologie 90, 1–70.
Ferrer, J., 1971b. Presencia de macroforaminíferos priabonienses en el Eoceno de Igualada. Acta Geologica Hispánica 6, 4–7.

Ferrer, J., Rosell, J., Reguant, S., 1968. Síntesis litoestratigráfica del Paleógeno del borde oriental de la depresión del Ebro. Acta Geologica Hispánica 3, 54–66.
Flügel, E., 1985. Diversity and environments of Permian and Triassic dasycladacean algae. In: Toomey, D.F., Nitecki, M.H. (Eds.), Paleoalgology: Contemporary Research and Applications. Springer, Berlin, pp. 344–351.
Franquès, J., 1996. Estudi paleoecològic de l'escull de la Trona. Unpublished Master Degree Thesis. University of Barcelona. . 115 pp.
Gandolfi, A., Giraldo-Gómez, V.M., Arena, L., Luciani, V., Papazzoni, C.A., Pignatti, J., Piazza, M., Kocsis, L., Baumgartner, C., Briguglio, A., 2025. Diverse ecological responses of foraminifera to the Middle Eocene Climatic Optimum (MECO) in shallow-water settings (Provençal Domain, NW Italy). Palaeogeography Palaeoclimatology Palaeoecology 661, 112697. https://doi.org/10.1016/j.palaeo.2024.112697.
Garcés, M., López-Blanco, M., Valero, L., Beamud, E., Oliva-Urcia, B., Vinyoles, A., Arbués, P., Cabello, P., Cabrera, L., 2020. Paleogeographic and sedimentary evolution of the south Pyrenean foreland basin. Marine and Petroleum Geology 113, 104105. https://doi.org/10.1016/j.marpetgeo.2019.104105.
Geel, T., 2000. Recognition of stratigraphic sequences in carbonate platform and slope deposits: empirical models based on microfacies analysis of Palaeogene deposits in southeastern Spain. Palaeogeography, Palaeoclimatology, Palaeoecology 155, 211–238. https://doi.org/10.1016/S0031-0182(99)00117-0.
Giraldo-Gómez, V.M., Briguglio, A., Baucon, A., Papazzoni, C.A., Pignatti, J., Gandolfi, A., Piazza, M., 2025. Benthic ecosystem variations along the middle Eocene Provençal drowning ramp. Rivista Italiana di Paleontologia e Stratigrafia 131. https://doi.org/10.54103/2039-4942/24033.
Gómez-Paccard, M., López-Blanco, M., Costa, E., Garcés, M., Beamud, E., Larrasoaña, J. C., 2011. Tectonic and climatic controls on the sequential arrangement of an alluvial fan/fan-delta complex (Montserrat, Eocene, Ebro Basin, NE Spain). Basin Research 23, 1–19. https://doi.org/10.1111/j.1365-2117.2011.00532.x.
Gradstein, F.M., Ogg, J.G., Schmitz, M.D., Ogg, G.M., 2020. The Geologic Time Scale 2020. Elsevier, Amsterdam, p. 1357.
Greiner, G.O.G., 1969. Recent benthic foraminifera; environmental factors controlling their deposition. Nature 223, 168–170.
Hallock, P., Glenn, E.C., 1986. Larger Foraminifera: a Tool for Paleoenvironmental Analysis of Cenozoic Carbonate Depositional Facies. PALAIOS 1, 55–64. https://doi.org/10.2307/3514459.
Hamon, N., Sepulchre, P., Lefebvre, V., Ramstein, G., 2013. The role of eastern Tethys seaway closure in the Middle Miocene Climatic transition (ca. 14 Ma). Climate of the Past 9, 2687–2702. https://doi.org/10.5194/cp-9-2687-2013.
Harvey, A.S., Woelkerling, W.J., Millar, A.J.K., 2003. An account of the Hapalidiaceae (Corallinales, Rhodophyta) in South-Eastern Australia. Australian Systematic Botany 16, 647–698. https://doi.org/10.1071/SB03008.
Held, I.M., Soden, B.J., 2006. Robust responses of the hydrological cycle to global warming. Journal of Climate 19, 5686–5699. https://doi.org/10.1175/JCLI3990.1.
Hohenegger, J., 2005. Estimation of environmental paleogradient values based on presence/absence data: a case study using benthic foraminifera for paleodepth estimation. Palaeogeography, Palaeoclimatology, Palaeoecology 217, 115–130. https://doi.org/10.1016/j.palaeo.2004.11.020.
Hottinger, L., 2001. Learning from the past. In: Levi-Montalcini, R. (Ed.), Frontiers of Life, Vol. 4, Part 2: Discovery and Spoliation of the Biosphere. Academic Press, London and San Diego, pp. 449–477.
Hottinger, L., 1983. Processes determining the distribution of larger foraminifera in space and time. Utrecht Micropaleontological Bulletin 30, 239–253.
Hottinger, L., 1997. Shallow benthic foraminiferal assemblages as signals for depth of their deposition and their limitations. Bulletin de la Société Géologique de France 168, 491–505.
Hottinger, L., 1998. Shallow benthic foraminifera at the Paleocene–Eocene boundary. Strata 1, 61–64.
Hottinger, L., Romero, J., Caus, E., 2001. Architecture and revision of the pellatispirines, planispiral canaliferous foraminifera from the late Eocene Tethys. Micropaleontology 47, 35–77.
Houben, A.J.P., Quaijtaal, W., Wade, B.S., Schouten, S., Brinkhuis, H., 2019. Quantitative organic-walled dinoflagellate cyst stratigraphy across the Eocene–Oligocene Transition in the Gulf of Mexico: a record of climate- and sea level change during the onset of Antarctic glaciation. Newsletters on Stratigraphy 52, 131–154. https://doi.org/10.1127/nos/2018/0455.
Houbrick, R.S., 1981. Anatomy, biology and systematics of *Campanile symbolicum* with reference to adaptive radiation of the *Cerithiacea* (*Gastropoda*: *Prosobranchia*). Malacologia 21, 263–289.
Hutchinson, D.K., Coxall, H.K., Lunt, D.J., Steinthorsdottir, M., de Boer, A.M., Baatsen, M., von der Heydt, A., Huber, M., Kennedy-Asser, A.T., Kunzmann, L., Ladant, J.-B., Lear, C.H., Moraweck, K., Pearson, P.N., Piga, E., Pound, M.J., Salzmann, U., Scher, H.D., Sijp, W.P., Śliwińska, K.K., Wilson, P.A., Zhang, Z., 2021. The Eocene–Oligocene transition: a review of marine and terrestrial proxy data, models and model–data comparisons. Climate of the Past 17, 269–315. https://doi.org/10.5194/cp-17-269-2021.
Inglis, G.N., Farnsworth, A., Lunt, D., Foster, G.L., Hollis, C.J., Pagani, M., Jardine, P.E., Pearson, P.N., Markwick, P., Galsworthy, A.M.J., Raynham, L., Taylor, K.W.R., Pancost, R.D., 2015. Descent toward the Icehouse: Eocene Sea surface cooling inferred from GDGT distributions. Paleoceanography 30, 1000–1020. https://doi.org/10.1002/2014PA002723.
Insalaco, E., 1998. The descriptive nomenclature and classification of growth fabrics in fossil scleractinian reefs. Sedimentary Geology 118, 159–186. https://doi.org/10.1016/S0037-0738(98)00011-6.
Institut Cartogràfic i Geològic de Catalunya (ICGC), 2024. Mapa geològic de Catalunya 1:50.000 [Scale 1:50,000]. Vector and image formats; ETRS89 UTM zone 31N. Institut Cartogràfic i Geològic de Catalunya, Barcelona.
James, N.P., 1997. The cool-water carbonate depositional realm. In: James, N.P., Clarke, J.A.D. (Eds.), Cool-Water Carbonates, 56. SEPM Special Publication, pp. 1–20. https://doi.org/10.2110/pec.97.56.0001.
Jaramillo-Vogel, D., Bover-Arnal, T., Strasser, A., 2016. Bryozoan beds in northern Italy as a shallow-water expression of environmental changes during the Oligocene isotope event 1. Sedimentary Geology 333, 9–18. https://doi.org/10.1016/j.sedgeo.2015.10.010.
Jardim, V., Grall, J., Barros-Barreto, M.B., Bizlen, A., Benoit, T., Braga, J.C., Brodie, J., Burel, T., Cabrito, A., Diaz-Pulido, G., Gagnon, P., Hall-Spencer, J.M., Helias, M., Auntunes Horta, P., Joshi, S., Kamennos, N.A., Kolzenburg, R., Krieger, E.C., Legrand, E., Page, T.M., Peña, V., Ragazzola, F., Rasmusson, L.M., Rendina, F., Schubert, N., Silva, J., Tâmega, F.T.S., Tauran, A., Burdett, H.L., 2025. A common terminology to unify research and conservation of coralline algae and the habitats they create. Aquatic Conservation: Marine and Freshwater Ecosystems 35, e70121. https://doi.org/10.1002/aqc.70121.
Johnson, J.H., 1961. Limestone-Building Algae and Algal Limestones. Colorado School of Mines, Golden, Colorado, p. 297.
Katz, M.E., Miller, K.G., Wright, J.D., Wade, B.S., Browning, J.V., Cramer, B.S., Rosenthal, Y., 2008. Stepwise transition from the Eocene greenhouse to the Oligocene icehouse. Nature Geoscience 1, 329–334. https://doi.org/10.1038/ngeo179.
Kazancı, N., Varol, B., 1990. Development of a mass flow-dominated fan-delta complex and associated carbonate reefs within a transgressive Paleocene succession, Central Anatolia, Turkey. Sedimentary Geology 68, 261–278. https://doi.org/10.1016/0037-0738(90)90014-K.
Kocsis, L., Ozsvárt, P., Becker, D., Ziegler, R., Scherler, L., Codrea, V., 2014. Orogeny forced terrestrial climate variation during the late Eocene–early Oligocene in Europe. Geology 42, 727–730. https://doi.org/10.1130/G35673.1.
Król, J.J., Kołodziej, B., Bucur, I.I., 2018. Coral reefs near the Eocene–Oligocene boundary in the northern Transylvanian Basin, Romania: composition and paleoenvironmental interpretation. Geological Journal 53, 565–579. https://doi.org/10.1002/gj.2918.
Ladant, J.-B., Donnadieu, Y., Lefebvre, V., Dumas, C., 2014. The respective role of atmospheric carbon dioxide and orbital parameters on ice sheet evolution at the Eocene–Oligocene transition. Paleoceanography 29, 810–823. https://doi.org/10.1002/2013PA002593.
Langbein, W.B., Schumm, S.A., 1958. Yield of sediment in relation to mean annual precipitation. Transactions of the American Geophysical Union 39, 1076–1084.
Lear, C.H., Elderfield, H., Wilson, P.A., 2000. Cenozoic deep-sea temperatures and global ice volumes from Mg/ca in benthic foraminiferal calcite. Science 287, 269–272.
Lear, C.H., Bailey, T.R., Pearson, P.N., Coxall, H.K., Rosenthal, Y., 2008. Cooling and ice growth across the Eocene–Oligocene transition. Geology 36, 251–254. https://doi.org/10.1130/G24584A.1.
Less, G., 1987. Paleontology and stratigraphy of the European Orthophragminae. Geologica Hungarica, Series Palaeontologica 51, 1–373.
Less, G., Özcan, E., 2012. Bartonian–Priabonian larger benthic foraminiferal events in the Western Tethys. Austrian Journal of Earth Sciences 105, 129–140.
Less, G., Özcan, E., Papazzoni, C.A., Stockar, R., 2008. The middle to late Eocene evolution of the nummulitid foraminifer Heterostegina in the Western Tethys. Acta Palaeontologica Polonica 53, 317–350.
Less, G., Özcan, E., Okay, A.I., 2011. Stratigraphy and larger foraminifera of the Middle Eocene to lower Oligocene shallow-marine units in the northern and eastern parts of the Thrace Basin, NW Turkey. Turkish Journal of Earth Sciences 20, 793–845. https://doi.org/10.3906/yer-1010-53.
Lokier, S.W., Wilson, M.E.J., Burton, L.M., 2009. Marine biota response to clastic sediment influx: a quantitative approach. Palaeogeography, Palaeoclimatology, Palaeoecology 281, 25–42. https://doi.org/10.1016/j.palaeo.2009.07.007.
López-Blanco, M., 2006. Stratigraphic and tectonosedimentary development of the Eocene Sant Llorenç del Munt and Montserrat fan-delta complexes (Southeast Ebro basin margin, Northeast Spain). Contributions to Science 3 (2), 125–148. https://doi.org/10.2436/20.7010.01.1.
López-Blanco, M., 2002. Sedimentary response to thrusting and fold growing on the SE margin of the Ebro basin (Paleogene, NE Spain). Sedimentary Geology 146, 133–154. https://doi.org/10.1016/S0037-0738(01)00170-1.
López-Blanco, M., Marzo, M., Burbank, D.W., Vergés, J., Roca, E., Anadón, P., Piña, J., 2000. Tectonic and climatic controls on the development of foreland fan deltas: Montserrat and Sant Llorenç del Munt systems (Middle Eocene, Ebro Basin, NE Spain). Sedimentary Geology 138, 17–39. https://doi.org/10.1016/S0037-0738(00)00142-1.
Luciani, V., Fornaciari, E., Papazzoni, C.A., Dallanave, E., Giusberti, L., Stefani, C., Amante, E., 2020. Integrated stratigraphy at the Bartonian–Priabonian transition: Correlation between shallow benthic and calcareous plankton zones (Varignano section, northern Italy). Geological Society of America Bulletin 132, 495–520. https://doi.org/10.1130/B35169.1.
Lunt, P., Luan, X., 2022. SE Asian Cenozoic larger Foraminifera: taxonomic questions, apparent radiation and abrupt extinctions. Journal of Earth Science 33, 1285–1306. https://doi.org/10.1007/s12583-022-1614-4.
Mancini, A., Brandano, M., Gaglianone, G., Mannetta, D., Ferràndez-Cañadell, C., 2025. Coralgal buildup in a mixed carbonate-siliciclastic succession of the upper Eocene Sant Martí Xic Formation (Orís, Vic, SE Ebro Basin, Spain). Geologica Acta 23 (15), 1–16. https://doi.org/10.1344/GeologicaActa2025.23.15.

Martín-Martín, M., Guerrera, F., Tosquella, J., Tramontana, M., 2021. Middle Eocene carbonate platforms of the westernmost Tethys. Sedimentary Geology 415, 105861. https://doi.org/10.1016/j.sedgeo.2021.105861.
Mateu-Vicens, G., Brandano, M., Gaglianone, G., Baldassarre, A., 2012. Seagrass-meadow sedimentary facies in a mixed siliciclastic–carbonate temperate system in the Tyrrhenian Sea (Pontinian Islands, western Mediterranean). Journal of Sedimentary Research 82, 451–463.
Miller, K.G., Wright, J.D., Fairbanks, R.G., 1991. Unlocking the ice house: Oligocene–Miocene oxygen isotopes, eustasy and margin erosion. Journal of Geophysical Research 96, 6829–6848. https://doi.org/10.1029/90JB02015.
Molina, E., Ortiz, N., Serra-Kiel, J., 1988. Implicaciones paleoecológicas de los foraminíferos en el Eoceno del Prepirineo Oscense (Sector de Arguis). Revista Espanola de Paleontologia 3, 45–58.
Morabito, C., Papazzoni, C.A., Lehrmann, D.J., Payne, J.L., Al-Ramadan, K., Morsilli, M., 2024. Carbonate factory response through the MECO (Middle Eocene climate optimum) event: insight from the Apulia Carbonate Platform, Gargano Promontory, Italy. Sedimentary Geology 461, 106575. https://doi.org/10.1016/j.sedgeo.2023.106575.
Moraweck, K., Uhl, D., Kunzmann, L., 2015. Estimation of late Eocene (Bartonian–Priabonian) terrestrial palaeoclimate: Contributions from megafloral assemblages from Central Germany. Palaeogeography, Palaeoclimatology, Palaeoecology 433, 247–258. https://doi.org/10.1016/j.palaeo.2015.05.023.
Morsilli, M., Bosellini, F.R., Pomar, L., Hallock, P., Aurell, M., Papazzoni, C.A., 2012. Mesophotic coral buildups in a prodelta setting (late Eocene, southern Pyrenees, Spain): a mixed carbonate–siliciclastic system. Sedimentology 59, 766–794. https://doi.org/10.1111/j.1365-3091.2011.01275.x.
Muñoz, J.A., 1992. Evolution of a continental collision belt: ECORS-Pyrenees crustal balanced cross-section. In: McClay, K.R. (Ed.), Thrust Tectonics. Chapman & Hall, London, pp. 235–246. https://doi.org/10.1007/978-94-011-3066-0_21.
Murray, J.W., 1973. Distribution and Ecology of Living Benthic Foraminiferids. Crane, Russak and Co., New York, p. 274.
Murray, J.W., 2006. Ecology and Applications of Benthic Foraminifera. Cambridge University Press, Cambridge, p. 426. https://doi.org/10.1017/CBO9780511535529.
Nebelsick, J.H., Bassi, D., Drobne, K., 2000. Microfacies analysis and palaeoenvironmental interpretation of lower Oligocene, shallow-water carbonates (Gornji Grad Beds, Slovenia). Facies 43, 157–176. https://doi.org/10.1007/BF02536989.
Nebelsick, J.H., Rasser, M.W., Bassi, D., 2005. Facies dynamics in Eocene to Oligocene circum-alpine carbonates. Facies 51, 197–217. https://doi.org/10.1007/s10347-005-0069-2.
Özcan, E., Less, G., Báldi-Beke, M., Kollányi, K., Kertész, B., 2007. Biometric analysis of middle and upper Eocene Discocyclinidae and Orbitoclypeidae (Foraminifera) from Turkey and updated orthophragmine zonation in the Western Tethys. Micropaleontology 52, 485–520. https://doi.org/10.2113/gsmicropal.52.6.485.
Özcan, E., Saraswati, P.K., Yücel, A.O., Ali, N., Hanif, M., 2018. Bartonian orthophragminids from the Fulra Limestone (Kutch, W India) and coeval units in Sulaiman Range, Pakistan: a synthesis of shallow benthic zone (SBZ) 17 for the Indian Subcontinent. Geodinamica Acta 30, 137–162. https://doi.org/10.1080/09853111.2018.1443654.
Özcan, E., Less, G., Jovane, L., Catanzariti, R., Frontalini, F., Coccioni, R., Giorgioni, M., Rodelli, D., Rego, E.S., Kayğılı, S., Rostami, M.A., 2019. Integrated biostratigraphy of the middle to upper Eocene Kırkgeçit Formation (Baskil section, Elazığ, eastern Turkey): larger benthic foraminiferal perspective. Mediterranean Geoscience Reviews 1, 55–90.
Papazzoni, C.A., Sirotti, A., 1995. Nummulite biostratigraphy at the Middle/Upper Eocene boundary in the northern Mediterranean area. Rivista Italiana di Paleontologia e Stratigrafia 101, 249–268. https://doi.org/10.13130/2039-4942/8566.
Papazzoni, C.A., Ćosović, V., Briguglio, A., Drobne, K., 2017. Towards a calibrated larger foraminifera biostratigraphic zonation: celebrating 18 years of the application of shallow benthic zones. Palaios 32, 1–4. https://doi.org/10.2110/palo.2016.043.
Pascher, K.M., Hollis, C.J., Bohaty, S.M., Cortese, G., McKay, R.M., Seebeck, H., Suzuki, N., Chiba, K., 2015. Expansion and diversification of high-latitude radiolarian assemblages in the late Eocene linked to a cooling event in the Southwest Pacific. Climate of the Past 11, 1599–1620. https://doi.org/10.5194/cp-11-1599-2015.
Pearson, P.N., McMillan, I.K., Wade, B.S., Dunkley Jones, T., Coxall, H.K., Bown, P.R., Lear, C.H., 2008. Extinction and environmental change across the Eocene–Oligocene boundary in Tanzania. Geology 36, 179–182. https://doi.org/10.1130/G24308A.1.
Pearson, P.N., Foster, G.L., Wade, B.S., 2009. Atmospheric carbon dioxide through the Eocene–Oligocene climate transition. Nature 461, 1110–1113. https://doi.org/10.1038/nature08447.
Persico, D., Villa, G., 2004. Eocene–Oligocene calcareous nannofossils from Maud Rise and Kerguelen Plateau (Antarctica): paleoecological and paleoceanographic implications. Marine Micropaleontology 52, 153–179. https://doi.org/10.1016/j.marmicro.2004.05.002.
Pilleri, G., Biosca, J., Via Boada, L., 1989. The Tertiary Sirenia of Catalonia. Brain Anatomy Institute, Ostermundigen.
Pisera, A., Busquets, P., 2002. Eocene siliceous sponges from the Ebro Basin (Catalonia, Spain). Geobios 35, 321–346. https://doi.org/10.1016/S0016-6995(02)00030-X.
Plancq, J., Mattioli, E., Pittet, B., Simon, L., Grossi, V., 2014. Productivity and sea-surface temperature changes recorded during the late Eocene–early Oligocene at DSDP Site 511 (South Atlantic). Palaeogeography, Palaeoclimatology, Palaeoecology 407, 34–44. https://doi.org/10.1016/j.palaeo.2014.04.016.
Plaziat, J., 1981. Late Cretaceous to late Eocene paleogeographic evolution of Southwest Europe. Palaeogeography, Palaeoclimatology, Palaeoecology 36, 263–320. https://doi.org/10.1016/0031-0182(81)90110-3.
Pomar, L., Baceta, J.I., Hallock, P., Mateu-Vicens, G., Basso, D., 2017. Reef building and carbonate production modes in the west-central Tethys during the Cenozoic. Marine and Petroleum Geology 83, 261–304. https://doi.org/10.1016/j.marpetgeo.2017.03.015.
Pound, M.J., Salzmann, U., 2017. Heterogeneity in global vegetation and terrestrial climate change during the late Eocene to early Oligocene transition. Scientific Reports 7, 43386. https://doi.org/10.1038/srep43386.
Puigdefàbregas, C., Muñoz, J.A., Marzo, M., 1986. Thrust belt development in the Eastern Pyrenees and related depositional sequences in the southern foreland basin. In: Allen, P.A., Homewood, P. (Eds.), Foreland Basins, 8. International Association of Sedimentologists Special Publication, pp. 229–246.
Puigdefàbregas, C., Muñoz, J.A., Vergés, J., 1992. Thrusting and foreland basin evolution in the Southern Pyrenees. In: McClay, K.R. (Ed.), Thrust Tectonics. Chapman & Hall, London, pp. 247–254. https://doi.org/10.1007/978-94-011-3066-0_22.
Racey, A., 2001. A review of Eocene nummulite accumulations: structure, formation and reservoir potential. Journal of Petroleum Geology 24, 79–100. https://doi.org/10.1111/j.1747-5457.2001.tb00662.x.
Rasser, M., 1994. Facies and palaeoecology of rhodoliths and acervulinid macroids in the Eocene of the Krappfeld (Austria). Beiträge zur Paläontologie 19, 191–217.
Rasser, M.W., 2000. Coralline red algal limestones of the late Eocene Alpine Foreland Basin in Upper Austria: component analysis, facies and paleoecology. Facies 42, 59–92.
Reguant, S., 1967. El Eoceno Marino de Vic (Barcelona), 68. Memorias del Instituto Geológico y Minero de España, p. 350.
Reguant, S., Colombo, F., Taberner, C., Barnolas, A., Serra-Kiel, J., Ortí, F., 1987. El Terciari de la Plana: Plantejaments i resultats plurals. Ausa XII 245–264.
Reguant, S., Fernández, J., Rodríguez-Fernández, Serra-Kiel, J., 1991. Bryozoan biofacies, zoarial forms and sedimentary environments in the Tertiary of Spain. In: Bigey, F.P. (Ed.), Bryozoaires actuels et fossiles, Bulletin de la Société des Sciences Naturelles de l'Ouest de la France, Mémoire Hors Série 1, pp. 361–370. Nantes.
Reijmer, J.J.G., 2021. Marine carbonate factories: Review and update. Sedimentology 68, 1729–1796. https://doi.org/10.1111/sed.12878.
Reiss, Z., Hottinger, L., 1984. The Gulf of Aqaba: Ecological Micropaleontology. In: Ecological Studies, 50. Springer-Verlag, Berlin Heidelberg, p. 354. https://doi.org/10.1007/978-3-642-69787-6.
Renema, W., 2002. Larger benthic foraminifera as environmental indicators. Scripta Geologica 124, 1–260.
Riba, O., Reguant, S., Colombo, F., Busquets, P., Vilaplana, M., Anadón, P., Marzo, M., Ramírez, A., Pueyo, J.J., Williams, R.C., 1975. Le bassin tertiaire catalan espagnol et ses gisements de potasse, 20. IX Congrès International de Sédimentologie, Nice, Livret guide de l'excursion, p. 84.
Riba, O., Reguant, S., Villena, J., 1983. Ensayo de síntesis estratigráfica y evolutiva de la Cuenca terciaria del Ebro. In: Libro Jubilar J.M. Ríos, 2, pp. 131–157.
Riding, R., 2002. Structure and composition of organic reef and carbonate mud mounds: concepts and categories. Earth-Science Reviews 58, 163–231. https://doi.org/10.1016/S0012-8252(01)00089-7.
Romero, J., 1996. Estudio de los foraminíferos bentónicos del límite Eoceno medio-Eoceno superior de la Cuenca de Igualada (Barcelona). Master's Degree thesis. Universitat Autònoma de Barcelona, Barcelona, p. 184.
Romero, J., Caus, E., 2000. Eventos neríticos en el límite Eoceno medio-Eoceno superior en el extremo oriental de la depresión del Ebro (NE de España). Revista de la Sociedad Geológica de España 13, 301–321.
Romero, J., Hottinger, L., Caus, E., 1999. Early appearance of larger foraminifera supposedly characteristic for the late Eocene in the Igualada Basin, NE Spain. Revista Espanola de Paleontologia 14, 79–92.
Romero, J., Caus, E., Rosell, J., 2002. A model for the palaeoenvironmental distribution of larger foraminifera based on late Middle Eocene deposits on the margin of the south Pyrenean basin (NE Spain). Palaeogeography, Palaeoclimatology, Palaeoecology 179, 43–56.
Rusciadelli, G., Shiner, P., 2018. Isolated carbonate platforms of the Mediterranean and their seismic expresión — searching for a paradigm. The Leading Edge 37, 492–502. https://doi.org/10.1190/tle37070492.1.
Salas, R., 1979. El sistema arrecifal del Eoceno Superior de la Cuenca de Igualada, Barcelona. Master's degree Thesis. University of Barcelona, p. 196.
Sanders, D., Baron-Szabo, R.C., 2005. Scleractinian assemblages under sediment input: their characteristics and relation to depositional environments (Middle Eocene, northern Calcareous Alps, Austria). Palaeogeography, Palaeoclimatology, Palaeoecology 222, 1–24. https://doi.org/10.1016/j.palaeo.2004.10.008.
Sanjuan, J., Martín-Closas, C., Serra-Kiel, J., Gallardo, H., 2012. Stratigraphy and biostratigraphy (charophytes) of the marine-terrestrial transition in the Upper Eocene of the NE Ebro Basin (Catalonia, Spain). Geologica Acta 10, 1–13. https://doi.org/10.1344/105.000001708.
Scheibner, C., Rasser, M.W., Mutti, M., 2007. The Campo section (Pyrenees, Spain) revisited: Implications for changing benthic carbonate assemblages across the Paleocene–Eocene boundary. Palaeogeography, Palaeoclimatology, Palaeoecology 248, 145–168. https://doi.org/10.1016/j.palaeo.2006.12.007.
Scher, H.D., Bohaty, S.M., Smith, B.W., Munn, G.H., 2014. Isotopic interrogation of a suspected late Eocene glaciation. Paleoceanography 29, 628–644. https://doi.org/10.1002/2014PA002648.
Schlager, W., 2003. Benthic carbonate factories of the Phanerozoic. International Journal of Earth Sciences 92, 445–464. https://doi.org/10.1007/s00531-003-0327-x.

Serra-Kiel, J., Reguant, S., 1991. Biofaciès de plate-forme aphotique silico-clastique avec bryozoaires et spongiaires (Éocène moyen, secteur oriental du bassin sud-pyrénéen). Geobios 24, 33–40.
Serra-Kiel, J., Hottinger, L., Caus, E., Drobne, K., Ferràndez, C., Jauhri, A.K., Less, G., Pavlovec, R., Pignatti, J., Samso, J.M., Schaub, H., Sirel, E., Strougo, A., Tambareau, Y., Tosquella, J., Zakrevskaya, E., 1998. Larger foraminiferal biostratigraphy of the Tethyan Paleocene and Eocene. Bulletin de la Société Géologique de France 169, 281–299.
Serra-Kiel, J., Travé, A., Mató i Palós, E., Saula Briansó, E., Ferràndez i Cañadell, C., Busquets, P., Tosquella i Angrill, J., Vergés i Masip, J., 2003a. Marine and transitional Middle/Upper Eocene units of the Southeastern Pyrenean Foreland Basin (NE Spain). Geologica Acta 1, 177–200. https://doi.org/10.1344/105.000001609.
Serra-Kiel, J., Mató, E., Saula, E., Travé, A., Ferràndez-Cañadell, C., Busquets, P., Samsó, J.M., Tosquella, J., Álvarez-Pérez, G., Franquès, J., Romero, J., 2003b. An inventory of the marine and transitional Middle/Upper Eocene deposits of the Southeastern Pyrenean Foreland Basin (NE Spain). Geologica Acta 1, 201–229. https://doi.org/10.1344/105.000001610.
Serra-Kiel, J., Tosquella, J., Samsó, J.M., Ferrández, C., 1994. Distribución ambiental de los macroforaminíferos del Paleoceno de la Cuenca Pirenaica. Comunicaciones de las X Jornadas de Paleontología, UCM, CSIC y SEP., pp. 189–191
Setiawan, J.R., 1983. Foraminifera and microfacies of the type Priabonian. Utrecht Micropaleontological Bulletin 29, 1–161.
Sheldon, N.D., Retallack, G.J., 2004. Regional paleoprecipitation records from the late Eocene and Oligocene of North America. The Journal of Geology 112, 487–494. https://doi.org/10.1086/421076.
Sheldon, N.D., Costa, E., Cabrera, L., Garcés, M., 2012. Continental climatic and weathering response to the Eocene–Oligocene transition. The Journal of Geology 120, 227–236. https://doi.org/10.1086/663984.
Śliwińska, K.K., Thomsen, E., Schouten, S., Schoon, P.L., Heilmann-Clausen, C., 2019. Climate- and gateway-driven cooling of late Eocene to earliest Oligocene Sea surface temperatures in the North Sea Basin. Scientific Reports 9, 4458. https://doi.org/10.1038/s41598-019-41013-7.
Somerville, I.D., Strogen, P., 1992. Ramp sedimentation in the Dinantian limestones of the Shannon Trough, Co. Limerick, Ireland. Sedimentary Geology 79, 59–75.
Strasser, A., Pittet, B., Hillgärtner, H., Pasquier, J.-B., 1999. Depositional sequences in shallow carbonate-dominated sedimentary systems. Sedimentary Geology 128, 201–221. https://doi.org/10.1016/S0037-0738(99)00070-6.
Straume, E.O., Faccenna, C., Becker, T.W., Steinberger, B., Licht, A., Sembroni, A., Gvirtzman, Z., Ballato, P., 2025. Collision, mantle convection and Tethyan closure in the Eastern Mediterranean. Nature Reviews Earth & Environment 6, 299–317. https://doi.org/10.1038/s43017-025-00653-2.
Suc, J.-P., Fauquette, S., Popescu, S.-M., Melinte-Dobrinescu, M.C., Huet, B., Sorrel, P., Semmani, N., Fournier, F., Bessedik, M., Zheng, Z., Truc, G., Ferry, S., Rubino, J.-L., Girard, V., Séranne, M., 2025. Late Eocene to early Miocene environments, vegetation and climate in southeastern France documented by palynology. Palaeogeography, Palaeoclimatology, Palaeoecology 659, 112625. https://doi.org/10.1016/j.palaeo.2024.112625.
Sun, J., Ni, X., Bi, S., Wu, W., Ye, J., Meng, J., Windley, B.F., 2014. Synchronous turnover of flora, fauna, and climate at the Eocene–Oligocene boundary in Asia. Scientific Reports 4, 7463. https://doi.org/10.1038/srep07463.
Taberner, C., 1984. Evolución ambiental y diagenética de los depósitos del Terciario inferior (Paleoceno y Eoceno) de la Cuenca de Vic. PhD thesis. University of Barcelona. , 1400 pp.
Taberner, C., Bosence, D.W.J., 1995. An Eocene biodetrital mud-mound from the southern Pyrenean foreland basin, Spain: An ancient analogue for Florida Bay mounds? In: Monty, C.L.V., Bosence, D.W.J., Bridges, P.H., Pratt, B.R. (Eds.), Carbonate Mud-Mounds – Their Origin and Evolution, 23. International Association of Sedimentologists Special Publication, pp. 423–437.
Taberner, C., Dinarès-Turell, J., Giménez, J., Docherty, C., 1999. Basin infill architecture and evolution from magnetostratigraphic cross-basin correlations in the southeastern Pyrenean foreland basin. GSA Bulletin 111, 1155–1174. https://doi.org/10.1130/0016-7606(1999)111<1155:BIAAEF>2.3.CO;2.
Teixell, A., Serra-Kiel, J., 1988. Sedimentología y distribución de foraminíferos en medios litorales y de plataforma mixta del Eoceno superior de la cuenca del Ebro (sector suroriental). Boletín Geológico y Minero 94, 871–885.
Thomas, E., 2007. Cenozoic mass extinctions in the deep sea: what disturbs the largest habitat on Earth? Geological Society of America Special Papers 424, 1–23.
Tomassetti, L., Benedetti, A., 2020. To be allochthonous or autochthonous? The late Paleocene–late Eocene slope sedimentary succession of the Latium–Abruzzi carbonate platform (Central Apennines, Italy). Facies 66, 6. https://doi.org/10.1007/s10347-019-0590-3.
Tomassetti, L., Benedetti, A., Brandano, M., 2016. Middle Eocene seagrass facies from Apennine carbonate platforms (Italy). Sedimentary Geology 335, 136–149. https://doi.org/10.1016/j.sedgeo.2016.02.002.
Torfstein, A., Steinberg, J., 2020. The Oligo–Miocene closure of the Tethys Ocean and evolution of the proto-Mediterranean Sea. Scientific Reports 10, 13817. https://doi.org/10.1038/s41598-020-70652-4.
Tosal, A., Sanjuan, J., Cartanyà, J., Martín-Closas, C., 2018. Taphonomy and palaeoecology of the uppermost Eocene flora from Sarral (Eastern Ebro Basin): Palaeoclimatic implications. Palaeogeography, Palaeoclimatology, Palaeoecology 497, 66–81. https://doi.org/10.1016/j.palaeo.2018.02.006.
Tosal, A., Valero, L., Sanjuan, J., Martin-Closas, C., 2019. Influence of short- and long-term climatic cycles on floristic change across the Eocene–Oligocene boundary in the Ebro Basin (Catalonia, Spain). Comptes Rendus Palevol 18, 925–947. https://doi.org/10.1016/j.crpv.2019.10.003.
Tosquella, J., Martín-Martín, M., Guerrera, F., 2022. The Eocene carbonate platform of the central-western Malaguides (Internal Betic Zone, S Spain) and its meaning for the Cenozoic paleogeography of the westernmost Tethys. Palaeogeography, Palaeoclimatology, Palaeoecology 602, 110840. https://doi.org/10.1016/j.palaeo.2022.110840.
Travé, A., 1992. Sedimentologia, petrologia i geoquímica (elements traça i isòtops) dels estromatòlits de la Conca Eocena Sudpirinenca. PhD Thesis. University of Barcelona, p. 396.
Travé, A., Serra-Kiel, J., Zamarreño, I., 1996. Paleoecological interpretation of transitional environments in Eocene carbonates (NE Spain). Palaios 11, 141–160.
Travé, A., Serra-Kiel, J., Ferràndez-Cañadell, C., 1999. Litho-biostratigraphy of the Bartonian in the Igualada area (South-Pyrenean Basin). Temas Geológico-Mineros ITGE 26, 513–517.
Tremblin, M., Hermoso, M., Minoletti, F., 2016. Equatorial heat accumulation as a long-term trigger of permanent Antarctic ice sheets during the Cenozoic. Proceedings of the National Academy of Sciences 113, 11782–11787. https://doi.org/10.1073/pnas.1608100113.
Tuya, F., Schubert, N., Aguirre, J., Basso, D., Bastos, E.O., Berchez, F., Bernardino, A.F., Bosch, N.E., Burdett, H.L., Espino, F., Fernández-García, C., Francini-Filho, R.B., Gagnon, P., Hall-Spencer, J.M., Haroun, R., Hofmann, L.C., Horta, P.A., Kamenos, N. A., Le Gall, L., Magris, R.A., Martin, S., Nelson, W.A., Neves, P., Olivé, I., Otero-Ferrer, F., Peña, V., Pereira-Filho, G.H., Ragazzola, F., Rebelo, A.C., Ribeiro, C., Rinde, E., Schoenrock, K., Silva, J., Sissini, M.N., Tâmega, F.T.S., 2023. Levelling-up rhodolith-bed science to address global-scale conservation challenges. Science of the Total Environment 892, 164818. https://doi.org/10.1016/j.scitotenv.2023.164818.
Ungaro, S., 1996. Adaptive morphological strategy of *Gypsina* (encrusting foraminifer). In: Cherchi, A. (Ed.), Autecology of Selected Fossil Organisms: Achievements and Problems, 3. Bollettino della Società Paleontologica Italiana Special, pp. 233–241.
Van Breedam, J., Huybrechts, P., Crucifix, M., 2022. Modelling evidence for late Eocene Antarctic glaciations. Earth and Planetary Science Letters 586, 117532. https://doi.org/10.1016/j.epsl.2022.117532.
van Hinsbergen, D.J.J., de Groot, L.V., van Schaik, S.J., Spakman, W., Bijl, P.K., Sluijs, A., Langereis, C.G., Brinkhuis, H., 2015. A paleolatitude calculator for paleoclimate studies. PLoS One 10, e0126946. https://doi.org/10.1371/journal.pone.0126946.
van Hinsbergen, D.J.J., Vaes, B., Boschman, L.M., Lom, N., van de Lagemaat, S.H.A., Advokaat, E.L., de Baar, S., Paridaens, J., Jarochowska, E., 2026. Paleolatitude.org 3.0: a calculator for paleoclimate and paleobiology studies based on a new global paleogeography model. PLoS One 21, e0346817. https://doi.org/10.1371/journal.pone.0346817.
Vergés, J., Burbank, D.W., 1995. Eocene–Oligocene thrusting and basin configuration in the eastern and central Pyrenees (Spain). Tectonics 14, 462–480.
Vergés, J., Muñoz, J.A., 1990. Thrust sequences in the southern Central Pyrenees. Bulletin de la Société Géologique de France 8, 265–271.
Vergés, J., Marzo, M., Santaeulària, T., Serra-Kiel, J., Burbank, D.W., Muñoz, J.A., Giménez-Montsant, J., 1998. Quantified vertical motions and tectonic evolution of the SE Pyrenean foreland basin. In: Mascle, A., Puigdefábregas, C., Luterbacher, H.P., Fernández, M. (Eds.), Cenozoic Foreland Basins of Western Europe, 134. Geological Society Special Publications, pp. 107–134. https://doi.org/10.1144/gsl.sp.1998.134.01.06.
Vergés, J., Fernàndez, M., Martínez, A., 2002. The Pyrenean orogen: pre-, syn-, and post-collisional evolution. Journal of Virtual Explorer 8, 55–74. https://doi.org/10.3809/jvirtex.2002.00058.
Waltham, D., Docherty, C., Taberner, C., 2000. Decoupled flexure in the South Pyrenean Foreland. Journal of Geophysical Research 105, 1637–1652. https://doi.org/10.1029/2000JB900064.
Wei, X., Yan, D., Luo, P., Jiang, P., Wang, H., Zhou, J., Cong, F., Yang, X., Niu, X., Li, T., Liu, L., Liu, E., 2020. Astronomically forced climate cooling across the Eocene–Oligocene transition in the Pearl River Mouth Basin, northern South China Sea. Palaeogeography, Palaeoclimatology, Palaeoecology 558, 109945. https://doi.org/10.1016/j.palaeo.2020.109945.
Westerhold, T., Marwan, N., Drury, A.J., Liebrand, D., Agnini, C., Anagnostou, E., Barnet, J.S.K., Bohaty, S.M., De Vleeschouwer, D., Florindo, F., Frederichs, T., Hodell, D.A., Holbourn, A.E., Kroon, D., Lauretano, V., Littler, K., Lourens, L.J., Lyle, M., Pälike, H., Röhl, U., Tian, J., Wilkens, R.H., Wilson, P.A., Zachos, J.C., 2020. An astronomically dated record of Earth's climate and its predictability over the last 66 million years. Science 369 (6509), 1383–1387. https://doi.org/10.1126/science.aba6853.
Whidden, K.J., Jones, R.W., 2012. Correlation of early Paleogene global diversity patterns of large benthic foraminifera with Paleocene and Eocene climatic events. Palaios 27, 235–251. https://doi.org/10.2110/palo.2010.p10-109r.
Wilson, M., 2012. Equatorial carbonates: an Earth systems approach. Sedimentology 59, 1–31. https://doi.org/10.1111/j.1365-3091.2011.01293.x.
Zachos, J.C., Pagani, M., Sloan, L., Thomas, E., Billups, K., 2001. Trends, rhythms, and aberrations in global climate 65 Ma to present. Science 292, 686–693. https://doi.org/10.1126/science.1059412.
Zachos, J.C., Dickens, G., Zeebe, R.E., 2008. An early Cenozoic perspective on greenhouse warming and carbon-cycle dynamics. Nature 451, 279–283.
Zakrevskaya, E., Less, G., Bugrova, E., Shcherbinina, E., Grigoryan, T., Sahakyan, L., 2020. Integrated biostratigraphy and benthic foraminifera of the middle-upper Eocene deposits of Urtsadzor section (Southern Armenia). Turkish Journal of Earth Sciences 29, 896–945. https://doi.org/10.3906/yer-1912-6.
Zhang, Y.G., Pagani, M., Liu, Z., Bohaty, S.M., DeConto, R., 2013. A 40-million-year history of atmospheric CO_2. Philosophical Transactions of the Royal Society A: Mathematical, Physical and Engineering Sciences 371, 20130096. https://doi.org/10.1098/rsta.2013.0096.